Norwegian University of Life Sciences
Faculty of Environmental Sciences
and Natural Resource Management (MINA)

Philosophiae Doctor (PhD)
Thesis 2018:68

Late Weichselian glacial dynamics and retreat patterns of the Fennoscandian Ice Sheet in Gausdal Vestfjell, south-central Norway, acquired from spatial data

Sen weichsel isdynamikk og isavsmeltings-mønster av Den fennoskandiske innlandsisen i Gausdal Vestfjell, sentrale Sør-Norge, basert på romlige data

Artūrs Putniņš

Late Weichselian glacial dynamics and retreat patterns of the Fennoscandian Ice Sheet in Gausdal Vestfjell, south-central Norway, acquired from spatial data

Sen weichsel isdynamikk og isavsmeltingsmønster av Den fennoskandiske innlandsisen i Gausdal Vestfjell, sentrale Sør-Norge, basert på romlige data

degree of Philosophiae Doctor (PhD) Thesis

Artūrs Putniņš

Norwegian University of Life Sciences
Faculty of Environmental Sciences and Natural Resource Management

Ås (2018)

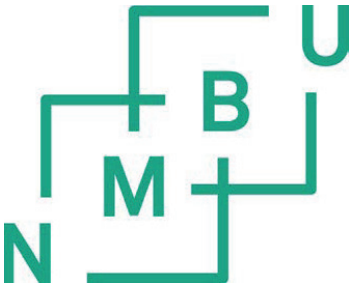

Thesis number: 2018:68
ISSN: 1894-6402
ISBN: 978-82-575-1536-2

PhD supervisors

Associate professor **Mona Henriksen** (Main supervisor),
Faculty of Environmental Sciences and Natural Resource Management (MINA)
Norwegian University of Life Sciences, P.O. Box 5003, 1432 Ås, Norway
Telephone: (+47) 67 23 18 17
E-mail: mona.henriksen@nmbu.no

Associate professor **Håvard Tveite** (Co-supervisor),
Faculty of Science and Technology (REALTEK),
Norwegian University of Life Sciences, P.O. Box 5003, 1432, Ås, Norway
Telephone: (+47) 67 23 15 48
E-mail: havard.tveite@nmbu.no

Professor **Jon Ytterbø Landvik** (Co-supervisor),
Faculty of Environmental Sciences and Natural Resource Management (MINA)
Norwegian University of Life Sciences, P.O. Box 5003, 1432 Ås, Norway
Telephone: (+47) 67 23 18 19
E-mail: jon.landvik@nmbu.no

Thesis Evaluation committee

Professor Dr. PhD **Johan Kleman** (First opponent),
Department of Physical Geography and Quaternary Geology, Stockholm University
106 91 Stockholm, Sweden
Telephone: (+46) 8 16 48 13
E-mail: johan.kleman@natgeo.su.se

Researcher Dr. PhD **Anna L.C. Hughes** (Second opponent),
Department of Earth Science, University of Bergen
P.O. Box 7803, 5020 Bergen, Norway
Telephone: (+47) 555 88 109
E-mail: anna.hughes@uib.no

Associate professor Dr. **Line Tau Strand** (committee coordinator),
Faculty of Environmental Sciences and Natural Resource Management, NMBU
P.O. Box 5003 NMBU, 1432 Ås, Norway
Telephone: (+47) 67 23 18 62
E-mail: line.strand@nmbu.no

Preface

First and foremost I would like to express my deepest gratitude to the team of my supervisors. Thank you, Jon, for coming up with the idea and project proposal to begin with. I would like to thank Håvard, for your willingness to teach me all those GIS skills and tricks that I did not know before, and for the encouragement to join the NMBU orienteering club where I could loosen up my mind from mapping and maps with… ...another type of maps. And certainly greatest thanks of all to Mona. Thank you for taking the lead in my supervision throughout the last four years. Thank you for picking me up at the airport in the rainy day of May 6th, 2014. And thank you being the *devil's advocate* so many times in the ever-evolving geological discussion throughout the course of my PhD.

I would like to thank the numerous colleagues at the Department of Environmental Sciences (MINA) for your kindness and willingness to provide an advice and support. Thank you, Nils-Otto, Sylvi, Rolf, Michael, Leif, Helen, Annne-Grethe, Håkon and Mirian. Furthermore, a special thanks to my fellow *comrades* – Perrine, Ellen and Sverre – the dream-team of the 'Geovann' corner, as well as Ivan and Daumantas. Thank you all for being much more than just colleagues on the same struggle, thank you for now being part of my life.

During these years I was privileged to gain academic experience beyond the PhD project alone. Thank you, Line, Trine, Jan, Jan and Ståle for your thrust and allowance to be part of *JORD210* and *OSCAR*.

I acknowledge Clay from the NMBU writing centre for the help on adding adhesion to my thesis.

In a brief retrospect, I also would like to thank Pēteris Blumbergs – my first orienteering coach and the first mentor in the fascinating process of map-making. My sincerest gratitude goes to Laimdota Jansone – my first geography teacher from the grammar-school years. Thank you for being the compass that guided me in the right direction starting with the invitation to participate in the *school of Vidzeme New geographers'* as well as the one particular conversation on the way to it that shifted my curiosity towards geomorphology. I do also acknowledge the scenic regional road P30 stretching through the Vidzeme Uplands, in Latvia (and, in particular, the 21st kilometre of it) around where this conversation took place.

I would like to thank Prof. Dr. PhD Vitālijs Zelčs for his guidance through my bachelor and master thesis, and the opportunity to be part of the geomorphological research team in the Faculty of Geography and Earth Sciences, University of Latvia.

I would like to acknowledge my mum and sister for believing in me even then when I had lost the belief in myself.

I would like to thank my father for teaching me the appreciation of nature since the early days of my childhood that lead me to where I am now. You will always be remembered for that even though you are not with us anymore.

Last, but certainly not the least – thank you Santa for being present in this journey of my life since the very first day of it!

Summary

Evidence-based geomorphological research (analyses of glacial landform record) is one of the commonly used types of glacial reconstructions applied for studying the past ice sheets. The work covered by this thesis contains a geomorphological data set of more than 17 000 glacial and glacifluvial landforms in Gausdal Vestfjell, south-central Norway. The study area is located in an inner region of the former Fennoscandian Ice Sheet (FIS) and contains a palaeogeological record on the flow pattern evolution and retreat during the Late Weichselian. The geomorphological mapping was carried out by exploiting the accessibility of high resolution LiDAR *(Light Detection And Ranging)* data and the capabilities provided by the latest advances in Geographical Information System (GIS) technologies such as terrain visualisations in an interactive 3D environment. A consequence of the '*age of LiDAR'* is the increase in the resolution of the findings with more and smaller-sized landforms being mapped, that earlier were likely to be left out as unrecognised. These small-sized landforms may provide information on relatively short-lived events representing changes of glacial dynamics. This is particularly the case when such landforms are found overlapping other larger landforms. The mapping results have been validated by field observations.

Since the manual mapping of landforms is a time consuming and potentially subjective process, part of the thesis explores the semi-automated mapping (SAM) techniques that may be a reliable and effective alternative for data extraction. Several SAM methods are proposed for glacial streamlined landform extraction, yet none was considered optimal for the extraction of glacial ice flow directions in a complex terrain, such as the study area in the Scandinavian Mountains. Therefore, the potential of the grayscale thinning (skeletonisation) application for the extraction of directional trends from the terrains is explored.

The meltwater landform domain is a valuable source of information on the dynamics of past ice sheets and their deglaciation. Possibly due to the uncertainties in establishing the correlations of spatial and temporal relations of (and, in particular, the marginal) meltwater landforms it has often had only a secondary role. Here, GIS tools were used to introduce a simple reference surface gradient and apply a vertical adjustment of the 'virtual ice surface' representing vertical down-wasting of ice in order to increase the credibility of meltwater landform correlations. This enabled to distinguish several important ice marginal positions and to reconstruct the significant events of deglaciation in a greater detail.

The study reveals a stepwise evolution of the FIS flow pattern during the Late Weichselian where a topography independent ice flow (Phase I) is followed by a regional (Phase II) that is subsequently replaced by a strongly channelized, topography-driven ice flow (Phase III with several substages). Prior to the ice disintegration, the ice flow was increasingly confined into valleys, likely separated by colder, less active ice. The deglaciation is characterised by a vertical down-melting of ice, dynamic evolution of the meltwater drainage systems that included temporary ice-dammed lakes and spillways, and deposition of various glacifluvial landforms.

Although the presented work can be considered as a local study from Gausdal Vestfjell, it improves our knowledge on the evolution and retreat of the FIS. Further, the proposed methods may find useful applications in other glacial geomorphology studies elsewhere.

Sammendrag

Bevisbaserte geomorfologiske undersøkelser (analyser av glasiale landformer) er en av de vanligste måtene å rekonstruere tidligere innlandsiser. Arbeidet som omfattes av denne avhandlingen inneholder et geomorfologisk datasett med mer enn 17 000 glasiale og glasifluviale landformer i Gausdal Vestfjell, midtre Sør-Norge. Studieområdet ligger i indre region av Den fennoskandiske innlandsisen (FIS) og inneholder et verdifullt geologisk arkiv om utviklingen av strømningsmønsteret og isavsmeltingen i sein weichsel. Geomorfologisk kartlegging ble utført ved å utnytte tilgjengeligheten av høyoppløselig LiDAR-data (*Light Detection And Ranging*) og å anvende de nyeste teknologiske framskrittene innen geografiske informasjonssystemer (GIS) som interaktive 3D-visualiseringer av terrenget. En konsekvens av denne 'LiDAR-epoken' er høyere oppløsning av kartleggingsfunnene med forekomst av langt flere og mindre landformer som sannsynligvis ville blitt oversett tidligere. Disse små-skala landformene kan gi informasjon om relativt kortvarige hendelser som representerer endringer i isdynamikken. Dette gjelder spesielt når slike landformer er funnet oppå andre større landformer. Kartleggingsresultatene er stadfestet med feltobservasjoner.

Siden manuell kartlegging av landformer er en tidkrevende og potensielt subjektiv prosess, blir det i avhandlingen utforsket om semi-automatiserte kartleggingsteknikker (SAM) kan være et pålitelig og effektivt alternativt for datautvinning. Det er foreslått flere SAM-metoder for utvinning av glasiale strømlinjede landformer, men ingen ble ansett som optimal for utvinning av isbevegelsesretninger i studieområdets komplekse terreng i de skandinaviske fjellene. Derfor utforskes potensialet i applikasjonen for gråtonetynning (*skeletonisation*) for utvinning av retningstrender i terrenget.

Smeltevannform-domenet er en verdifull informasjonskilde til isdynamikken til tidligere innlandsis og isavsmeltingen. Muligens på grunn av usikkerhetene i å etablere romlige og tidsmessige korrelasjoner mellom smeltevannlandformene (spesielt for de marginale), har de ofte bare hatt en sekundær rolle. For å øke troverdigheten til slike korrelasjoner ble GIS-verktøyene brukt til å introdusere en enkel referanse-overflategradient og anvende en vertikal justering av denne "virtuelle isoverflaten" som representerer vertikal nedsmelting av is. Dette gjorde det mulig å skille mellom flere viktige isfrontposisjoner og i å rekonstruere de viktigste deglasiasjonshendelsene i større detalj.

Studien viser en trinnvis utvikling av strømningsmønsteret til FIS i sein weichsel der en topografisk uavhengig isbevegelse (fase I) følges av en regional fase II som seinere erstattes av en sterkt kanalisert, topografisk avhengig isbevegelse (fase III med flere undertrinn). Før isen smeltet bort ble isbevegelsen mer og mer begrenset til dalbunnene, sannsynligvis adskilt av mindre aktiv, kald is. Deglasiasjonen er preget av en vertikal nedsmelting av is, dynamisk utvikling av dreneringssystemene med smeltevann som inkluderer kortvarige isdemte innsjøer og smeltevannsløp og avsetning av ulike glasifluviale landformer.

Selv om det presenterte arbeidet kan betraktes som en lokal studie fra Gausdal Vestfjell, har den forbedret vår kunnskap om utviklingen og tilbakesmeltingen av FIS. Videre kan de foreslåtte metodene bli anvendt i andre glasial-geomorfologiske studier andre steder.

Kopsavilkums

Pierādījumos balstītie ģeomorfoloģiskie pētījumi (glaciālo reljefa formu analīze) ir viens no biežāk pielietotajiem rekonstruckiju veidiem pagātnes ledusvairogu pētījumos. Doktora disertācijas ietvaros veiktais pētījums sevī ietver informāciju par vairāk kā 17 tūkstošiem dažādu glacigēno un ledāja kušanas ūdeņu reljefa formām no Gausdālas Vestfjelas (Gausdal Vestfjell) apkārtnes, centrālajā Dienvidnorvēģijā. Pētījuma teritorija atrodas bijušā Fenoskandijas ledusvairoga centrālā apgabala iecirknī, un tājā ir atrodamas vērtīgas paleoģeoloģiskās liecības par apledojuma plūsmu attīstību vēlā Vislas apledojuma laikā un ledusvairoga kušanu leduslaikmeta beigu posmā. Ģeomorfoloģiskā kartēšana tika veikta izmantojot augstas izšķirtspējas LiDAR (lāzerskenēšanas) datu pieejamību un Ģeogrāfisko Informācijas Sistēmu (ĢIS) sniegtās iespējas, kā piemēram, reljefa vizualizāciju interaktīvajā 3-dimensiju vidē. Likumsakarīgi, ka LiDAR laikmets ir atnesis izšķirtspējas pieaugumu, kā rezultātā ir iespējams kartēt un datu kopā ietvert vairāk un izmēros mazākas reljefa formas, kuras agrāk būtu palikušas nepamanītas. Šīs mazizmēra reljefa formas iespējams var sniegt ieskatu relatīvi īslaicīgos notikumos ledus plūsmu dinamikas attīstībā. Tas jo īpaši ir attiecināms gadījumos, kad šīs mazizmēra reljefa formas ir atrodamas pārklājamies uz citām, lielākām reljefa formām. Pētījuma ietvaros iegūtie kartēšanas rezultāti ir apstiprināti ar lauka darbos gūtajiem novērojumiem.

Tā kā manuāla reljefa formu kartēšana ir laikiepiltīgs un potenciāli subjektīvs process, daļa no doktora disertācijā ietvertā pētījuma apskata (semi-)automātiskās kartēšanas metodžu pielietošanu kā potenciāli uzticamu un efektīvu alternatīvu datu ieguvei. Kaut arī pastāv dažas reljefa formu automātiskās atpazīšanas metodes, neviena no esošajām metodēm nav uzskatāma par piemērotu datu par ledus plūsmu virzieniem ieguvei sarežģītos reljefa apstākļos, kādi ir satopami pētījuma teritorijā, Skandināvijas kalnu grēdas centrālajā apgabalā. Tāpēc pelēktoņu (grayscale) retināšanas rīkā balstīta reljefa virzienu noteikšanas metode, tiek apskatīta kā alternatīva esošajām metodēm.

Ledājkušanas ūdeņu reljefa formas sevī ietver vērtīgu informācijas avotu par ledusvairogu plūsmas dinamiku un to atkāpšanos leduslaikmeta beigu posmā. Taču, iespējams tieši neskaidrību un problemātikas dēļ, kāda pastāv saistībā ar ledāja kušanas reljefa formu (un jo īpaši marginālo) korelāciju izveidošanu, ledājkušanas ūdeņu reljefa formām bieži ir bijusi tikai otršķirīga nozīme. Šī darba ietvaros tika pielietoti ĢIS rīki, lai ieviestu vienkāršotu atsauces virsmu - 'virtuālo ledāja virsmu', ar mērķi uzlabot marginālo ledājkušanas ūdeņu reljefa formu korelācijas. Šādas atskaites virsmas ieviešana ir veicinājusi ledāja marginālo pozīciju noteikšanu un galcilo rekonstrukciju izveidi daudz augstākā detaizācijas pakāpē kā līdz šim.

Veiktais pētījums atklāj pakāpeniskumu Fenoskandijas ledusvairoga ledus plūsmu dinamiskas attīstībā vēlā Vislas apledojuma laikā, kur no topogrāfiski neatkarīgas plūsmas (fāze I) tā pāriet reģionālā (fāze II) ar zināmu zemledāja topogrāfijas ietekmi, līdz tā iegūst izteiktu kanālveida (fāze III un tās paveidi) raksturu. Pirms ledusvairoga aprimšanas, ledus plūsma pakāpeniski tika arvien vairāk novirzīta ielejās, starp tām valdot stagnata un aprimuša ledus apstākļiem. Deglaciāciju galvenokārt raksturo ledus biezuma pakāpeniska samazināšanās un dinamiska ledājkušanas ūdeņu sistēmu attīstību, kura ietver īslaicīgu ledājkušanas ūdeņu baseinu, ledājkušanas ūdeņu pārteces kanālu eksistenci kā arī akumulatīvo ledājkušanas ūdeņu reljefa formu veidošanos.

Kaut arī šis pētījums ir raksturojams kā lokālas nozīmes pētījums Gausdālas Vestfjelas apkārtnei, tas sniedz nozīmīgu papildinājumu mūsu zināšanās par Fenoskandijas ledusvairoga attīstību un deglacācijas gaitu. Turklāt, šī darba ietvaros piedāvātās metodes ir potenciāli pielietojamas glaciālās ģeomorfoloģijas pētījumos citviet seno apledojumu skartajās teritorijās.

Table of Contents

Preface ... 3
Summary ... 4
Sammendrag ... 5
Kopsavilkums ... 6
List of papers ... 8
Scope of Thesis ... 9
1. Introduction ... 10
Historical background ... 10
Concept of geomorphological inversion ... 10
Present and future perspectives ... 11
Study area ... 12
Sediment cover ... 13
Bedrock and the topographic sensitivity ... 14
Previous research within the study area ... 15
2. Materials and Methods ... 16
LiDAR ... 16
Input data for remote sensing ... 17
Geomorphological mapping ... 18
Fieldwork ... 20
(Semi-) automated mapping methods ... 20
Reference gradient surface use for meltwater landform correlations ... 21
3. Extended summary of papers ... 23
Paper I ... 23
Paper II ... 24
Paper III ... 25
4. Results and discussion ... 26
LiDAR implications on mapping of landforms ... 26
Evaluation of the proposed methods ... 29
Extracting and visualising glacial ice flow directions by using the Grayscale Thinning and directional trend analyses ... 29
Application and use of the reference gradient surface for analysing the meltwater features and deglaciation pattern ... 34
Reconstructed ice flow, retreat patterns and dynamics ... 34
5. Conclusions ... 38
6. Research Outlook ... 39
References ... 41

List of papers

Paper I

Putniņš, A., Henriksen, M. (2017) Reconstructing the flow pattern evolution in inner region of the Fennoscandian Ice Sheet by glacial landforms from Gausdal Vestfjell area, south-central Norway. Quaternary Science Reviews 163, 56-71. DOI: 10.1016/j.quascirev.2017.03.008. *Reprinted with kind permission of Elsevier.*

Paper II

Putniņš, A., Tveite, H. Extracting and visualizing glacial ice flow directions from Digital Elevation Models using Grayscale Thinning and directional trend analyses. *Submitted to Computers and Geosciences.*

Paper III

Putniņš, A., Henriksen, M. Final stages of deglaciation reconstructed from meltwater landforms in the Upper Etne valley, south-central Norway. *Manuscript. Prepared for submission to Boreas.*

Scope of Thesis

The broad research objective of this thesis is to improve the general understanding of the evolution and deglaciation of the former Fennoscandian Ice Sheet at one of its inner regions by using the latest remote sensing and spatial data applicable for glacial reconstructions. The main focus of the thesis is to reveal new insights in the evolution and deglaciation of Late Weichselian ice sheet in Gausdal Vestfjell, south-central Norway by implementing the latest opportunities provided by the LiDAR (laser scanning) data and GIS technologies as the main tools for geomorphological mapping.

The specific aims of the thesis are to investigate the following research questions:

- **Paper I** tackles the question – what were the glacial dynamics of the Fennoscandian Ice Sheet at its inner region close to the ice divide during the last glaciation?
- **Paper II** investigates the ways in how the information on previous glacial ice flow directions can be recognized in and extracted from the digital elevation models (DEMs) in a (semi-) automated manner.
- **Paper I** and **III** are exploring the spatial and temporal changes of the ice dynamics like ice flow patterns, glacial velocity and subglacial hydrology, and the ice extent of the last Fennoscandian Ice Sheet during its deglaciation.
- **Papers II** and **III** address methodological possibilities and constraints of GIS tools and how can new approaches be implemented and used to improve the efficiency of data collection and analyses used for glacial reconstructions?

1. Introduction

Historical background

Since the early 19th century when the first scientific acknowledgement of Ice Age occurred (Esmark, 1824, 1826; Agassiz, 1841), and the introduction of the solar forcing theory (Milankovic, 1930), an ever-growing bulk of observations, studies and theories have shaped the disciplines of glacial geomorphology and Quaternary geology (c.f. Ingólfsson & Landvik, 2013; Hestmark, 2018; Menzies 2018). At an early stage the studies on the former ice sheet extents in the Northern Hemisphere were carried out by field documentation – identifying marginal moraines, striae, erratics and investigating the till sheets extents (c.f. Hestmark, 2018). Later, with the development of aerial photography technique, remote sensing became the primary tool for landform mapping allowing to extend the coverage of study areas (Keman et al., 2006). The advancement of dating techniques have added the geochronological perspective to the ice sheets (e.g. Svendsen et al., 2004; Jahns, 2007; Goehring et al., 2008; Hughes et al., 2016). The further scientific development on analysing other geochronological records like isotope analyses of ice cores (e.g. Rasmussen et al., 2006, 2014;), Mg/Ca ratio records in foraminifera (e.g. Hennissen et al., 2015) and isotope compositions in cave speleothems (e.g. Bar-Matthews et al., 2003) has led to the identification of the existence of numerous glaciations of Pleistocene and to the general acceptance of the glacial – interglacial climatic cyclicity (c.f. Mangerud et al., 2011; Paillard, 2015). Yet, due to several reasons (like the limitations of ^{14}C dating technique or simply because of the amount of evidence) our overall knowledge is more concentrated on the last glacial cycle.

Concept of geomorphological inversion

The glacial reconstructions can be grouped into three main approaches: numerical modelling based on climatic records, physical properties and the behaviour of present-day ice sheets (e.g. Patton et al., 2017); models that assess the isostatic rebound of Earth's crust (e.g. Lambeck et al., 2014, 2017); and analyses of geomorphological record (assemblages of sediments and landforms) used as indicators for the ice dynamics and thermal conditions (e.g. Clark et al., 2017). The latter are the so-called evidence-based reconstructions (c.f. Clark & Meehan, 2001).

Several evidence-based glacial reconstructions of ice sheets have been established for the Late Weichselian in the Northern Hemisphere (e.g. Kleman et al., 1997; Clark et al., 2017; Margold et al., 2018). The methodological framework of such reconstructions was formalised roughly around the

turn of millennia by the work of two independent research groups – in Sweden (Kleman & Borgström, 1996; Kleman et al., 1997; De Angelis & Kleman, 2005; Kleman et al., 2006), and in the UK (Boulton & Clark, 1990a, b; Clark, 1997, 1999; Clark & Meehan, 2001; Greenwood & Clark, 2009a,b). This has led to some confusion in terminology. In the concept of '*process of inversion*'– where the information on properties and glaciological processes of ice sheets are acquired by inverting geomorphological and geological records, Kleman and others (2006) define that the main *tool* for establishing glacial reconstructions is the recognition of *swarms*. This is a cartographical representation of coherent directional landform systems that can be traced to particular formative conditions. However, terms like *fans* (Kleman & Borgstrom, 1996) and *flow-sets* (Boulton & Clark, 1990a,b) are also commonly used to refer to landform systems representing similar glacial events as the given definition of swarms. The difference is that for construction of flow-sets (Boulton & Clark, 1990a,b; Hughes et al., 2014; Clark et al., 2017), only a single genetic group (like streamlined glacial landforms or ribbed moraine ridges) is used, whereas the entire landform assemblages are used to distinguish different fan (and swarm) types (Kleman & Borgström, 1996; Kleman & Glasser, 2007; Kleman et al., 2006). In addition, Kleman and others (2006) emphasize the capability of the frozen-bed conditions to preserve older landscapes, and express the importance of the meltwater pattern analyses to be used as a separate entity (the 'deglacial envelope'). The importance of meltwater landform analyses for establishing the ice retreat pattern reconstructions is also acknowledged by Greenwood and others (2007).

Within this thesis, the term 'flow set' is used to refer to a single, cartographical unit grouping relevant landforms representing a single glacial phase that has left a landscape imprint from which the flow patterns were observed. The members of the two landform groups of streamlined glacial landforms and ribbed moraine ridges are used in conjunction as they are regarded as a process continuum (c.f. Ely et al., 2016). The 'deglacial envelope' is analysed as a separate entity.

Present and future perspectives

The formalisation of the inversion concept (Kleman et al., 2006; Greenwood & Clark, 2009a,b) in combination with the advances of other methodologies (e.g. Patton et al., 2017;Lambeck et al., 2014, 2017) and the ever growing 'volume' of dating results (c.f. Hughes et al., 2016; Stroeven et al., 2016) have improved glacial reconstructions and thus the understanding of the past ice sheets. Furthermore, this increasing glaciological understanding of the past has improved our perception of the stability of the present-day ice sheets in Greenland and Antarctica. Yet there is a need for further

research also here. For glacial geomorphology, this would imply incorporating the latest technological achievements of remote sensing, Geographical information systems (GIS), and concepts as the ones emphasising further incorporation of meltwater processes (Greenwood et, al. 2016; Storrar & Livingstone (2017). Furthermore, it is important to establish detailed glacial reconstructions that may be used as input for future climate change predictions (c.f. Vaughan et al., 2013). Understanding the past, like how the climate forced the FIS deglaciation (Goehring et al., 2008), is a key for understanding present processes (c.f. Hein et al., 2016) and to provide convincing predictions of the near and further future (Paul, 2015).

Study area

Gausdal Vestfjell is the study area covered within this thesis. It is located in Oppland County, south-central Norway. It lays roughly in between Lillehammer (c. 50 km SE) and the Jotunheimen mountain region (c. 50 km NW) – the highest part of the Scandinavian Mountains (Fig.1). The Jotunheimen mountain region had functioned as one of the primary accumulation areas during the build-up of the FIS prior to the Last Glacial Maximum (LGM) (Mangerud et al., 2011). The area was one of the last to become deglaciated (Hughes et al., 2016; Stroeven et al., 2016) (Fig. 1C).

The study area has a rather complex topography. It can be described as an undulating upland plateau generally sloping towards the SE. Several topographic highs encounter the plateau, a W-E oriented mountain ridge in the N (highest peak Skaget 1685 m a.s.l.), the Kjølafjellet ridge in the SW, and the Synnfjell ridge in the SE. In addition, several elevated areas (1100 up to 1325 m a.s.l.) exist within the plateau area itself. The low-lying areas are commonly occupied by several water bodies that are linked by rivers (Fig. 1D). The two largest rivers – Fjelldokka and Etne river – emerge in close proximity to each other at the foothill of the northern ridge (near mount Skaget) flowing towards E and SE before continuing into deep glacial eroded valleys. The western and eastern borders of the study area are drawn along the upper slopes of the Rauddalen and Øystre Slidre valleys (in W) and the Vestre Gausdal valley (in E).

The fact that almost two thirds of the area is located within the Langsua National Park and the adjacent nature reserves (Fig. 1D) has been a limitation for conducting large-scale excavations on the identified landforms.

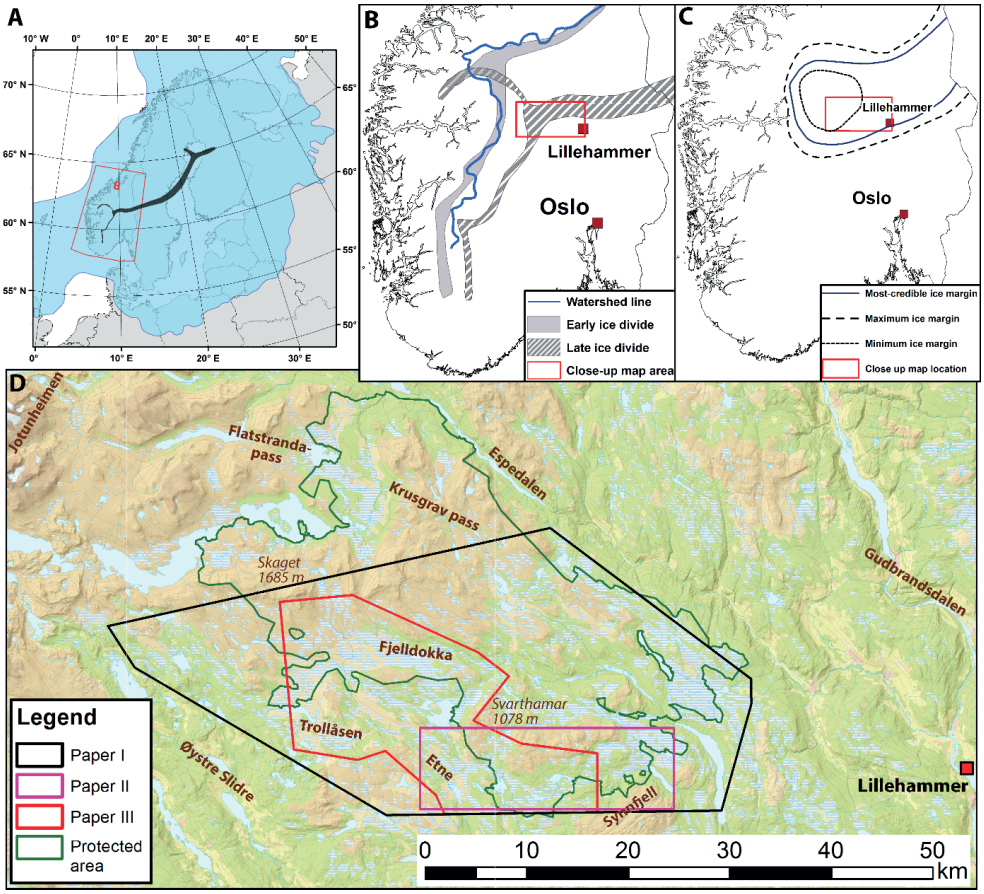

Figure 1. Overview of the study area covered in this thesis. **A.** The Fennoscandian Ice Sheet at its maximum position during the Late Weichselian (according to Svendsen et al., 2004) with ice divide in dark (according to Kleman et al., 1997). **B.** Overview map of southern Norway with watershed and ice divide locations (according to Vorren, 1977). **C.** Minimum, maximum and most-credible ice margin locations at 10 ka (according to Hughes et al. 2016). **D.** Map of Gausdal Vestfjell with outlines of areal extent covered in each paper and protected areas (Langsua National Park and several nature reserves).

Sediment cover

Sediment cover within the study area varies spatially primarily depending on the topography. Continuous cover of till deposits (in considerable thickness covering the underlying bedrock) is present on the valley floors, whereas the valley sides and hilltops either contain thin, discontinuous glacial deposits or have the bedrock exposed (Carlson & Sollid, 1979). Some sub-till sediments (glaciofluvial and glaciolacustrine deposits) of Mid-Weichselian interstadial age have been reported roughly 50 km E of the study area (Bergersen & Garnes, 1971, 1972, 1981) while no descriptions of such findings exist for the study area (**Paper I**).

Assemblages of glacifluvial deposits such as eskers, kames, outwash fans and deltas and sheet covers associated with previous meltwater basins, as well as erosional landforms (various meltwater channels and over-washed surfaces) are abundant within the study area (Carlson & Sollid, 1979, 1983; **Paper I & paper III**). In addition, Holocene deposits (Carlson & Sollid, 1979, 1983; Garnes & Bergersen, 1980) like peat and fluvial sediments are present throughout the study area.

Bedrock and the topographic sensitivity

The bedrock within the study area consists of metamorphosed sedimentary rocks of Precambrian to Ordovician age composed in series of thrust sheets (nappes) formed during the Caledonian orogeny (Heim et al., 1977). Metamorphosed arkose, greywacke sandstone, and conglomerate of Late Precambrian age as well as quartzite of Middle to Late Ordovician age (belonging to the Jotun-Valdres Nappes Complex) are present in the northern and central parts, whereas slate, sandstone and limestone of Cambrian to Middle Ordovician age (the Synnfjell Nappe) are found in southern and southeastern parts (Heim et al., 1977). The rocks are highly deformed by faulting, thrusting, and stacking in a NE-SW direction and have a high degree of schistosity. In addition, metamorphic plutonic basement rocks (metadiorite) of Precambrian age (Nickelsen, 1988; Siedlecka et al., 1987) are found in several localities forming the present-day topographic highs within the plateaus.

Several authors have pointed out that the bedrock rheology and the underlying topography had an effect on the behaviour of former ice-sheets (Glasser & Bennett, 2004; Glasser & Warren, 1990; Knight, 2011). Therefore, such rheological differences as described above can influence mechanisms behind the flow pattern evolution of previous ice sheets. These effects are mainly defined by the nature of interactions at the ice-bed interface, and are strongly controlled by bedrock type and structure as these determine the permeability and mechanical break-up of the bedrock, as well as micro-topography and larger-scale undulations of subglacial terrain. Therefore, these factors affect the spatial and temporal patterns of the subglacial thermal and hydraulic regime including the organization of subglacial meltwater and sediments altering the glacial dynamics (Knight, 2011). Such topographical control on the glacial dynamics induced by the underlying bedrock rheology have been noticed within the study area (**Paper I**).

Previous research within the study area

Earlier work on the former FIS glacial reconstructions in the Gausdal Vestfjell area is primarily associated with till deposits or glacial striations in Gudbrandsdalen (Fig. 1D) and its tributary valleys (Bergersen & Garnes, 1972,1981; Garnes & Bergersen, 1980). Bergersen and Garnes (1972) identified four glaciation phases within the Gudbransdalen area: *the initial phase* (ice streams followed the valleys), *the main phase* (little or no movement dependency on the topography), *later inland phase* (large variations in the directions of striae and till fabrics suggesting continuous shifting of flow directions) and the deglaciation phase (characterized by meltwater drainage along stagnant ice). Later, Vorren (1977), by combining this and other researches, established a unified reconstruction of the ice divide migration and the ice movement for southern Norway during the Weichselian. He distinguished four main phases of different ice movement directions, of which the two latest ones are related to the late Weichselian period. The ice divide migration from the watershed region towards the east (Fig. 1B) might have happened between Phase 2 and 3 (around 25 000 – 27 000 years BP). As suggested by Vorren (1977), Phase 3 can be correlated with the *later inland phase* (Bergersen & Garnes, 1972). This phase is assumed to indicate the maximum extent of the Weichselian ice sheet (18 000 – 20 000 yrs. B.P.) whereas Phase 4 is assigned to represent the Preboreal age (Vorren, 1977). The transition from Phase 3 to Phase 4 is thought to be gradual although with some definite halts (sub-phases) that might represent periods of stagnation / readvance during deglaciation. The changes in ice-divide position have resulted from the general decrease of ice sheet extent (Vorren, 1977). Different hypotheses have been forwarded about the evolution of this phase speculating either there has been one ice divide (Lunde, 1956) that influenced the flow, or several local ice flow centres (Bergersen & Garnes, 1972; Mangerud, 1964). Vorren (1977) states that these views do not necessarily contradict each other, suggesting that a single ice divide existed prior the multiple local flow centres.

The existence of a phase with topography-independent ice movements (*the main phase* by Bergersen & Garnes, 1972) were confirmed by Sollid and Sørbel (1994). Judging by the orientation, they point out that the uppermost streamlined landforms were formed by ice movements independent of topography, therefore, clearly underneath a thick ice sheet, prior to the deglaciation. These have later been preserved from reworking. Sollid and Sørbel (1994) use this to argue that, due to the topography, differences in the subglacial bed thermal regime have existed. This principle has been explained in detail by the theory of sticky spots (Stokes et al., 2007).

2. Materials and Methods

Geomorphology is an eclectic science with a considerable heritage and history of its own, yet, recently, it has become further integrated within other natural, computer and social sciences to provide the knowledge and data about our constantly changing Earth (Griffiths et al., 2011; Tooth & Viles, 2014). The geomorphological studies target on investigating the processes behind the formation of landforms. Thus, reconstructing past changes, is a key force for understanding present-day processes and anticipating future processes (Tooth & Viles, 2014). This, in particular applies for glacial geomorphology, as it is the basis of evidence based glacial reconstructions and the 'concept of inversion' (Kleman et al., 2006). This section provides a brief overview of existing methodology and concepts currently used in glacial geomorphology and highlights the methods used in this thesis. Furthermore, it also provides the background for the method development and testing carried out as part of this thesis.

LiDAR

Since the development of the first laser in 1960 (Maiman, 1960), the evolvement of geodetic laser scanning (GLS) technologies made it possible to determine the coordinates of billions of surface points over hundreds of kilometres in a time- and cost-efficient way (Carter et al., 2007). After the first experiments with airborne lasers around the 1970s (Link, 1969; Link & Collins, 1981), there has been a rapid advancement of airborne laser scanning (ALS), airborne laser swath mapping (ALSM) or airborne LiDAR *(Light Detection And Ranging)* technology (Wehr & Lohr, 1999; Carter et al., 2007; Nelson, 2013). LiDAR is a type of active transmitter and sensor that, similarly to radar, transmits a signal in near infrared or visible green part of the spectrum towards the ground and records the returning reflected signal (Fig.2). The time interval (delay) between transmission and reception of the reflected signal determines the distance (Baltsavias, 1999; Wehr & Lohr, 1999) between the sensor and the target. This can be a tree canopy (the first return of a single pulse) or the ground surface (last return) (Lefsky et al., 2002; Nelson, 2013).

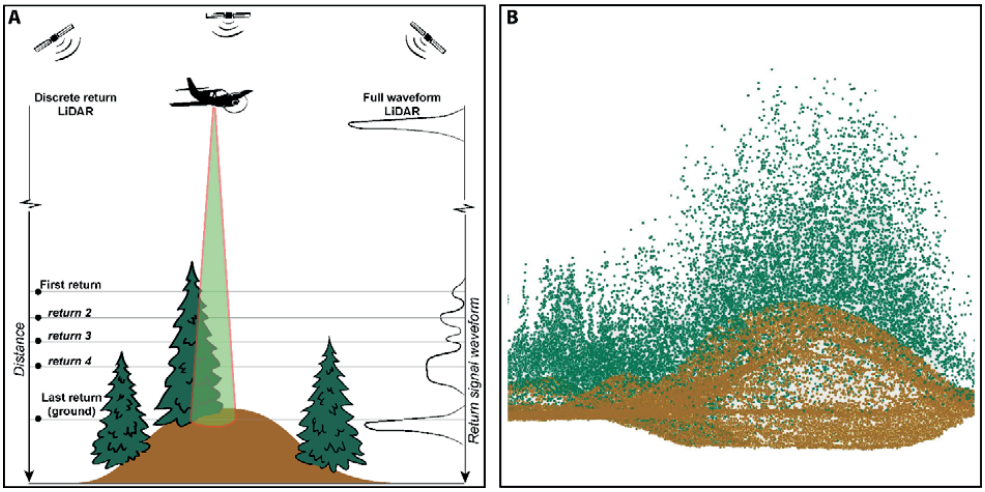

Figure 2. Principles of LiDAR. **A.** Schematic data acquisition using LiDAR scanning technique (author's contribution based upon various sources). **B.** Example of an exaggerated LiDAR point cloud in a 3D view. Brown dots represent reflected ground points (last return) and green dots represent vegetation (various returns).

The ability to record multiple returns simultaneously, measuring the ground points under vegetated areas, as well as the high resolution of the data, and the capability to detect a ground surface hidden under dense canopies are likely the reasons for the rapid adaptation of LiDAR in forestry, archaeology as well as geomorphology field (Baltsavias, 1999; Carter et al., 2007; Lefsky et al., 2002; Nelson, 2013). Although LiDAR is considered superior to aerial photogrammetry and other earlier remote sensing technologies due to the high-resolution capabilities (Baltsavias, 1999; Lefsky et al., 2002), it has technological flaws of its own. Apart from the computational power demands imposed by the large size of the raw data sets, LiDAR also has accuracy problems in complex terrains with dense vegetation or debris cover, as well as in terrains with particularly steep (near vertical) slopes (Hodgson & Bresnahan, 2004, Lefsky et al., 2002; Nelson et al., 2009).

Input data for remote sensing

The remote sensing analyses of glacial and meltwater landforms in this thesis were carried out with the LiDAR data provided by the Norwegian Mapping Authority (*Kartverket;* www.kartverket.no). The datasets have been acquired in various scanning cycles in accordance to the technical specifications of Kartverket – using the Euref-89 UTM zone 32 coordinate system and (depending on the scan date) various geoid models as the height reference. Similarly, the data point cloud density varies from 10 to 100 points/m^2 depending on the age of the dataset. Approximately half of the study area has data coverage with 100 DTM point cloud density (100 points/m^2).

The LiDAR datasets were processed using LAStools and ESRI ArcGIS (versions 10.3, 10.4.1 and 10.5) software. In ArcGIS, LAS datasets (LAS – is the standard file format for LiDAR data) were compiled. Further, these datasets were used for the data filtering operations (using the control and ground points only), for data visualizations via the 3D View window (Fig.3) and, subsequently, for Digital Elevation Model (DEM) and hill-shade image calculations. A horizontal resolution of 3 m was used for DEM and hill-shade images.

Various additional data sources (WMS services), like aerial imagery and topographic maps (provided by *Kartverket*), were used to aid the landform identification process in cases of uncertainty, e.g. to exclude man-made objects like road fragments, ditches, mounds or walls. Moreover, maps of Quaternary deposits, as well as the resource maps provided by the Geological Survey of Norway (NGU), were used in some cases to validate identified landforms, for example, whether a landform consist of sediments or is due to a bedrock feature.

Geomorphological mapping

The geomorphological mapping was performed to establish a database of identified landforms containing streamlined landforms, moraine ridges (ribbed moraine), and glacifluvial landforms and meltwater basins. Landforms were mapped either by identifying their plan form in the horizontal plane (based on their profile curvature) and drawn along the break of a slope, as suggested by Hughes and others (2010), or by identifying the crest-line of landform features (for eskers).

Often geomorphological mapping is performed by enhancing landform appearance in DEMs using the simulated solar shading (hill-shading). However this may introduce the so-called azimuth bias (Clark et al., 2001; Smith & Clark, 2005; Smith & Wise, 2007; Hughes et al., 2010), where some linear landforms are less visible when shaded from certain azimuths, whereas hill-shading of other azimuths may make some *landforms* appear where they actually do not exist in the terrain. To overcome this bias, Smith and Clark (2005) have suggested to use a pair of orthogonal hill-shading images or, ideally, to combine the hill-shading with an additional slope curvature image. Here, data visualizations in ArcGIS 3D View window (Fig.3) were preferred for landform mapping because of the simplicity and because it allowed a continuous interaction with the LAS dataset by adjusting the height exaggeration or the contour intervals used in the 3D image. The LAS Dataset visualization in the 3D View window (pop-up window in ArcGIS) allowed a better, detailed outcome for the smallest landforms (Table 1 in **Paper I**) that would otherwise be left out. Since the direct digitizing from oblique views onto a 2D or 3D GIS layer is currently not widely available (Smith & Clark, 2005) the actual mapping of landforms was carried out in the main software window (‘data view’ layout).

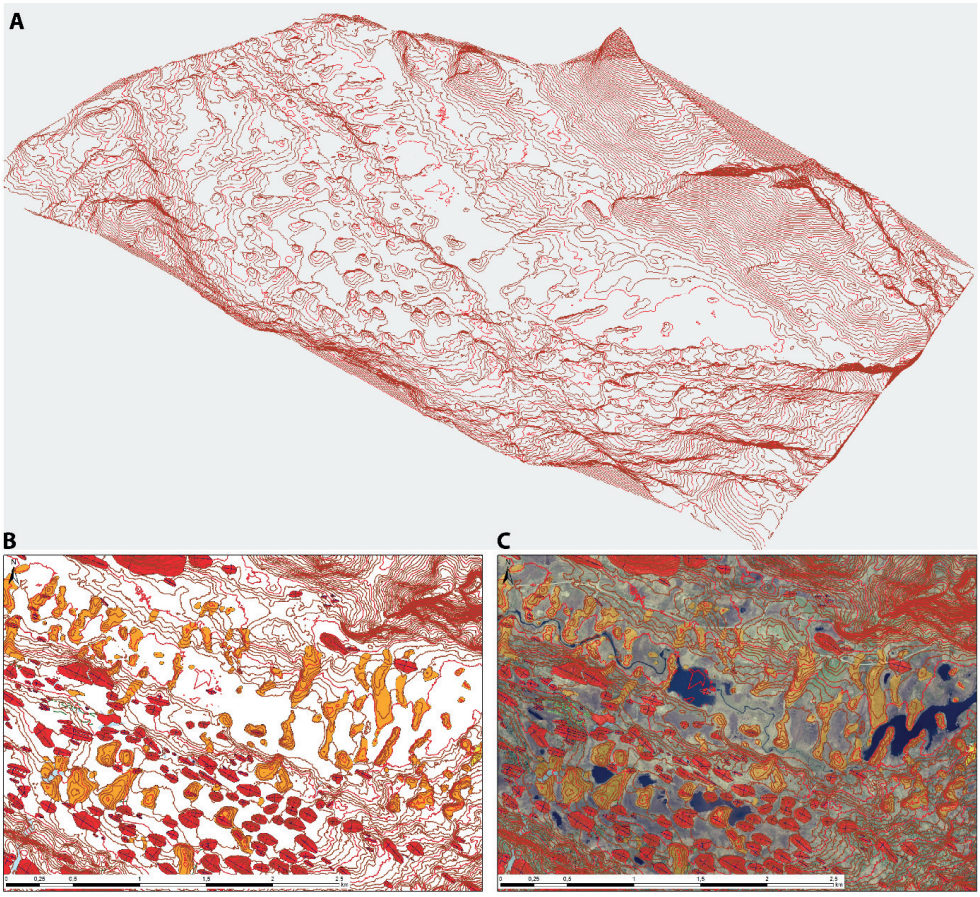

Figure 3. Ground surface representation using LAS Dataset tools functionally (ArcGIS). **A.** Terrain visualisation in 3D view. **B.** 2D (plane) view with mapped landforms. **C.** Plane view with aerial image in background.

While delineating the break-of-slope outlines of individual landforms, the morphometric parameters (width (W) and length (L)) of streamlined landforms and ribbed moraine ridges were extracted manually. Although an automated extraction of landform dimensions was considered following the methodology proposed by Napieralski and Nalepa (2010), a decision in favour of manual extractions was made due to the frequent occurrence of complex landform configurations. The relative height (H) of landforms was extracted following the methodology proposed by Spagnolo and others (2012). These were then checked manually for errors and to identify possible overlapping landforms.

Further, primarily interpretation accuracy of streamlined landforms (high, medium, low or non-reliable at all) was added to the dataset to be later re-assessed after the field reconnaissance. The assessment of interpretation accuracy (**Paper I**) was determined by using the following

characteristics: (a) object size; (b) object shape and configuration; (c) structural orientation of the underlying bedrock within the area, (d) object overall location and orientation in the terrain (hilltop, slope, or valley floor), (e) object relations to nearby objects, (f) possible other types of interpretation (if there is a different explanation of genesis, the reliability is decreased) and (g) other aspects like sedimentary or bedrock feature. I.e. distinctively shaped drumlins or small flutes overlying other landforms are regarded (in terms of accuracy) as more trustable than large-scale drumlins (crag-and tails or rock drumlins), oddly shaped roches moutonnées located on hilltops and glacial lineations forming successive chains at valley sides, which can also be interpreted as kames.

Fieldwork

Fieldwork was carried out over the course of several summers (2014, 2015 and 2018) with the main *session* conducted in the summer of 2015. The work has primarily focused on ground truthing of ambivalent mapped landforms. Along with the ground truthing, glacial striations were documented at ten localities, and sediment outcrops were investigated for the internal structure and sedimentary composition (ribbed moraine ridges - eight localities, streamlined landforms - three localities). Only two ribbed moraine ridges and one streamlined landform were further sectioned and visualized in **Paper I** to illustrate the sedimentary composition. Sedimentary composition was described using the lithofacies classification modified from Eyles and others (1983). In some outcrops, the clast fabric measurements were carried out to document ice-bed stress patterns. Further, from these the ice flow directions during the landform formation was deduced. The dip slope and dip direction were measured for 25 matrix-supported clasts ranging from 1 to 10 cm with a/b ratio 1.5 (Larsen & Piotrowski, 2003). The fabric measurements results were presented in **Paper I** using points and two-sigma Kamb contours on an equal area, lower-hemisphere Schmidt net plotted in StereoNet© for Windows.

(Semi-) automated mapping methods

Spatial distribution pattern analysis of subglacial landforms is a well-known tool for establishing glacial reconstructions of previous ice sheets (Kleman et al., 1997; Boulton & Hagdorn, 2006; Hubbard et al., 2009; Ross et al., 2009; Greenwood & Clark, 2009a, b; Clark et al., 2012; Hughes et al., 2014; also **Paper I)**. Considering the large areal extents of the study areas and the fact that manual landform mapping is time consuming and often subjective (Smith, 2011; Clark et al., 2001; Smith &

Clark, 2005; Hughes et al., 2010), there is a need for alternative methods. Consequently, there have been several recent attempts on developing a reliable, objective and efficient (semi-) automated mapping (SAM) methods for subglacial streamlined landforms (d'Oleire-Oltmanns et al., 2013; Hillier et al., 2015; Jorge & Brennand, 2017; Smith et al., 2009; Saha et al., 2011; Yu et al., 2015; Wang et al., 2017). Still issues with the proposed methods exist. First, as explained in **Paper II**, these methods often are applied on relatively simple areas that predominantly contain well pronounced streamlined glacial landforms (the drumlin fields of lowlands) and are lacking the 'noise' of other glacial landforms (ribbed moraine ridges, eskers), inherited bedrock topography or man-made artefacts (i.e. settings far from the complexity of Scandinavian Mountains). Second, the proposed methods may require rather complex raster pre-processing that masks out objects introducing noise (Hillier et al., 2015; Jorge & Brennand, 2017). Third, the proposed techniques often require a pre-existing dataset of manually mapped landforms as input (Saha et al., 2011).

Together, these issues form a methodological challenge that has to be overcome before SAM methods can be applied in more complex, real-world terrain with minimal supervision. In **Paper II**, an approach based on the grayscale thinning (Biagioni and Eriksson, 2012) of slope rasters is presented for extracting the directional trends from a complex terrains and is validated against manual reconstructions of glacial ice flow directions (**Paper I**). Extracting the directional trends from a terrain in this way provides a quantitative assessment that should be preferred over potentially biased visual observations (eye-bailing; Piégay, 2017).

Reference gradient surface use for meltwater landform correlations

The problems of correlating meltwater landforms over distances along the valley sides exist in areas with complex topography (Clark et al., 2012). Since the exact surface configuration of the previous ice sheet is unknown, the use of simple correlations along the same elevation may lead to erroneous and misleading interpretations (**Paper III**). Instead, landforms should be correlated by referring to a gradient of the previous ice surface rather than by using horizontal correlations along the mountain and valley sides. In **Paper III**, the ice surface gradient of 1% steepness representing the *Krusgrav phase* of Garnes and Bergersen (1980) for the nearby Gudbrandsdalen area (Fig. 1) was used as the reference.

The reference gradient surface (**Paper III**) was implemented by, first, geo-locating the exact profile line of the *Krusgrav phase* used in figures in Garnes and Bergersen (1980). Then, the elevation values (Z) were assigned for start- and end-points of a profile line of 1% gradient set to the Flatstranda pass,

where the ice surface during the Krusgrav phase was at about 1300 m a.s.l., by using simple calculations. The profile line and points (containing Z values) were then copied parallel roughly 25 km southwards so that the surface gradient covered the area of interest. Then, in ArcGIS, the gradient surface was generated using the **'**Natural Neighbours' **i**nterpolation and a 5x5 m resolution. Further, the generated reference gradient surface was used for analysing the spatial and temporal relations of meltwater landforms (**Paper III**) in both ArcGIS and ArcScene ESRI software. ArcScene software was used to visualize the possible ice marginal positions of the Krusgrav phase and other stages by utilizing the 'Base heights' option capabilities (in Layer properties), where the elevation was set to be *'Floating on a custom surface'*. Here the DEM was used for visualizing the terrain, whereas the gradient surface was used for the *Virtual Ice surface.* Further, the *Virtual Ice surface* was slid along the vertical (z) axis, visualising different ice surface positions above and below the Krusgrav phase. This enabled to identify several potentially meaningful, possible ice marginal positions – stages (in m) above or below the Krusgrav phase surface described in **Paper III**.

3. Extended summary of papers

Authors' contributions are stated at the end of each paper summary, and in the acknowledgements section at the end of each of the three papers in the appendix.

Paper I

Reconstructing the flow pattern evolution in inner region of the Fennoscandian Ice Sheet by glacial landforms from Gausdal Vestfjell area, south-central Norway. Putniņš & Henriksen, 2017. Quaternary Science Reviews, 163, 56-71.

This study presents the flow pattern evolution reconstructions for an inner region of the former Fennoscandian Ice Sheet, established from manually mapped glacial landforms in Gausdal Vestfjell area (south-central Norway). More than 17 000 landform features, mapped from detailed LiDAR data sets, have been used as input for the glacial reconstructions.

The analysis of spatial distribution patterns of identified landforms (mainly streamlined landforms and ribbed moraine ridges) have enabled to establish a reconstruction of the glacial events during the Late Weichselian glaciation. The reconstructed patterns reveal that the ice flow has evolved from a topography independent ice flow (Phase I) to a relatively long-existing regional (Phase II) before transforming into a strongly channelized, topography driven ice flow (Phase III). Further, several sub-stages of Phase III are distinguished. These sub-stages are characterized by flow sets becoming increasingly confined into the valleys separated by likely colder, less active ice prior to a complete deglaciation by down-melting of ice. The ice divide migration and the ice surface lowering seem to be the main reasons that caused changes in the ice flow pattern.

The limited number of sediment outcrops investigated within ribbed moraine ridges suggest that the sediments (well-sorted sediments) have a different primary origin (e.g. fluvial and/or lacustrine) prior to the deformation, likely by an overriding glacier. The observed intrusions interpreted as clastic dykes, together with the presence of flame structures, suggest depositional conditions with high water saturation and overloading.

Morphological evidences from the study area suggest that the formation of a ribbed moraine can occur both when the ice flow slows down and when it speeds up, forming respectively broad fields and elongated belts of ribbed moraines.

My contribution to this work included input data gathering and processing prior the mapping of landforms, conducting the morphological mapping and GIS analyses of landforms, and writing and revising the manuscript. Mona Henriksen participated in the conceptual study design, ground truthing (fieldwork), data interpretation and discussion, as well as revision of the manuscript. In addition, Jon Landvik has contributed to the study design and data interpretation (discussion) at an early stage.

Paper II

Extracting and visualising glacial ice flow directions from Digital Elevation Models using Grayscale Thinning and directional trend analyses. Putniņš & Tveite. Manuscript. Prepared for submitted to Computers and Geosciences.

In this study the capabilities of extracting the directional trends from terrains by applying the grayscale thinning skeletonisation is explored focusing on the potential applications of reconstructing the flow directions of previous ice sheets. Since the manual mapping of landforms used for flow pattern reconstructions is a time consuming and subjective process, developing reliable and effective (time saving) methods for data extraction, like (semi-)automated mapping (SAM) techniques may optimise the research within geomorphology and Quaternary geology field. Although many of the proposed (semi-)automated object-based methods are regarded as objective and fast, implementing them is a rather complex process and the existing SAMs still have their flaws and unresolved issues. Therefore, there is a need for less-complex alternatives that can extract data on glacial ice flow directions.

The paper presents a method for the extraction of directional trends from terrains based on grayscale-thinning of rasters. It shows the preliminary results of the grayscale thinning application on slope rasters and directional trend extractions from both artificial (synthetically generated) and real terrain surfaces. Grayscale thinning is preferred to traditional binary thinning due to its flexibility. The grayscale thinning approach respects variation in steepness by using several intervals within the thresholding range simultaneously.

The tests carried out on the artificial surfaces reveal that a landform feature has to be at least six (raster) cells wide to be properly detected by the method. The application on real-world terrain data illustrates the robustness of the approach. Various thresholding methods applied for skeletonisation (5 equal intervals, quantile distribution, 10 equal intervals) produce rather similar results, suggesting that the lower and upper boundaries of the thresholding range (here 3 and 33 degrees) have a strong control on the outcome. The demonstrated robustness suggests that the method is a promising tool for extracting directional trends from terrains and thus for reconstructing glacial flow patterns. However, further effort on minimizing the effects of noise (like over-representation of raster angles) and increasing the signal to noise ratio is needed, as well as additional testing on other terrain types.

I have contributed to this work by selecting and creating the DEM surfaces to be analysed and compared with the reference data (manually mapped landforms), by carrying out the data processing and analysing, and by writing and revising the manuscript. Håvard Tveite was responsible for implementing and is the author of both QGIS plugins (the 'Thin grayscale image to skeleton' and 'Line Direction Histogram') used in this paper. Both authors were responsible for the conceptual study design, data interpretation, discussion and revision of manuscript.

Paper III

Final stages of deglaciation reconstructed from meltwater landforms in the Upper Etne valley, south-central Norway. Putniņš & Henriksen. Manuscript. Prepared for submission to Boreas.

The study focuses on analysing the geomorphological and geological record of meltwater landforms in an attempt to reconstruct the sequence of final deglaciation events of the Fennoscandian Ice Sheet in the upper part of the Etne river valley and its adjacent areas. The study analyses the association of the channelized flow phase (phase 3) and its sub-stages (reported in **Paper I**). It assesses the findings in the context of vertical down-wasting of ice.

The analyses of spatial and temporal distribution patterns for marginal meltwater landforms are often complicated due to the complexity of terrain and lack of information on the past ice surface. This is the general limitation that inhibits the possibilities of establishing accurate correlations of meltwater landforms over some distances along the valley sides. To increase the reliability of findings, a reference surface gradient has been introduced and used for correlations.

The use of reference surface gradient has allowed us to delineate several significant deglacial stages (expressed as m above and below the Krusgrav phase). The findings made it possible to establish detailed reconstructions for the upper Etne river valley and adjacent areas. These give an insight in the distribution of different thermal conditions and the evolution of the retreat pattern within the inner region of the Fennoscandian Ice sheet.

My contribution to this work was the conceptual study design, input processing prior to the landform mapping, conducting the morphological mapping and ground truthing (fieldwork), implementation of the reference surface gradient and GIS analyses of landforms, writing and revising the manuscript. Mona Henriksen participated in the conceptual study design, ground truthing (fieldwork), data interpretation (discussion) and revision of the manuscript.

4. Results and discussion

LiDAR implications on mapping of landforms

The recent increase of accessibility and coverage of the high resolution LiDAR data sets (and DEMs) has positively contributed to the studies of glacial geomorphology (e.g. Dowling et al., 2015; Dowling & Möller, 2016; Sookhan et al., 2018; and **Paper I**). Firstly, the overall general effect of the increased spatial resolution is a higher number of mapped small-sized landforms of both glacigenic and glacifluvial types, that were likely left out earlier from the analysis. This changes the overall distribution of landform metrics, shifting the mode and median of landform dimension data towards the lower-end (Table 1 in **Paper I**; Figs 4, 5). Secondly, small-sized landforms may represent relatively short lived events of glacial dynamics (cf. Fig. 3 in Fredin et al., 2013). This is particularly the case when such landforms are found overlapping other larger landforms (Fig. 4). The effects of cell size of DEMs (coarse resolution) on the landform appearance are well demonstrated by Napieralski and Nalepa (2010).

The findings of mapped landforms presented in **Paper I** show a morphometric large variety of streamlined subglacial landforms and ribbed moraine (Fig. 5). The established map on the relative height of mapped landforms (Supplement 3 in **Paper I**) reveals relations between bedrock presence and the height of streamlined landforms. Mapped streamlined landforms with noticeable bedrock presence have distinctly the largest relative heights, which is in accordance with the findings of Hillier and others (2013). The ribbed moraine ridges with the largest relative heights are on the other hand found within the central parts of valley floors. Furthermore, the most elongated streamlined landforms are predominantly found on the larger, undulating plateau-like uplands or along some valley sides, where deposits of continuous cover and great thickness (varying from a half to a few meters) are present (Carlson & Sollid, 1979; 1983). This is in accordance with the observations from topographically different settings of the FIS in Närke drumlin field in south–central Sweden (Dowling et al., 2015; Möller & Dowling, 2016,2018), suggesting that the same processes are involved in the subglacial streamlined landform formation.

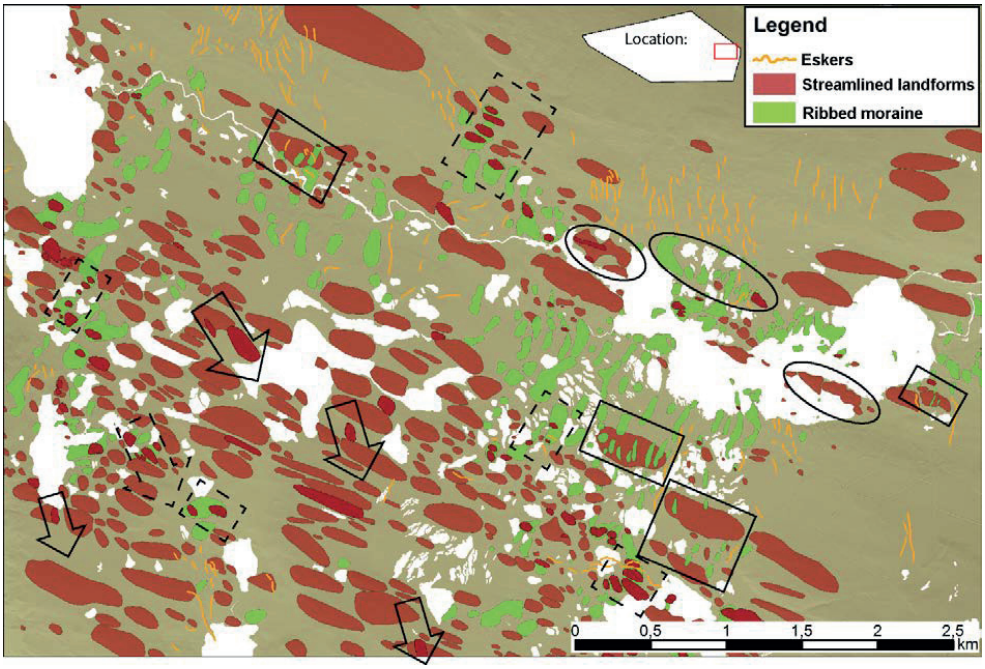

Figure 4. Mapped landforms used for establishing flow pattern reconstructions. Example from the eastern part of the study area (**Paper I**). In ellipses – streamlined landforms being reworked into ribbed moraine. In boxes – ribbed moraine ridges on top of streamlined landforms. In dashed boxes – streamlined landforms on top of ribbed moraine ridges. Inside arrows - streamlined landforms on top of other (older) streamlined landforms. Note eskers of both systems (parallel and transverse to the ice flow) overlying other landforms.

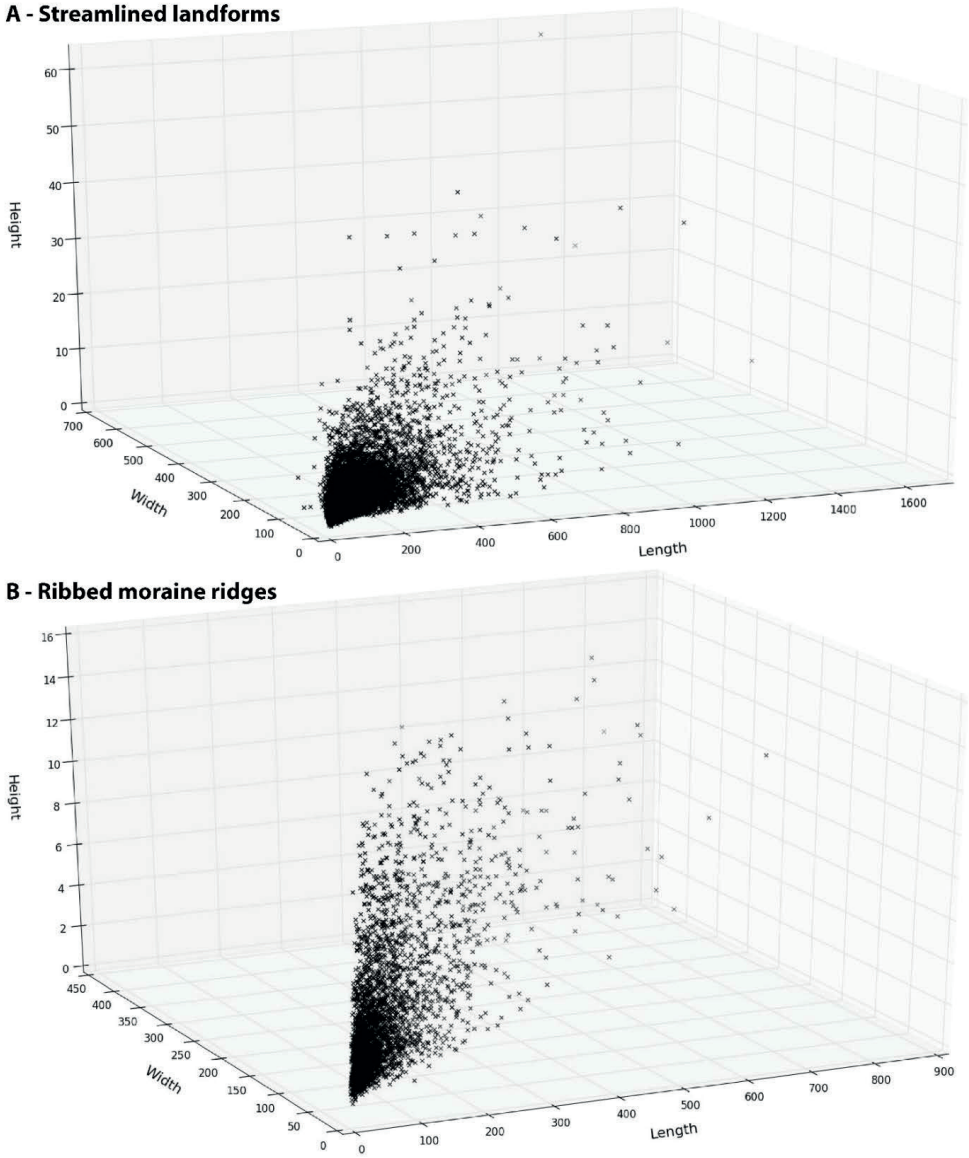

Figure 5. Dimensions of mapped glacigenic landforms (in meters). **A.** Streamlined glacial landforms. **B.** Ribbed moraine ridges. For more details on brief statistics see **Paper I**, Supplement 1.

Evaluation of the proposed methods

Extracting and visualising glacial ice flow directions by using the Grayscale Thinning and directional trend analyses

The preliminary tests of the application of grayscale thinning (of slope rasters) for the terrain analyses with the aim of extracting directional trends that could be used for reconstructing the previous ice flow directions (**Paper II**) have shown rather promising results. The findings presented in **Paper II** suggest that the method is rather robust and that the minimum and maximum values of the threshold range are of higher importance to the outcome than the selection of threshold intervals itself. Yet, **Paper II** also illustrates the issues to overcome (such as reducing the raster noise effects) for the method to achieve its full potential.

Two major issues exist that should be elaborated further – **(a)** can the grayscale thinning (skeletonisation) outcome be regarded as a credible representation of the real-world terrain (landforms); and **(b)** how is the proposed method better for streamlined subglacial landform detection than the manual mapping or other existing SAM techniques?

Whereas the manual mapping of landforms (as well as most of the other proposed SAM techniques) would usually represent the concave breaks of slope (landform outlines) or ridge crests, the grayscale thinning processing outcome will contain lines that roughly represent the mid-section part of slope, with often additional (perpendicular) lines breaching over the ridge crests (particularly common for narrower landforms) that is rather regarded as noise (**Paper II**). When extracting the directional trends from these datasets, these short line segments are contributing to reducing the overall signal strength, whereas the orientation of mean directional trend (and thus, the detected previous ice flow direction) is more dependent on longer lines (built-in function for weighting line length in the histogram plugin).

Regarding the latter, the proposed method, as well as other existing SAM techniques for streamlined subglacial landforms (Table 1), are time-efficient and a quantitative assessment that should be preferred over potentially biased 'eye-bailing' visual observations or manual mapping (Tooth & Viles, 2014; Piégay, 2017). Yet, the proposed method at its present (preliminary) state cannot be applied for straight-forward interpretations, and an expert knowledge and inspection (or as, suggested in **Paper II** – a repeated processing with higher input resolution) should be involved in the interpretation to explain the variations and outliers in extracted directional trends.

Table 1. Overview of the existing SAM methods proposed for streamlined subglacial landform extractions.

Method		Test area		
Name	Authors	Location	Approx. size (km)	Elevation (m. a.s.l)
Geomorphons mapping adaption for drumlins	Sărășan et al., 2018	Eberfinger drumlin field, German Alps	5 x 6	597 – 705
Localized contour tree approach	Wang et al., 2017	New York drumlin field, USA	35 x 60	74 – 212
Normalized closed contour method	Jorge and Brennad, 2017	Puget Lowland, Washington	10 x 14	*No data*
Landform elements mask method	–"–	–"–	–"–	–"–
Curvature Based Relief Separation (CBRS)	Yu et al., 2015	Wadena drumlin field, Minnesota, USA	30 x 50	372 – 466
Multiresolution segmentation for delimiting drumlins	Esnak et al., 2014	central Scotland	8 x 13	0 – 189
An Object-Based Workflow to Extract Landforms at Multiple Scales From Two Distinct Data Types	d'Oleire-Oltmanns et al., 2013	Eberfinger drumlin field, German Alps	5.2 x 7.8	597 – 705
semi-automated contour selection (SACS) *(as named by Yu et al. (2015))*	MacLachlan and Eyles, 2013	Peterborough drumlin field in central Ontario, Canada	20 x 35	9 – 396
An object-oriented approach to automated landform mapping of drumlins	Saha et al., 2011	Chautauqua drumlin field, NW Pennsylvania & upstate New York	11 x 12	*No data*
The Cookie Cutter: A method for obtaining a quantitative 3D description of 595 glacial bedforms *	Smith et al., 2009	Central Scotland	*No data*	*No data*
'Shadow mapping' *(as named by Yu et al. (2015))*	Pelletier, 2008	Drumlin fields in northern central New York State and eastern Wisconsin	*No data*	*No data*
Residual relief separation	Hiller and Smith, 2008	Lough Gara, Ireland,	20 x 30	50 – 250
Methods for the visualization of digital elevation models for landform mapping*	Smith and Clark, 2005	–"–	–"–	–"–
Thin grayscale thinning of rasters	Putniņš and Tveite (**Paper II**)	Gausdal Vestfjell, South central Norway	8 x 25	780 – 1324

* - Papers by Smith and Clark (2005) and Smith and others (2009) do not cover the landform extraction directly, yet they are important in the general context of SAM methods and techniques used within glacial geomorphology.

A conceptual difference between the proposed method in **Paper II** and other SAM techniques (Table 1) is the use of simple slope rasters (without any additional noise-filtering operations applied) rather than other, more complex datasets as the input. In addition, the case-study area in Gausdal Vestfjell (Fig. 1D) has one of the highest difference in elevation (Table 1) and can therefore be regarded as being more complex than other studies. This, as well as the findings reported in **Paper II**, allow to suggest that the application of grayscale thinning may produce reasonable results in less complex terrains. Another conceptual difference exist between this and other existing SAM methods. The grayscale thinning (skeletonisation) process generates a line dataset as an output whereas most of the other existing SAM methods produce polygonal datasets.

To provide a conclusive answer if the proposed method is better than the other SAM methods, a comparison of results of grayscale thinning should be compared to datasets gathered by and

analysed by another (or several) existing SAM methods (Table 1). The fact that the terrain is taken as a spatial continuum so that the proposed method cannot provide straight-forward information on landform metrics may be considered as a drawback by many glacial geomorphologists. Yet, the presented findings (**Paper II**) point out the potential of the method application for regional studies (preferably on rasters with coarser resolution), where the extraction (and visualisation) of glacial ice flow directions is the primary goal; and the selection of areas with the directional trend outliers to be inspected further in detail, the secondary goal. Furthermore, several of the other existing methods propose a noise reduction by filtering prior to landform extraction, which often includes manually set azimuthal/directional information of the mean direction of previous ice flow (Eisank et al., 2014; Hillier & Smith, 2012; Hillier et al., 2015; Jorge & Brennand, 2017). Within this context the automated extraction of directional trends could be used as a proxy for such filtering operations. Using computationally extracted values for adjusting the filtering settings may reduce the bias potentially introduced by manual *'fine-tuning'*. Finally, the simplicity and robustness of the proposed method suggests that it may have a further potential for applications within other branches of geomorphology, where extracting the directional trends are of high importance (e.g. dunes, structural geology) for analysing the forcing mechanisms behind land surface formation processes.

To demonstrate the grayscale thinning (**Paper II**) application for extracting the directional trends from a different (previously glaciated) terrains, an example is given from the Múlajökull glacial foreland in Iceland (Figs 6, 7). Figures 6 and 7 illustrate the method's capability of extracting the directional trends from the terrain, whereas the interpretation of extracted trends (drumlins, end moraines or *the noise*), as well as the choice of tile size and configuration is left to the user (as emphasised in **Paper II**). Yet, applicability of the proposed method on regional scale, awaits testing on datasets with larger aerial extents.

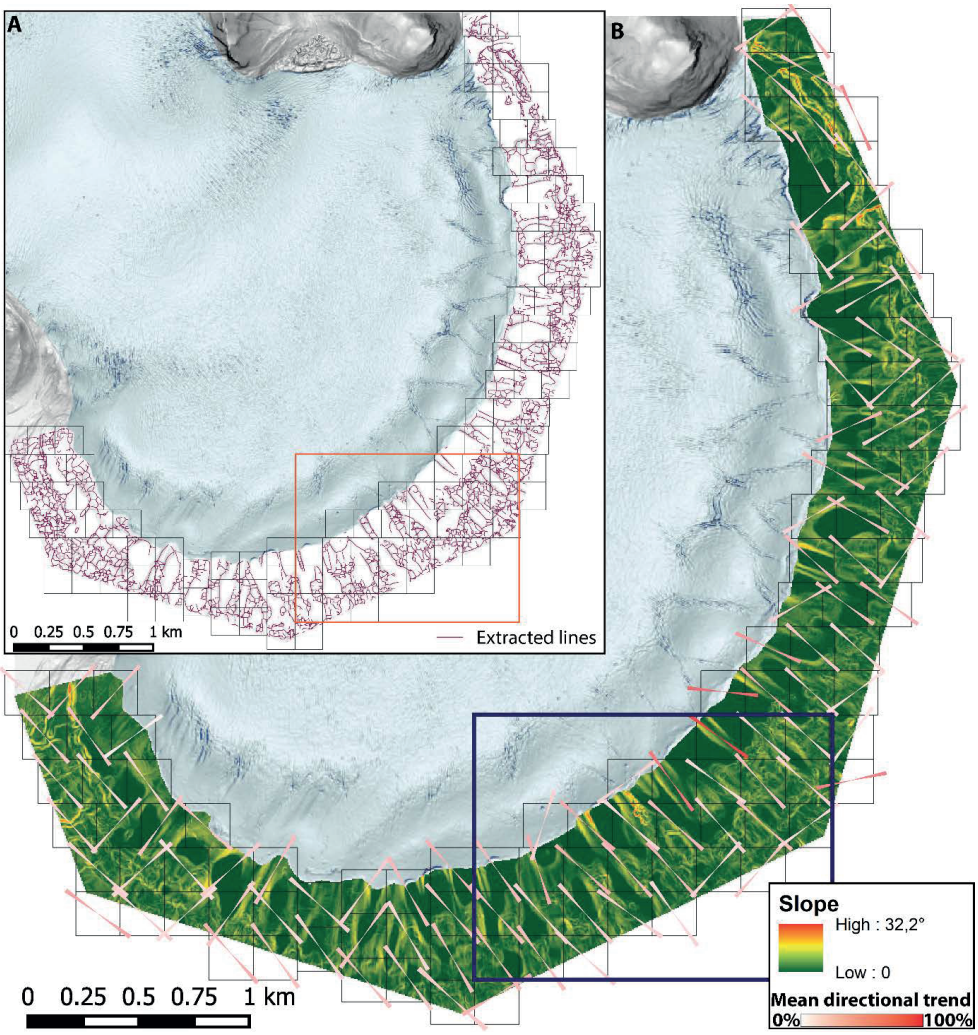

Figure 6. Grayscale thinning application on slope raster (5m resolution) from the Múlajökull glacial foreland, Iceland generated from 2008 LiDAR DEM (downloaded from National Land Survey of Iceland web service). For detailed geomorphological site description please see Benediktsson and others (2016). Boxes in both panels indicate the close-up area shown in Fig.7. **A.** Skeletonisation (Slope range 3 to 33°, 5 equal intervals) outcome dataset after the 'raster to polyline' transformation (in ArcGIS, with 'simplify lines' option) and the 'snake' smoothing (GRASS) applied. See **Paper II** for detailed processing work-flow description. Black squares represent tiles (200x200m) used for directional trend extraction. **B.** Extracted directional trends using tiles (black squares), with slope raster as background. Trends extracted using the same settings as described in **Paper II.**

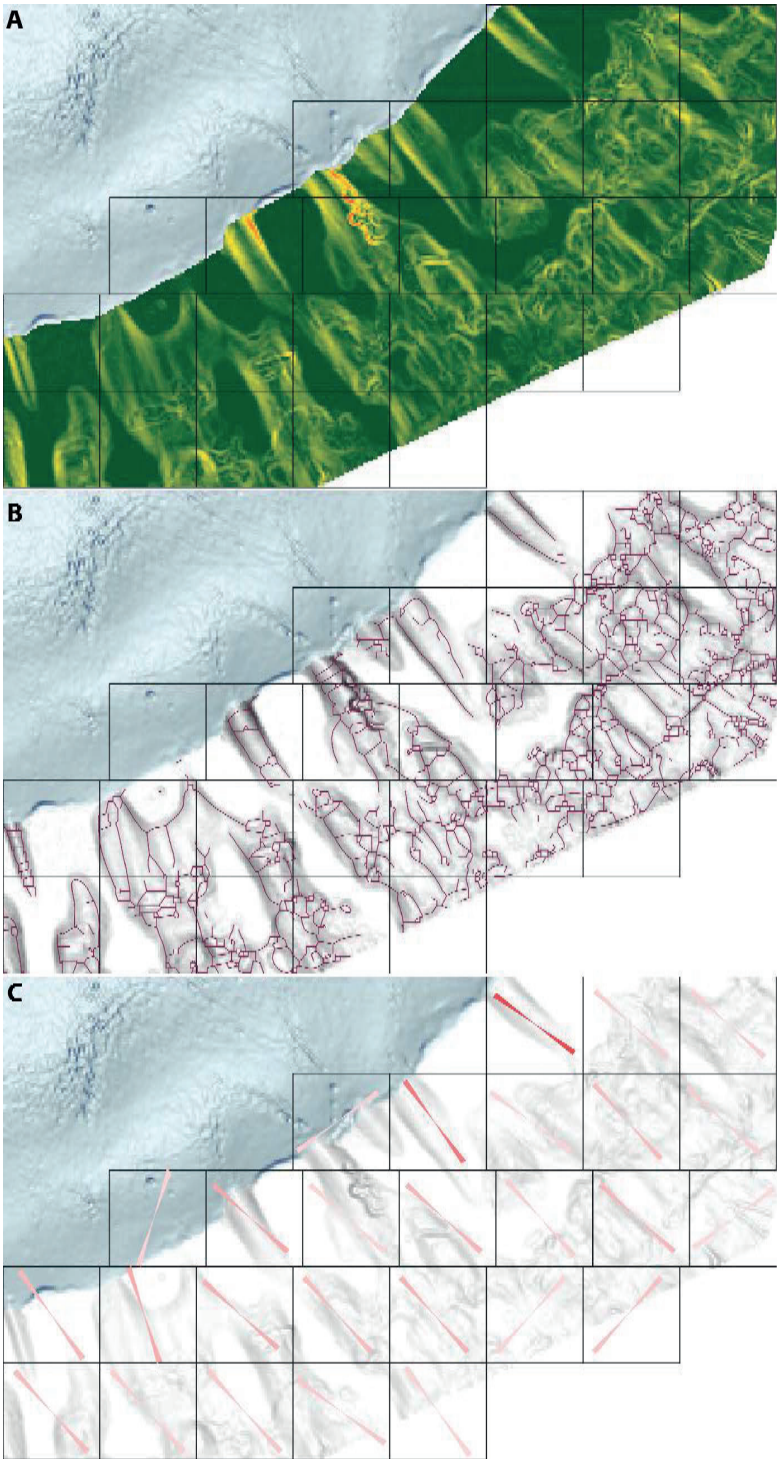

Figure 7. close-up area from Fig. 6. **A.** Slope raster. **B.** Line dataset with slope (in grayscale) as background. **C.** Extracted mean directional trends.

Application and use of the reference gradient surface for analysing the meltwater features and deglaciation pattern

The simple, static reconstruction of vertical thinning of ice (Garnes & Bergersen, 1980) using available GIS tools (**Paper III**) has improved the correlations of meltwater landforms over distances and interpretation of the deglaciation pattern for the Gausdal Vestfjell area with more details. The need for caution when establishing the retreat patterns have been emphasised before (Clark et al., 2012). **Paper III** has also pointed out some main issues that exist for this method – **(a)** the choice of gradient to be used as the reference surface; **(b)** the accuracy of correlations in areas oriented oblique to the reference surface gradient; and **(c)** the possible influx of ice from the west. Within the given context, questioning the gradient (1%) accuracy used in **Paper III** implies questioning the validity of the Krusgrav phase (Garnes & Bergersen, 1980). Although the proposed reconstructions of Garnes and Bergersen (1980) are generally accepted (**Paper I**), Garnes and Bergersen (1980) themselves point out that the gradient of an earlier phase (prior the Nunatak phase) might have been less than 1%. In addition, the later stages are recognized as more-topography dependent suggesting even larger variations in the ice surface gradient, from <1% in inner areas to 2-4% at the distal parts of the ice sheet. Combined with the 'static' nature of the approach, this implies that the accuracy of such assumptions should be primarily met with an awareness on these issues. Yet, the findings presented in **Paper III** show a reasonable match between the reference surface and the lateral meltwater channels (as well as the other meltwater features like kames), thus implying that the 1% gradient is accurate for at least some stages of deglaciation.

Reconstructed ice flow, retreat patterns and dynamics

Following the work of Garnes and Bergersen (1980), the deglaciation of FIS by down wasting of ice is confirmed by numerous studies (Sollid & Sørbel, 1994; Goehring et al., 2008; Mangerud et al., 2011; Hughes et al., 2016; also **Paper I**). However, when establishing the flow pattern reconstructions and interpreting the sequence of deglacial events the main focus often has been on glacigenic landform types (and landform assemblages) and the ice marginal positions (as in Clark *et al.* 2012; also **Paper I**), with limited attention for meltwater landforms (Greenwood *et al.* 2007; Storrar & Livingstone, 2017). With a warming climate and the potential of using the past conditions to predict the future, the influence of meltwater drainage on the dynamics of ice sheets is acknowledged (Greenwood *et al.,* 2016). Therefore the meltwater landforms are regaining attention as valuable records on the hydrology and dynamics of past ice sheets.

In this context, and as the meltwater features form a significant role in the reconstructions by Garnes and Bergersen (1980), further analyses of the glacial reconstructions presented in **Paper I** can provide detailed information on the final deglaciation stages of the FIS in Gausdal Vestfjell. In Figure 8, the ice flow patterns established in **Paper I** are combined with several significant deglaciation stages (above and below the Krusgrav phase) depicted by using the reference surface gradient (**Paper III)**.

This, in combination with the ice thickness estimations (Fig. 11 in **Paper III**) allow us to distinguish the areas that were the first to become under stagnant and dead ice conditions (at higher elevations) while active ice flow continued in valleys (as acknowledged by Garnes & Bergersen, 1980; Sollid & Sørbel, 1994). Figure 8 also indicates the areas that could still be affected by influx of ice from the west (marked as the same colour code for flow 'Phase II') with the possible down-valley extent of the last ice flows, as well as the disintegration of ice into smaller (dead) ice remnants. Furthermore, this indicates that in some parts (mainly in west) of the study area, the overall sequence of the sub-stages of Phase III presented in **Paper I** should be adjusted (as such possibility has been acknowledged in **Paper I**), although the relative sequence still remains rather accurate. The established deglacial reconstructions (Fig. 8) indicate a transitional mode of the ice retreat from east to west, where the areas in east (Fjelldokka) become deglaciated first while an active ice flow still remained in west (in Etne and Østre Slidre valleys). This westward retreat pattern of ice is in line with the presented general reconstructions of the last stages of the FIS that the last remaining glaciers were probably located on the floors of deep valleys near the former ice divide (Hughes et al., 2016).

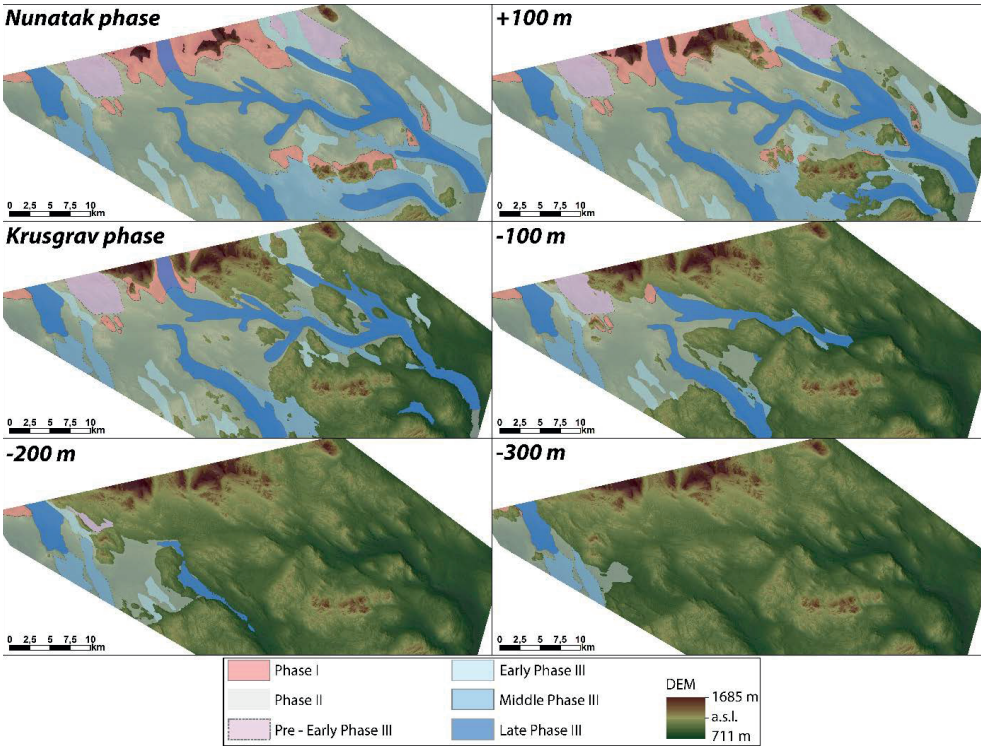

Figure 8. Established ice flow phases (**Paper I**) overlaid on various representative deglacial stages identified in **Paper III**. For details on reconstructed flow phases see **Paper I**, Fig.7 and Supplement 2.

The extensive presence of soft-sediment bedforms (**Paper I**, Supplement 2) points to widespread warm-based conditions during the last glaciation, at some periods. This does not exclude stages of cold-based ice as the warm-based conditions may have a large landscape imprint (cf. Landvik et al., 2014). The spatial relations between the streamlined landforms and ribbed moraine observed in the study area support the suggestion that these glacial landforms represent a continuum of landform formation process along the ice-bed interface (e.g. Aario, 1977; Rose, 1987; Everest et al., 2005; Dunlop et al., 2008; Stokes et al., 2013; Ely et al., 2016), and thus a bedform assemblage (Stokes & Clark, 1999, 2001; Clark & Stokes, 2003; Stokes et al, 2008). However, Möller and Dowling (2018) argue it to only be a morphological continuum (shape and size distribution) and use the subglacial bedform examples from Sweden to illustrate that different, unrelated processes can lead to landforms with very similar morphology, i.e. the equifinality.

The findings presented in **Paper I** that the ribbed moraine are found in various topographical settings (plateaus, valley sides, floors of valleys dipping the same and opposite to the ice-flow directions), as well as the evidence that landform formation occurred both during the slow-down and speed-up of

ice, correspond well with the concept of equifinality. Various re-worked streamlined landforms and ribbed moraine ridges on top of streamlined landforms (slow-down ice flow) and ribbed moraine ridges overlaid by streamlined landforms, both belonging to the same phase (a speed-up) can be taken as evidence. Therefore, the 'ribbed moraine' should be regarded as a geomorphic term used for a polygenetic landform group (identifying transverse-to-ice-flow ridges). Further, analysing the reconstructed flow patterns, the ribbed moraine formation seems to have occurred prior to the latest stages of phase II (by deceleration) and of phase III (by acceleration). As discussed above, if the established flow patterns (**Paper I**) are to-be adjusted from the deglacial perspective (**Paper III**), it is possible that even more of the ribbed moraine ridges should be assigned to the channelized flow phase (phase III). Further, this and the other findings collected within this thesis have allowed to establish a *'time – development diagram'* (Fig. 9). The diagram summarises the observations within the context of their occurrence in space (relative to the ice margin) and time (the LGM and the complete deglaciation). Although some absolute dates are given in the diagram to constrain the time frame, the time scale should be treated as a relative sequence of events (change of flow phases).

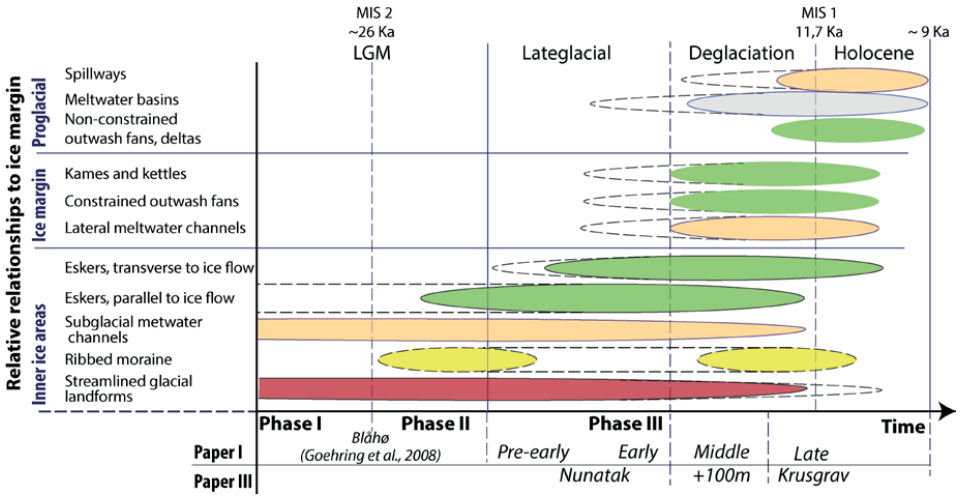

Figure 9. The time–process development diagram based on the findings for study area. Filled ellipses indicate periods of landform formation that are relatively certain. Dashed extensions indicate when the landform formation is plausible, yet the initiation / stop cannot be completely determined. Various colours used for infill represents the colours used on maps in **Paper I** (for glacigenic landforms) and **Paper III** (for glacifluvial landforms).

The transition from the phase I to phase II (Fig. 9) is marked by the onset of vertical thinning and it may have initiated at ~26 ^{10}Be ka as suggested by dating results (c.f. Goehring et al., 2008) from Mt. Blåhø, ca. 70 km N of the study area (**Paper I**). A timing which corresponds with the Marine Isotope Stage (MIS) 2. MIS 2 marks the 'global LGM' defined by minimum global sea level (Svedsen et al., 2004). Yet, since the ice sheets around the world reached their maximum extents at different times

(and often asynchronously within the different sectors of theirs) during the last glaciation the 'global LGM' concept has recently been re-evaluated (Hughes et al., 2013). Instead, due to this asynchrony, a more local use of the LGM has been suggested. The Deglaciation – Holocene transition (Fig. 9) is marked by the MIS 1 (c.f. Hughes et al., 2013). As suggested by Hughes and others (2016), the rapid deglaciation of the FIS was complete by 9 ka (Fig. 9), yet none of the phases (**Paper I**) or stages (**Paper III**) of the glacial reconstructions established within this thesis are constrained by any geochronological dating. Therefore, there is a potential for future research (see ch.6).

5. Conclusions

The findings presented in this thesis reveal new insights in the Late Weichselian evolution and deglaciation of the Fennoscandian Ice Sheet at one of its inner regions. The thesis attempts to understand the processes behind the glacial dynamics and the involvement of meltwater hydrology in the deglaciation.

The main conclusions are the following:

- The flow pattern reconstructions from glacial landforms (**Paper I**) demonstrate a stepwise evolution from the topographically independent flow (phase I), with the maximum ice sheet thickness succeeded by the regional flow (phase II), and a further transition to the channelized flow (phase III). The sub-divisions of the channelized flow (phase III) reveal a gradual increase in the flow dependency on the overall topography, while the areas in between the ice flows became under less active and developed cold-based conditions (as demonstrated by **Paper III**).
- The local mode of deglaciation in the study area in Gausdal Vestfjell reveals a westward transition of the ice retreat pattern (**Paper III**), in accordance with the assumption that the last remaining glaciers were located on the floors of deep valleys near the former ice divide.
- Two distinct types of esker systems are recognised (**Papers I** and **III**). The parallel-to-ice flow esker systems likely fed the subglacial drainage network within the valleys during phase III, whereas the transverse-to-ice flow esker systems are presumably representing late stages of deglaciation, when glacifluvial material filled in the crevasses of dead ice.

- The evidence that ribbed moraine were formed under both slow-down and speed-up of the ice flow (**Paper I**) suggests that these landforms belong to a polygenetic landform group (identifying transverse-to-ice-flow ridges), and that the landforms of this group are a subject to the principles of equifinality.
- The *'age of LiDAR'* and the capabilities provided by present-day GIS software makes it possible to establish detailed reconstructions and come up with innovating (**Papers II and III**) approaches that several decades ago, when the first research on glacial history was conducted within the Gausdal Vestfjell area, would seem incredible.

6. Research Outlook

When summarising the results covered in this thesis, a number of subjects can be suggested for potential future research:

- A continued exploration of the study area in detail. This would imply either further analysing the findings (like the relations between the landform metrics and morphology and the underlying bedrock rheology) or gathering additional data on sedimentary composition, internal structure, as well as expanding the study area to the nearby adjacent territories.
- Dating the reconstructed glacial - deglacial patterns by either relative or absolute age determination. This would imply a careful selection of localities for collecting samples to be analysed with pollen analyses, radiocarbon, luminescence (TL, OSL), and cosmic nuclide (^{10}Be) dating techniques. For instance, applying ^{10}Be dating in Skaget (the highest summit in north – 1685 m a.s.l) and other peaks within the study area (like Svarthamar, 1078 m a.s.l) could provide additional information on the age chronology. However, the issues and error bounds of various dating methods have to be taken into consideration (c.f. Hughes et al., 2016). Whilst radiocarbon dating can produce the most accurate results, the lack of organic material suitable for dating may be the matter. In the given context, the latest advance of OSL dating technique should be mentioned (Jenkins et al., 2018), since it presents promising results for dating cobbles within the glacifluvial deposits that (for sand-sized sediments) previously have been considered as challenging due to the dose sensitivity to the water content (i.e. clay particles in it).
- Using the established landform database (**Paper I**) to provide a valuable empirical input that can be used for calibrating the numerical modes used for ice-sheet modelling and, in

particular, for increasing the details of models. Or, *vice versa*, a detailed model illustrating the ice surface changes (based on the Nye's equations (Nye, 1952) and, for example, the following work of Ng and others (2010)) could be used in addition to the findings presented in **Paper III** to enhance (add more *dynamics*), validate or reject (i.e. *falsify* according to Popper, 1959) the proposed reconstruction of the last stages of FIS. This leads to a rhetorical question: Can a '*fine-tuning*' of a numerical model be really used to test a simpler, narrative and field-observations based reconstructions? It is likely that a combination of both will further push the boundaries within glacial geomorphology.

- Continued development and testing of the proposed methods (**Papers II** and **III**) would be beneficial. This should include the application on other previously glaciated areas and, as it stands for application of the Grayscale thinning, a different geomorphological settings.

References

Aario, R., 1977. Classification and terminology of morainic landforms in Finland. Boreas 6, 87-100.

Agassiz, L., 1841. On glaciers, and the evidence of their having once existed in Scotland. Ireland.

Baltsavias, E.P., 1999. Airborne laser scanning: basic relations and formulas. ISPRS Journal of photogrammetry and remote sensing 54, 199-214.

Bar-Matthews, M., Ayalon, A., Gilmour, M., Matthews, A., Hawkesworth, C.J., 2003. Sea–land oxygen isotopic relationships from planktonic foraminifera and speleothems in the Eastern Mediterranean region and their implication for paleorainfall during interglacial intervals. Geochimica et Cosmochimica Acta 67, 3181-3199.

Benediktsson, Í.Ö., Jónsson, S.A., Schomacker, A., Johnson, M.D., Ingólfsson, Ó., Zoet, L., Iverson, N.R., Stötter, J., 2016. Progressive formation of modern drumlins at Múlajökull, Iceland: stratigraphical and morphological evidence. Boreas 45, 567-583.

Bergersen, O.F., Games, K., 1971. Evidence of sub-till sediments from a Weichselian interstadial in the Gudbrandsdalen valley, Central Norway. Norsk Geogr. Tidsskr 25, 99-108.

Bergersen, O.F., Garnes, K., 1972. Ice Movements and Till Stratigraphy in the Gudbransdal Area. Preliminary Results. Norsk Geologisk Tidsskrift 26, 1-16.

Bergersen, O.F., Garnes, K., 1981. Weichselian in central South Norway: the Gudbrandsdal Interstadial and the following glaciation. Boreas 10, 315-322.

Biagioni, J., Eriksson, J., 2012. Map inference in the face of noise and disparity, Proceedings of the 20th International Conference on Advances in Geographic Information Systems. ACM, Redondo Beach, California, pp. 79-88.

Boulton, G., Clark, C.D., 1990a. The Laurentide Ice Sheet through the last glacial cycle: drift lineations as a key to the dynamic behaviour of former ice sheets. Transactions of the Royal Society of Edinburgh, Earth Sciences 81, 327-347.

Boulton, G., Clark, C.D., 1990b. A highly mobile Laurentide Ice Sheet revealed by satellite images of glacial lineations. Nature 346.

Boulton, G., Hagdorn, M., 2006. Glaciology of the British Isles Ice Sheet during the last glacial cycle: form, flow, streams and lobes. Quat. Sci. Rev. 25, 3359-3390.

Boulton, G., Smith, D., Jones, S., Newsome, J., 1985. Glacial geology and glaciology of the last mid-latitude ice sheets. Journal of the Geological Society of London 142, 447-474.

Carlson, A.B., Sollid, J.L., 1979. Fullsenn, kvartærgeologisk kart 1717 III - 1:50 000. Norges geologiske undersøkelse, Trondheim.

Carlson, A.B., Sollid, J.L., 1983. Fullsenn Beskrivelse til kvartærgeologisk kart 1717 III – M 1:50 000 Norges geologiske undersøkelse 390. 1-35 NGU, Trondheim.

Carter, W., Shrestha, R., Clint Slatton, K., 2007. Geodetic Laser Scanning. Physics Today 60, 12, 41

Clark, C.D., 1993. Mega-scale glacial lineations and cross-cutting ice-flow landforms. Earth Surface Processes and Landforms 18, 1-29.

Clark, C.D., 1997. Reconstructing the evolutionary dynamics of former ice sheets using multi-temporal evidence, remote sensing and GIS. Quat. Sci. Rev. 16, 1067-1092.

Clark, C.D., 1999. Glaciodynamic context of subglacial bedform generation and preservation. Annals of Glaciology 28, 23-32.

Clark, C.D., Hughes, A.L.C., Greenwood, S.L., Jordan, C., Sejrup, H.P., 2012. Pattern and timing of retreat of the last British-Irish Ice Sheet. Quat. Sci. Rev. 44, 112-146.

Clark C. D., Ely J. C., Greenwood S. L., Hughes A. L. C., Meehan, R., Barr I. D., Bateman M. D., Bradwell, T., Doole, J., Evans D. J. A., Jordan C. J., Monteys, X., Pellicer X. M. & Sheehy, M. 2017: BRITICE Glacial Map, version 2: a map and GIS database of glacial landforms of the last British–Irish Ice Sheet. Boreas 47, 11-18.

Clark, C.D., Meehan, T.M.R., 2001. Subglacial bedform geomorphology of the Irish Ice Sheet reveals major configuration changes during growth and decay. Journal of Quaternary Science 16, 483-496.

d'Oleire-Oltmanns, S., Eisank, C., Drăgut, L., Blaschke, T., 2013. An Object-Based Workflow to Extract Landforms at Multiple Scales From Two Distinct Data Types. IEEE Geoscience and Remote Sensing Letters 10, 947-951.

De Angelis, H., Kleman, J., 2005. Palaeo-ice streams in the northern Keewatin sector of the Laurentide ice sheet. Annals of Glaciology 42, 135-144.

Dowling, T.P.F., Spagnolo, M., Möller, P., 2015. Morphometry and core type of streamlined bedforms in southern Sweden from high resolution LiDAR. Geomorphology 236, 54-63.

Dunlop, P., Clark, C.D., Hindmarsh, R.C.A., 2008. Bed Ribbing Instability Explanation: Testing a numerical model of ribbed moraine formation arising from coupled flow of ice and subglacial sediment. Journal of Geophysical Research: Earth Surface 113.

Eisank, C., Smith, M., Hillier, J., 2014. Assessment of multiresolution segmentation for delimiting drumlins in digital elevation models. Geomorphology 214, 452-464.

Ely, J.C., Clark, C.D., Spagnolo, M., Stokes, C.R., Greenwood, S.L., Hughes, A.L.C., Dunlop, P., Hess, D., 2016. Do subglacial bedforms comprise a size and shape continuum? Geomorphology 257, 108-119.

Esmark, J., 1824. Bidrag til vor jordklodes historie. Magazin for Naturvidenskaberne 2, 28-49.

Esmark, J., 1826. Remarks tending to explain the geological history of the Earth. Edinburgh New Phil. Journal 3.

Eyles, N., Eyles, H.C., Miall, D.A., 1983. Lithofacies types and vertical profile models; an alternative approach to the description and environmental interpretation of glacial diamict and diamictite sequences. Sedimentology 30, 393-410.

Everest, J., Bradwell, T., Golledge, N., 2005. Subglacial landforms of the tweed palaeo-ice stream. Scottish Geographical Journal 121, 163-173.

Fredin, O., Bergstrøm, B., Eilertsen, R., Hansen, L., Longva, O., Nesje, A., Sveian, H., 2013. Glacial landforms and quaternary landscape development in Norway. Quaternary Geology of Norway, Geological Survey of Norway Special Publication 13, 5-25.

Garnes, K., Bergersen, O.F., 1980. Wastage features of the inland ice sheet in central South Norway. Boreas 9, 251-269.

Glasser, N.F., Bennett, M.R., 2004. Glacial erosional landforms: origins and significance for palaeoglaciology. Prog. Phys. Geogr. 28, 43-75.

Glasser, N.F., Warren, C.R., 1990. Medium Scale Landforms of Glacial Erosion in South Greenland; Process and Form. Geografiska Annaler. Series A, Physical Geography 72, 211-215.

Goehring, B.M., Brook, E.J., Linge, H., Ralsbeck, G.M., Yiou, F., 2008. Beryllium-10 exposure ages of erratic boulders in southern Norway and implications for the history of the Fennoscandian Ice Sheet. Quat. Sci. Rev. 27, 320-336.

Greenwood Sarah, L., Clark Chris, D., Hughes Anna, L.C., 2007. Formalising an inversion methodology for reconstructing ice-sheet retreat patterns from meltwater channels: application to the British Ice Sheet. Journal of Quaternary Science 22, 637-645.

Greenwood, S.L., Clark, C.D., 2009a. Reconstructing the last Irish Ice Sheet 1: changing flow geometries and ice flow dynamics deciphered from the glacial landform record. Quat. Sci. Rev. 28, 3085-3100.

Greenwood, S.L., Clark, C.D., 2009b. Reconstructing the last Irish Ice Sheet 2: a geomorphologically-driven model of ice sheet growth, retreat and dynamics. Quat. Sci. Rev. 28, 3101-3123.

Greenwood, S.L., Clason, C.C., Helanow, C., Margold, M., 2016. Theoretical, contemporary observational and palaeo-perspectives on ice sheet hydrology: Processes and products. Earth-Science Reviews 155, 1-27.

Griffiths, J.S., Smith, M.J., Paron, P., 2011. Chapter One - Introduction to Applied Geomorphological Mapping, in: Smith, M.J., Paron, P., Griffiths, J.S. (Eds.), Developments in Earth Surface Processes. Elsevier, pp. 3-11.

Heim, M., Schärer, U., Milnes, G., 1977. The nappe complex in the Tyin-Bygdin-Vang region, central southern Norway. Norsk Geologisk Tidsskrift 57, 171-181. Oslo.

Hein, A., Woodward, J., Marrero, S., Dunning, S., Steig, E., P H T Freeman, S., M Stuart, F., Winter, K., Westoby, M., Sugden, D., 2016. Evidence for the stability of the West Antarctic Ice Sheet divide for 1.4 million years.

Hennissen, J.A.I., Head, M.J., De Schepper, S., Groeneveld, J., 2015. Increased seasonality during the intensification of Northern Hemisphere glaciation at the Pliocene–Pleistocene boundary ~2.6 Ma. Quat. Sci. Rev. 129, 321-332.

Hestmark, G., 2018. Jens Esmark's mountain glacier traverse 1823 – the key to his discovery of Ice Ages. Boreas 47, 1-10.

Hillier, J.K., Smith, M., 2008. Residual relief separation: digital elevation model enhancement for geomorphological mapping. Earth Surface Processes and Landforms 33, 2266-2276.

Hillier, J.K., Smith, M.J., 2012. Testing 3D landform quantification methods with synthetic drumlins in a real digital elevation model. Geomorphology 153-154, 61-73.

Hillier, J.K., Smith, M.J., Clark, C.D., Stokes, C.R., Spagnolo, M., 2013. Subglacial bedforms reveal an exponential size–frequency distribution. Geomorphology 190, 82-91.

Hillier, J.K., Sofia, G., Conway, S.J., 2015. Perspective – synthetic DEMs: A vital underpinning for the quantitative future of landform analysis? Earth Surf. Dynam. 3, 587-598.

Hodgson, M., Bresnahan, P., 2004. Accuracy of Airborne LIDAR-Derived Elevation: Empirical Assessment and Error Budget.
Hubbard, A., Bradwell, T., Golledge, N., Hall, A., Patton, H., Sugden, D., Cooper, R., Stoker, M., 2009. Dynamic cycles, ice streams and their impact on the extent, chronology and deglaciation of the British-Irish ice sheet. Quat. Sci. Rev. 28, 758-776.
Hughes, A.L.C., Clark, C.D., Jordan, C.J., 2010. Subglacial bedforms of the last British Ice Sheet. Journal of Maps 6, 543-563.
Hughes, A.L.C., Clark, C.D., Jordan, C.J., 2014. Flow-pattern evolution of the last British Ice Sheet. Quat. Sci. Rev. 89, 148-168.
Hughes, A.L.C., Gyllencreutz, R., Lohne, Ø.S., Mangerud, J., Svendsen, J.I., 2016. The last Eurasian ice sheets – a chronological database and time-slice reconstruction, DATED-1. Boreas 45, 1-45.
Hughes, P.D., Gibbard, P.L., Ehlers, J., 2013. Timing of glaciation during the last glacial cycle: evaluating the concept of a global 'Last Glacial Maximum' (LGM). Earth-Science Reviews 125, 171-198.
Ingólfsson, Ó., Landvik, J.Y., 2013. The Svalbard–Barents Sea ice-sheet – Historical, current and future perspectives. Quat. Sci. Rev. 64, 33-60.
Jahns, S., 2007. Palynological investigations into the Late Pleistocene and Holocene history of vegetation and settlement at the Löddigsee, Mecklenburg, Germany. Vegetation History and Archaeobotany 16, 157-169.
Jenkins, G.T.H., Duller, G.A.T., Roberts, H.M., Chiverrell, R.C., Glasser, N.F., 2018. A new approach for luminescence dating glaciofluvial deposits - High precision optical dating of cobbles. Quat. Sci. Rev. 192, 263-273.
Jorge, M.G., Brennand, T.A., 2017. Semi-automated extraction of longitudinal subglacial bedforms from digital terrain models – Two new methods. Geomorphology 288, 148-163.
Kleman, J., Borgstrom, I., 1996. Reconstruction of paleo-ice sheets:the use of geomorphological data. Earth Surface Processes and Landforms 21, 893-909.
Kleman, J., Glasser, N.F., 2007. The subglacial thermal organisation (STO) of ice sheets. Quat. Sci. Rev. 26, 585-597.
Kleman, J., Hattestrand, C., Borgstrom, I., Stroeven, A., 1997. Fennoscandian palaeoglaciology reconstructed using a glacial geological inversion model. J. Glaciol. 43, 283-299.
Kleman, J., Hättestrand, C., Stroeven, A.P., Jansson, K.N., De Angelis, H., Borgström, I., 2006. Reconstruction of palaeo-ice sheets - inversion of their glacial geomorphological record. Glacier Science and Environmental Change, 192-198.
Knight, J., 2011. Subglacial processes and drumlin formation in a confined bedrock valley, northwest Ireland. Boreas 40.
Lambeck, K., Purcell, A., Zhao, S., 2017. The North American Late Wisconsin ice sheet and mantle viscosity from glacial rebound analyses. Quat. Sci. Rev. 158, 172-210.
Lambeck, K., Rouby, H., Purcell, A., Sun, Y., Sambridge, M., 2014. Sea level and global ice volumes from the Last Glacial Maximum to the Holocene. Proceedings of the National Academy of Sciences 111, 15296-15303.
Landvik, J.Y., Alexanderson, H., Henriksen, M., Ingólfsson, Ó., 2014. Landscape imprints of changing glacial regimes during ice-sheet build-up and decay: a conceptual model from Svalbard. Quat. Sci. Rev. 92, 258-268.
Larsen, K.N., Piotrowski, A.J., 2003. Fabric Pattern in a Basal Till Succession and Its Significance for Reconstructing Subglacial Processes. Journal of Sedimentary Research 73, 725-734.
Lefsky, M.A., Cohen, W.B., Parker, G.G., Harding, D.J., 2002. Lidar Remote Sensing for Ecosystem Studies. BioScience 52, 19-30.
Link, L., 1969. Capability of airborne laser profilometer to measure terrain roughness, Proceedings, 6th Symposium on Remote Sensing of Environment, pp. 189-196.
Link, L., Collins, J., 1981. Airborne laser systems in terrain mapping. Proceedings, 15th International Symposium on Remote Sensing of Environment, Vol. 1, pp. 95 -110.
Lunde, T., 1956. Isavsmeltningen i et område sør for Sjodalen. University thesis, Oslo (unpubl.).
Maclachlan, C.J., Eyles, H.C., 2013. Quantitative geomorphological analysis of drumlins in the Peterborough drumlin field, Ontario, Canada. Geografiska Annaler: Series A, Physical Geography 95, 125-144.
Maiman, T.H., 1960. Stimulated optical radiation in ruby.
Mangerud, J., 1964. Isavsmeltningen i og omkring midtre Gudbransdal. Norsk Geologisk Undersøkelse 223, 223 - 274.
Mangerud, J., Gyllencreutz, R., Lohne, Ø., Svendsen, J.I., 2011. Chapter 22 - Glacial History of Norway, in: Ehlers, J., Gibbard, P.L., Hughes, P.D. (Eds.), Developments in Quaternary Sciences. Elsevier, pp. 279-298.

Margold, M., Stokes, C.R., Clark, C.D., 2018. Reconciling records of ice streaming and ice margin retreat to produce a palaeogeographic reconstruction of the deglaciation of the Laurentide Ice Sheet. Quat. Sci. Rev. 189, 1-30.

Menzies, J., 2018. Glacial Geomorphology☆, Reference Module in Earth Systems and Environmental Sciences. Elsevier.

Milankovich, M., 1930. Mathematical climatology and the astronomical theory of climate change. Handbuch der Klimatologie 1, 1-176.

Möller, P., Dowling, T.P.F., 2016. Streamlined subglacial bedforms on the Närke plain, south-central Sweden – Areal distribution, morphometrics, internal architecture and formation. Quat. Sci. Rev. 146, 182-215.

Möller, P., Dowling, T.P.F., 2018. Equifinality in glacial geomorphology: instability theory examined via ribbed moraine and drumlins in Sweden. GFF 140, 106-135.

Napieralski, J., Nalepa, N., 2010. The application of control charts to determine the effect of grid cell size on landform morphometry. Computers & Geosciences 36, 222-230.

Nelson, A., Reuter, H.I., Gessler, P., 2009. Chapter 3 DEM Production Methods and Sources, Geomorphometry - Concepts, Software, Applications, pp. 65-85.

Nelson, R., 2013. How did we get here? An early history of forestry lidar1. Canadian Journal of Remote Sensing 39, S6-S17.

Ng, F.S.L., Barr, I.D., Clark, C.D., 2010. Using the surface profiles of modern ice masses to inform palaeo-glacier reconstructions. Quat. Sci. Rev. 29, 3240-3255.

Nickelsen, R.P., 1988. Fullsenn 1717 III, berggrunnskart M 1:50 000. Norges geologiske undersøkelse.

Nye, J.F., 1952. A Method of Calculating the Thicknesses of the Ice-Sheets. Nature 169, 529-530.

Paillard, D., 2015. Quaternary glaciations: from observations to theories. Quat. Sci. Rev. 107, 11-24.

Patton, H., Hubbard, A., Andreassen, K., Auriac, A., Whitehouse, P.L., Stroeven, A.P., Shackleton, C., Winsborrow, M., Heyman, J., Hall, A.M., 2017. Deglaciation of the Eurasian ice sheet complex. Quat. Sci. Rev. 169, 148-172.

Paul, J.D., 2015. A question of uniformitarianism: Has the geological past become the key to humanity's future? Anthropocene 9, 70-74.

Pelletier, J.D., 2008. Quantitative modeling of earth surface processes. Cambridge University Press.

Piégay, H., 2017. Quantitative Geomorphology, International Encyclopedia of Geography.

Popper, K.R., 1959. The logic of scientific discovery. Hutchinson, London.

Stokes, R.C., Lian, B.O., Tulaczyk, S., Clark, C.D., 2008. Superimposition of ribbed moraines on a palaeo-ice-stream bed: implications for ice stream dynamics and shutdown. Earth Surface Processes and Landforms 33, 593-609.

Rasmussen, S.O., Andersen, K.K., Svensson, A., Steffensen, J.P., Vinther, B.M., Clausen, H.B., Siggaard-Andersen, M.L., Johnsen, S.J., Larsen, L.B., Dahl-Jensen, D., 2006. A new Greenland ice core chronology for the last glacial termination. Journal of Geophysical Research: Atmospheres 111.

Rasmussen, S.O., Bigler, M., Blockley, S.P., Blunier, T., Buchardt, S.L., Clausen, H.B., Cvijanovic, I., Dahl-Jensen, D., Johnsen, S.J., Fischer, H., Gkinis, V., Guillevic, M., Hoek, W.Z., Lowe, J.J., Pedro, J.B., Popp, T., Seierstad, I.K., Steffensen, J.P., Svensson, A.M., Vallelonga, P., Vinther, B.M., Walker, M.J.C., Wheatley, J.J., Winstrup, M., 2014. A stratigraphic framework for abrupt climatic changes during the Last Glacial period based on three synchronized Greenland ice-core records: refining and extending the INTIMATE event stratigraphy. Quat. Sci. Rev. 106, 14-28.

Rose, J., 1987. Drumlins as part of a glacier bedform continuum. Drumlin symposium. Manchester, 1985, 103-116.

Ross, M., Campbell, J.E., Parent, M., Adams, R.S., 2009. Palaeo-ice streams and the subglacial landscape mosaic of the North American mid-continental prairies. Boreas 38, 421-439.

Saha, K., Wells, N.A., Munro-Stasiuk, M., 2011. An object-oriented approach to automated landform mapping: A case study of drumlins. Computers & Geosciences 37, 1324-1336.

Sărășan, A., Józsa, E., Ardelean, C.A., Drăguț, L., 2018. Sensitivity of geomorphons to mapping specific landforms from a digital elevation model: A case study of drumlins. Area 0.

Siedlecka, A., Nystuen, J.P., Englund, J.O., Hossack, J., 1987. Lillehammer- berggrunnskart M. 1:250 000. Norges geologiske undersøkelse, Trondheim.

Smith, M.J., 2011. Chapter Eight - Digital Mapping: Visualisation, Interpretation and Quantification of Landforms, in: Smith, M.J., Paron, P., Griffiths, J.S. (Eds.), Developments in Earth Surface Processes. Elsevier, pp. 225-251.

Smith, M.J., Clark, C.D., 2005. Methods for the visualization of digital elevation models for landform mapping. Earth Surface Processes and Landforms 30, 885-900.

Smith, M.J., Rose, J., Gousie, M.B., 2009. The Cookie Cutter: A method for obtaining a quantitative 3D description of glacial bedforms. Geomorphology 108, 209-218.
Smith, M.J., Wise, S.M., 2007. Problems of bias in mapping linear landforms from satellite imagery. International Journal of Applied Earth Observation and Geoinformation 9, 65-78.
Sollid, J.L., Sørbel, L., 1994. Distribution of Glacial Landforms in Southern Norway in Relation to the Thermal Regime of the Last Continental Ice Sheet. Geografiska Annaler. Series A, Physical Geography 76, 25-35.
Sookhan, S., Eyles, N., Putkinen, N., 2018. LiDAR-based mapping of paleo-ice streams in the eastern Great Lakes sector of the Laurentide Ice Sheet and a model for the evolution of drumlins and MSGLs. GFF 140, 202-228.
Spagnolo, M., Clark, C.D., Hughes, A.L.C., 2012. Drumlin relief. Geomorphology 153-154, 179-191.
Stokes, C.R., Clark, C.D., 1999. Geomorphological criteria for identifying Pleistocene ice streams. Annals of Glaciology 28, 67-74.
Stokes, C.R., Clark, C.D., 2001. Palaeo-ice streams. Quat. Sci. Rev. 20, 1437-1457.
Stokes, C.R., Clark, C.D., Lian, O.B., Tulaczyk, S., 2007. Ice stream sticky spots: A review of their identification and influence beneath contemporary and palaeo-ice streams. Earth-Science Reviews 81, 217-249.
Stokes, C.R., Spagnolo, M., Clark, C.D., Ó Cofaigh, C., Lian, O.B., Dunstone, R.B., 2013. Formation of mega-scale glacial lineations on the Dubawnt Lake Ice Stream bed: 1. size, shape and spacing from a large remote sensing dataset. Quat. Sci. Rev. 77, 190-209.
Storrar, R.D., Livingstone, S.J., 2017. Glacial geomorphology of the northern Kivalliq region, Nunavut, Canada, with an emphasis on meltwater drainage systems. Journal of Maps 13, 153-164.
Stroeven, A.P., Hättestrand, C., Kleman, J., Heyman, J., Fabel, D., Fredin, O., Goodfellow, B.W., Harbor, J.M., Jansen, J.D., Olsen, L., Caffee, M.W., Fink, D., Lundqvist, J., Rosqvist, G.C., Strömberg, B., Jansson, K.N., 2016. Deglaciation of Fennoscandia. Quat. Sci. Rev. 147, 91-121.
Svendsen, J.I., Alexanderson, H., Astakhov, V.I., Demidov, I., Dowdeswell, J.A., Funder, S., Gataullin, V., Henriksen, M., Hjort, C., Houmark-Nielsen, M., Hubberten, H.W., Ingólfsson, O., Jakobsson, M., Kjær, K.H., Larsen, E., Lokrantz, H., Lunkka, J.P., Lyså, A., Mangerud, J., Matiouchkov, A., Murray, A., Möller, P., Niessen, F., Nikolskaya, O., Polyak, L., Saarnisto, M., Siegert, C., Siegert, M.J., Spielhagen, R.F., Stein, R., 2004. Late Quaternary ice sheet history of northern Eurasia. Quat. Sci. Rev. 23, 1229-1271.
Tooth, S., Viles, H., 2014. 10 reasons why is important Geomorphology, in: Geomorphology, B.S.f. (Ed.).
Vaughan, D.G., Comiso, J.C., Allison, I., Carrasco, J., Kaser, G., Kwok, R., Mote, P., Murray, T., Paul, F., Ren, J., 2013. Observations: cryosphere. Climate change 2103, 317-382.
Vorren, T.O., 1977. Weichselian ice movement in South Norway and adjacent areas. *Boreas 6*, 247-257.
Wang, Y., Han, L., Xiao, S., Wang, J., Zhai, X., 2017. A novel statistical approach to remove salt-and-pepper noise. Journal of Statistical Computation and Simulation 87, 2538-2548.
Wehr, A., Lohr, U., 1999. Airborne laser scanning—an introduction and overview. ISPRS Journal of photogrammetry and remote sensing 54, 68-82.
Yu, P., Eyles, N., Sookhan, S., 2015. Automated drumlin shape and volume estimation using high resolution LiDAR imagery (Curvature Based Relief Separation): A test from the Wadena Drumlin Field, Minnesota. Geomorphology 246, 589-601.

Paper I

Putniņš, A., Henriksen, M. (2017) Reconstructing the flow pattern evolution in inner region of the Fennoscandian Ice Sheet by glacial landforms from Gausdal Vestfjell area, south-central Norway. Quaternary Science Reviews 163, 56-71.

Quaternary Science Reviews 163 (2017) 56–71

Contents lists available at ScienceDirect

Quaternary Science Reviews

journal homepage: www.elsevier.com/locate/quascirev

Reconstructing the flow pattern evolution in inner region of the Fennoscandian Ice Sheet by glacial landforms from Gausdal Vestfjell area, south-central Norway

Artūrs Putniņš*, Mona Henriksen

Faculty of Environmental Sciences and Natural Resource Management, Norwegian University of Life Sciences, P.O. Box 5003, 1432 Ås, Norway

ARTICLE INFO

Article history:
Received 5 October 2016
Received in revised form
6 January 2017
Accepted 6 March 2017
Available online 21 March 2017

Keywords:
Streamlined subglacial landforms
Ribbed moraine
Fennoscandian Ice Sheet
Flow pattern reconstruction
Deglaciation
Scandinavia
LiDAR

ABSTRACT

More than 17 000 landforms from detailed LiDAR data sets have been mapped in the Gausdal Vestfjell area, south-central Norway. The spatial distribution and relationships between the identified subglacial bedforms, mainly streamlined landforms and ribbed moraine ridges, have provided new insight on the glacial dynamics and the sequence of glacial events during the last glaciation. This established evolution of the Late Weichselian ice flow pattern at this inner region of the Fennoscandian Ice Sheet is stepwise where a topography independent ice flow (Phase I) are followed by a regional (Phase II) before a strongly channelized, topography driven ice flow (Phase III). The latter phase is divided into several substages where the flow sets are becoming increasingly confined into the valleys, likely separated by colder, less active ice before down-melting of ice took place. A migrating ice divide and lowering of the ice surface seems to be the main reasons for these changes in ice flow pattern. Formation of ribbed moraine can occur both when the ice flow slows down and speeds up, forming respectively broad fields and elongated belts of ribbed moraines.

1. Introduction

The configuration of the Fennoscandian Ice Sheet (FIS) and its complex evolution in time and space during the Weichselian glaciation have been the subject of research for a long time (Böse et al., 2012; Hughes et al., 2016; Kleman and Glasser, 2007; Kleman et al., 1997; Mangerud et al., 1979, 2011; Svendsen et al., 2004). This includes the discussion on the causes of the ice divide migration (Fig. 1) and the implications of this on the ice sheet dynamics, e.g. the initiation of the Norwegian Channel Ice Stream (NCIS) (Mangerud et al., 2011). The consequence of this likely lead to an enhanced drainage of large parts of southern Norway and central Sweden and a subsequent lowering the ice surface (Svendsen et al., 2015; Sejrup et al., 2009). The study area, Gausdal Vestfjell in south-central Norway (Fig. 1), is located upstream from the NCIS (Ottesen et al., 2005) and in close proximity to the later, migrated ice divide (Vorren, 1977). Such geographical setting (an inner region of the last ice sheet) also determines that this area has been one of the last parts of the FIS to become deglaciated. Therefore, it has a high importance on reconstructing the ice sheet development, glacial dynamics and the deglaciation. Numerous scientists have emphasized the significance of glacial bedforms – streamlined terrain and ribbed moraine – as the indicators of glacial dynamics (e.g. Briner, 2007; Clark, 1993, 1997; Dunlop and Clark, 2006a, 2006b; Hättestrand, 1997; Hättestrand and Kleman, 1999; Hughes et al., 2014; Knight, 2010, 2011; Roberts and Long, 2005; Spagnolo et al., 2012, 2014; Stokes et al., 2011, 2013; Trommelen and Ross, 2010). The analysis of distribution of glacial landforms on a regional scale is the primary tool for the ice flow pattern reconstructions with the so-called flowset (*ice-flow vector* by Hughes et al. (2014)) or the palaeoglacial approach (Boulton and Hagdorn, 2006; Clark et al., 2012; Greenwood and Clark, 2009a, 2009b; Greenwood et al., 2007; Hubbard et al., 2009; Hughes et al., 2014; Kleman et al., 1997; Ross et al., 2009).

The latest development within Geographic Information Systems (GIS) and the increasing accessibility of *Light Detection and Ranging* (LiDAR) terrain data have made it possible to create a high accuracy geomorphological maps further used for glacial reconstructions, and by so it has contributed to the development of geomorphology and Quaternary geology. The extensive mapping conducted within this study provides insight on the distribution and morphostratigraphical relationships of the glacial landforms and thus reveals

* Corresponding author.
E-mail address: arturs.putnins@nmbu.no (A. Putniņš).

http://dx.doi.org/10.1016/j.quascirev.2017.03.008
0277-3791/

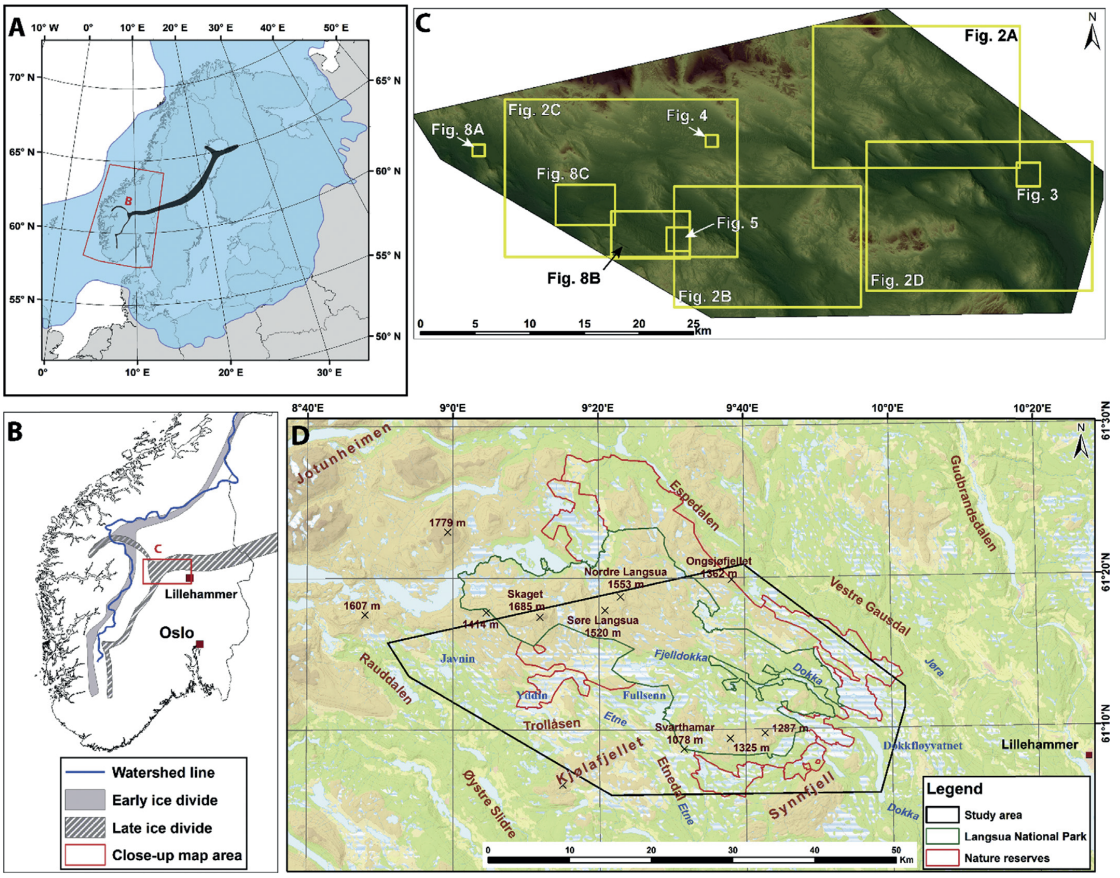

Fig. 1. **A.** The Fennoscandian Ice Sheet at its maximum position during the Late Weichselian (according to Svendsen et al., 2004) with ice divide in dark (according to Kleman et al., 1997). **B.** Overview map of southern Norway with watershed and ice divide locations (according to Vorren, 1977). **C.** Overview map with locations of other map figures. **D.** Map of Gausdal Vestfjell with outlines of the study area and the protected Langsua National Park and nature reserve areas. Some additional location names are shown in Figs. 2 and 7.

new information on the glacial dynamics during the last glaciation. Based on the identified ice flow patterns, a detailed reconstruction of glacial events from the Late Weichselian and deglaciation in the Gausdal Vestfjell area are established.

2. Study area

Gausdal Vestfjell is located in Oppland County, south-central Norway, situated c. 50 km W of Lillehammer and 50 km SE of the Jotunheimen mountain region (Fig. 1). Jotunheimen is the highest part of the Scandinavian Mountains, which has functioned as one of the primary accumulation areas during the buildup of the FIS prior to the LGM (Mangerud et al., 2011). The study area shows a diverse and relatively complex topography (Fig. 1C). In general, it can be described as an undulating upland plateau, gently sloping towards the SE. The plateau is surrounded by several topographic highs, a W-E oriented mountain ridge in the N (highest peak Skaget 1685 m a.s.l.), the Kjølafjellet ridge in the SW, and the Synnfjell ridge in the SE. Within the plateau area itself, several elevated areas (1100 up to 1325 m a.s.l.) exist. Low-lying areas are commonly occupied by several natural or dammed water bodies that are linked by rivers (Fig. 1D). The two largest ones, the Fjelldokka and Etne rivers, emerge from the foothill of the northern ridge and flow towards the SE, continuing into deep glacial eroded valleys. The western border of the study area is drawn at the upper valley slope of the Rauddalen and Øystre Slidre valleys, while the eastern is along the Vestre Gausdal valley. Almost two thirds of the study area is located within the Langsua National Park and adjacent nature reserves (Fig. 1D) having different degrees of nature protection status limiting the possibilities for excavations.

2.1. Bedrock

The bedrock in the study area is mainly composed of metamorphosed sedimentary rocks of Precambrian to Ordovician age in nappes emplaced during the Caledonian orogeny (Heim et al., 1977). The northern and central part of the area consists of metamorphosed arkose, greywacke sandstone, and conglomerate of Late Precambrian age, and quartzite of Middle to Late Ordovician age belonging to the Jotun-Valdres Nappes Complex. In the southern and southeastern part, slate, sandstone and limestone of Cambrian to Middle Ordovician age form the Synnfjell Nappe (Heim et al.,

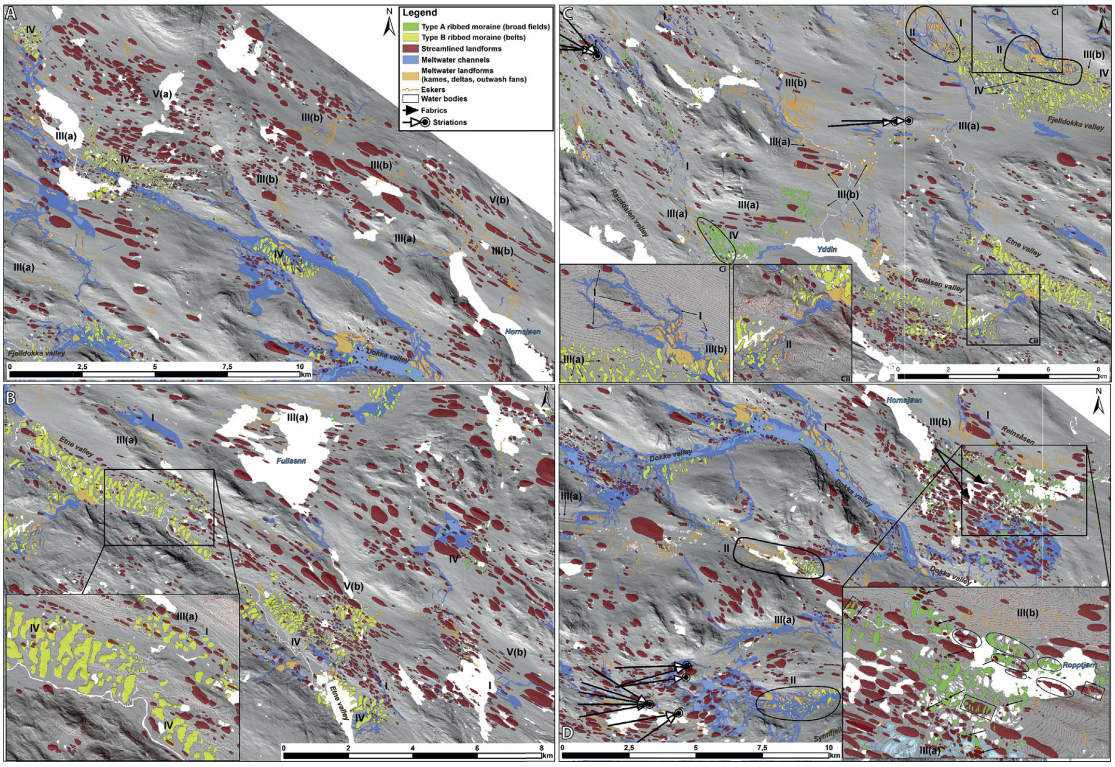

Fig. 2. Distribution pattern and spatial relationships of identified landforms plotted on DEM hillshade image from four parts of the study area. See Fig. 1C for location and supplement no. 2 for a detailed map. Roman numbers indicate: (I) lateral meltwater channels; (II) close spatial relations between meltwater landforms and ribbed moraine; (III) various esker system patterns oriented (a) parallel and (b) transverse to the general ice flow direction; (IV) spatial relations between streamlined terrain and ribbed moraine ridges with streamlined landforms located both on top and in between the ribbed moraines; (V) different modes of streamlined landforms being mainly (a) round and oval shaped and (b) distinctly more elongated (L/W ratio > 3). **A.** Northern part. **B.** Southern part. Close-up (5 m contour intervals) of the ribbed moraine belt (type B) in Etne valley. **C.** Western part. Close-ups (5 m contour intervals) showing (Ci) meandering lateral meltwater channel (I) and (Cii) ribbed moraine and meltwater landform spatial relations (II). **D.** Eastern part. Close-up (2.5 m contour intervals) of a broad ribbed moraine field (type A) from the plateau S of Reinsåsen with various modes of the streamlined landforms transforming into ribbed moraines. Reworked streamlined landforms in circles, overlying ribbed moraines in boxes, and the smaller streamlined landforms with varying orientation partly overlying ribbed moraine and older streamlined landforms marked by arrows.

1977). Rocks of this formation are highly deformed by faulting, thrusting, and stacking in a N-S direction and have a high degree of schistosity. In addition, there are several localities where metamorphic plutonic basement rock (metadiorite) of Precambrian age are found (Nickelsen, 1988; Siedlecka et al., 1987). These plutonic rock formations are usually found in elevation heights that stand out from the overall terrain.

2.2. Sediment cover

The sediment cover in Gausdal Vestfjell differs due to the influence of the terrain topography as well as changes in depositional environment throughout the glacial history. Noticeably, an extensive amount of the sediment cover is made up by different till deposits that vary spatially in thickness throughout the study area (Carlson and Sollid, 1979). Deposits of continuous cover and great thickness (usually from a half to a few meters) that hide the structures of the underlying bedrock are found mainly in topographic lows and valley floors. Elsewhere (e.g. on valley sides and hilltops) glacial deposits have a discontinuous nature with frequent bedrock outcrops. Previous research on till lithology conducted in this area suggests a dominant gravely sandy matrix dominated by the local bedrock material. This suggests a short transportation prior to deposition (Carlson and Sollid, 1983). Glaciofluvial deposits, in association with landforms such as eskers, kames, deltas, and outwash fans or in form of sheet covers (related to previous meltwater basins), are widespread within the study area. There is also a common occurrence of peat and fluvial sediments deposited during the Holocene (Carlson and Sollid, 1979, 1983; Garnes and Bergersen, 1980). Sub-till sediments (glaciofluvial and glaciolacustrine deposits) of Mid-Weichselian interstadial age (Bergersen and Garnes, 1971, 1972, 1981) are found in several places in the nearby main valley of Gudbrandsdalen (Fig. 1D). However, there are no descriptions of similar findings within the study area.

2.3. Previous research

Previous reconstructions of the FIS deglaciation in the Gausdal Vestfjell area (Bergersen and Garnes, 1972, 1983; Garnes and Bergersen, 1980; Olsen, 1985) are mainly based on the

investigations of till deposits and glacial striations at Gudbrandsdalen and its tributary valleys (Fig. 1D). Based on their observations, Bergersen and Garnes (1972, 1983) and Garnes and Bergersen (1977, 1980) identified four phases of the last glaciation in the Gudbrandsdalen area. These are (i) *the initial phase* (ice flow followed the valleys), (ii) *the main phase* (little or no movement dependency on the topography), (iii) *later inland phase* (large variations in the directions of striae and till fabrics suggesting continuous shifting of flow directions) and (iv) *the deglaciation phase* (characterized by meltwater drainage along stagnant ice). All these phases had a predominant SE ice flow in Gausdal Vestfjell. Combining this and other research, Vorren (1977) established a unified reconstruction of the ice divide migration and the ice movement for southern Norway during the Weichselian. According to him, there are four main phases of different ice movement directions, the two youngest ones related to the Late Weichselian. The ice divide migration from the watershed region towards the E (Fig. 1B) might have happened between their Phases 2 and 3 (around 25–27 ka BP) (Vorren, 1977). Vorren (1977) suggests that Phase 3 should be correlated with the maximum extent of the Weichselian ice sheet (the LGM) (Fig. 1A) and with the *later inland phase (iii)* of Bergersen and Garnes (1972). Nesje et al. (1988) on the other hand, state that the ice divide migration towards the SE and E (Fig. 1B) was a result of a backward lowering of the ice sheet during the ice marginal retreat from its LGM position at the continental shelf edge to coastal and fjord areas of western Norway. Therefore, Phase 2 should represent the maximum extent of the Weichselian ice sheet while Phase 3 most likely represents a period of marginal retreat (Nesje et al., 1988). Most reconstructions of the ice divide for the entire FIS at its maximum position (e.g. Kleman et al., 1997) place it over the Gulf of Bothnia continuing westward to the eastern (late) ice divide in southern Norway (Fig. 1A). At the deglaciation, Sollid and Sørbel (1994) acknowledged a change from warm-to cold-based ice conditions at higher inland areas (such as Gausdal Vestfjell) as streamlined landforms in these areas are found together with extensive supraglacial and lateral drainage systems. Garnes and Bergersen (1980) supposed that stagnant and dead ice was located at higher elevations while active ice was flowing in the valleys as the inland ice sheet gradually down-wasted. This *deglaciation phase (iv)* of Bergersen and Garnes (1972) corresponds to Vorren's (1977) Phase 4, assigned to represent the Preboreal age (Early Holocene).

3. Materials and methods

The glacial landforms within our study area were mapped manually using several digital input data sources. Laserscan data sets (LiDAR) provided by the Norwegian Mapping Authority (*Kartverket*) is the primary source of terrain information. Landform recognition and determination was carried out using ESRI software ArcGIS version 10.3 that supports operations with .LAS files, such as data filtering (using ground points only) and data visualizations in 3D View window. The point cloud density for LiDAR data varies in range from 10 to 100 points per square meter depending on the age of the dataset. Approximately half of the study area has data coverage with 100 DTM point cloud density (100 points per m^2). Later, for visualization purposes, a Digital Elevation Model (DEM) of 3 m horizontal resolution was processed from the LiDAR data set and a hillshade image from the DEM. Additionally, WMS servers of aerial imagery and topographic maps were used to aid the landform identification in cases of uncertainty, e.g. to exclude man-made objects like road fragments, ditches, mounds or walls. Maps of Quaternary deposits as well as various resource maps provided by the Geological Survey of Norway (NGU) were in some cases used to validate identified landforms, for example, whether a landform consist of sediments or is due to a bedrock feature. Landform's plan form in the horizontal plane were mapped based on their profile curvature and drawn along the break of a slope. A file geodatabase was established to store and organize the identified landforms (Table 1), incorporating streamlined landforms, moraine ridges (ribbed moraine), and glaciofluvial landforms. The following parameters of streamlined landforms and ribbed moraine ridges were included: landform configuration (polygon feature), axis of width (W) and length (L) (polyline features), landform type, and relative height (H) (obtained as described in Spagnolo et al. (2012)). Simple morphometric analyses of these parameters are presented in Supplement no. 1 and 3. No morphometric information was acquired for meltwater landforms (eskers and meltwater channels) as only their location in the terrain was used further in this study and due to their complex form, often consisting of more than one feature per landform. Further, interpretation accuracy of streamlined landforms (high, medium, low or not reliable at all) was added to the dataset and reassessed after field investigation. This assessment of interpretation accuracy was determined by following characteristics: (a) object size, (b) object shape and configuration, (c) structural orientation of the underlying bedrock within the area, (d) object overall location and orientation in the terrain (either on a hilltop, slope, or valley floor), (e) object relation to nearby objects, (f) possible other types of interpretation (if there is a different explanation of genesis, the reliability is decreased) and (g) other aspects like sedimentary or bedrock feature. For example, distinctively shaped drumlins (located in the central parts topographic lows (valleys) or plateaus that is characterized by thick drift sheet) or small flutes overlying other landforms are regarded (in terms of accuracy) as more trustable than large-scale drumlins (crag-and-tails or rock drumlins), oddly shaped roche moutonnées located on hilltops and glacial lineations forming successive chains at valley sides, which can also be interpreted as kames.

As an important part of the study, landforms with uncertainties regarding their genesis were investigated during fieldwork. Along with the landform ground truthing, fieldwork also included collecting data on glacial striations (ten localities), as well as investigating and documenting the sediment outcrops to acquire information of internal structure and sedimentary composition of ribbed moraine ridges (eight localities) and streamlined landforms (three localities). Only two localities from ribbed moraine ridges and one from streamlined landform were further visualized and included in the paper to illustrate the sedimentary composition. A lithofacies classification modified from Eyles et al. (1983) was used in describing the sediments. Clast fabric measurements were carried out to document ice-bed stress patterns and from that deduces ice flow directions during the formation of streamlined landform. The dip and dip direction was measured for 25 matrix-supported clasts ranging from 1 to 10 cm with a/b ratio $\geq$1.5 (Larsen and Piotrowski, 2003). The results of the fabric measurements are presented as points and two-sigma Kamb contours on an equal-area, lower-hemisphere Schmidt net plotted in StereoNet© for Windows.

The field inspection led to an increase in the quality of acquired data and to a decreased quantity of previously identified landforms. Furthermore, the established assessment of reliability for streamlined landforms was evaluated during the field inspection. However, as field investigation is a time consuming process, and with 1190 km^2 to cover, it is impossible to fully exclude all errors in the geomorphic dataset and some of the identified landforms may have been interpreted imprecisely regarding their genesis. Only the identified streamlined landforms with interpretation accuracy assessed as high or medium of (8155 out of 9547 in total) are used for further processing (relative height estimation) and analyses within this research.

Table 1
Summary of identified landforms included in database.

	Landform feature type	Count	Length (m)			Width (m)			Relative height (m)		
			Min	Max	Mean	Min	Max	Mean	Min	Max	Mean
Subglacial bedforms	Streamlined landforms (including low or no reliability)	9547 *Further used:* 8155	12.7	1687.8	140.8	4.12	666.2	57.7	0.2	62	4
	Ribbed moraine	3105	12.8	766.6	118.2	9.1	354.4	64.2	0.5	14.7	3.8
Meltwater landforms	Meltwater channel features	1322									
	Meltwater features (kames, outwash fans, deltas)	537									
	Eskers (lines)	2653	8.2	1685	110						
Total		**17 164**									

Table 2
Overview of the lithofacies code used to describe the outcrops. Modified from Eyles et al., (1983), following Möller (2005).

Lithofacies code	Lithofacies type description: grain size, grain support system, internal structures
D(G/S/Si/C)	Diamicton, gravely, sandy, silty, clayey. One or more grain-size code letter used in brackets
D( )mm	Diamicton, matrix-supported, massive
D( )ms	Diamicton, matrix-supported, stratified
GSm	Gravely sand, massive
Sm	Sand, massive
SiSm	Silty sand, massive
SSim	Sandy silt, massive
GSpc	Gravely sand, planar cross-laminated
Spc	Sand, planar cross-laminated

4. Results

A total of 17 164 landforms and landform features were identified and included in the database. These landforms are grouped into (a) subglacial bedforms including streamlined ridges within streamlined terrain and transverse to ice-flow moraine ridges within ribbed moraine areas, and (b) meltwater landforms including eskers, meltwater channels, kames, outwash fans and deltas (Table 1) (Fig. 2). The established database is further used to analyze the spatial relations among the landforms in a manner to establish the deglaciation pattern.

4.1. Subglacial bedforms

4.1.1. Streamlined landforms

For simplicity, we use the term 'streamlined landforms' in this paper to refer to the broad family of glacially streamlined terrain landforms including flutes, drumlins, rock drumlins, crag-and-tails, roche moutonnées and glacial lineations (as defined by Stokes et al. (2013)). This use is without restricting the variety of their shape and size or without unambiguously linking them to a certain formation mechanism as the only plausible cause. The 8155 identified streamlined landforms classified with medium or high reliability, have morphological parameters varying within a wide range (Table 1). The relative height varies from 0.2 m up to 62.2 m. However, there is only one feature higher than 50 m while 13 others are forming a cluster around 40 m (see supplement no. 1). This suggests that the highest landform is an outlier and is thus excluded as unrepresentative, resulting in a change of the interpretation accuracy class of this particular landform to 'low'.

Streamlined landforms are found at various elevation levels throughout the whole study area (Fig. 2, supplement no. 2). The most prominent (widest and highest) ones are often situated in close relation to local topographic bumps (Fig. 2A, supplement no. 3), and therefore indicating either the importance of bedrock presence (rock core), or a diminished streamlining due to the lack of sediment or porewater, or a combination of both at their formation. Less distinct (lower and narrower) streamlined landforms are located on slopes and topographic lows (Fig. 2, supplement no. 3). It is in this setting that the most elongated ones (L/W ratio > 3) often appear located on the shadow (lee) side of larger topographic bumps throughout the study area (Fig. 2A and B). The majority of such more elongated features are located either around Etne valley (Fig. 2B) or in the eastern part of the study area (Fig. 2D). The smallest of the identified streamlined landforms are often found in close association with ribbed moraine, either on top of ridge crests or between them (Fig. 2B and C, supplement no. 2).

Only a few outcrops of the streamlined landforms are available in the study area. At Reinsåsen (Figs. 2D and 3), the uppermost 2 m of the middle of a drumlin consists of compact, matrix-supported diamicton with numerous cobbles and boulders. The diamicton is in the upper ca. 1 m sandy while it is silty sandy below. Clast orientations are strong ($S_1 = 0.87$ and 0.89) indicating a depositional stress transfer towards SE and SSE (Fig. 3). A 5–15 cm thick massive, sandy silt lens is found within the diamicton. The diamicton at Reinsåsen is interpreted as a subglacial traction till due to its compact, unsorted character and strong fabric orientations (Evans et al., 2006) where the fabric analyses suggest ice movement towards SE, slightly more southerly directed than the orientation of the drumlin. The two other investigated exposures are as well in drumlins revealing similar compact, matrix-supported sandy diamicton, also interpreted as subglacial till.

4.1.2. Ribbed moraines

A total of 3105 features were identified as ribbed moraine ridges, and taken into account for analysis. The morphological parameters (length, width, relative height) of the ridges varies within a broad range (Table 1). There are no obvious outliers and the data show relative homogeneity of height distribution (supplement no. 1).

It is observed that moraine ridges either tend to be agglomerated into broad fields, our type A ribbed moraine area (Fig. 2D), or elongated belts located on the valley floors, our type B ribbed moraine area (Fig. 2B and C). The type A ribbed moraine is seen preferentially in the eastern part of the study area, while type B ribbed moraine is found throughout the whole study area (Fig. 2). Ribbed moraine ridges of type A are considerably smaller in

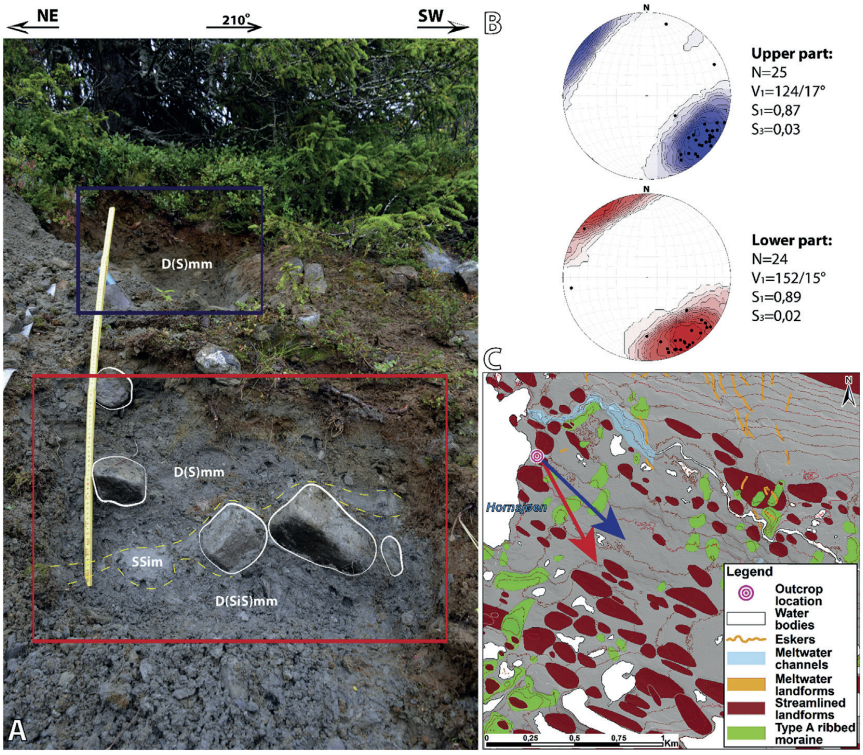

Fig. 3. Sediment outcrop near the top of a streamlined landform (drumlin) at Reinsåsen located on the plateau S of the lake Hornsjøen. **A**. Photo of outcrop (scale 1 m long) with identified lithofacies (for lithofacies code descriptions see Table 2), stippled lines outline sediment boundaries. The boxes represent the parts where fabric measurements were taken. Color code: blue – upper part, red – lower part. **B**. Contoured stereoplots of clast fabric measurements. **C.** Glacial landform map of the Reinsåsen area (2.5 m contour intervals). Colored arrow lines represent the ice flow direction as interpreted from fabrics measurements. Note the overlying landforms: smaller streamlined landforms and eskers on top of both ribbed moraine ridges and larger streamlined landforms, and ribbed moraine ridges on top of larger streamlined landforms. (For interpretation of the references to colour in this figure legend, the reader is referred to the web version of this article.)

geometry (length and width, and the relative height) than type B (Fig. 2B). The distance between the ribbed moraine ridge crests (or the 'wavelength' proposed by Dunlop and Clark, 2006b) tend to be wider for type A. Moraine belts are from around 2 km up to 16 km in length and, on average are around 1 km wide. Noticeable ribbed moraine belts are located in Fjelldokka (755 features, Figs. 2C and 4) and Etne valleys (Fig. 2B), and the ridges there tend to have the highest relative heights and largest width and length parameters of all the identified ribbed moraines. The most distinct ridges are located in the middle parts of all the ribbed moraine belts (supplement no. 3).

The few investigated sediment outcrops from the ribbed moraine ridges reveal a relatively complex inner structure that consist of both diamictons and sorted sediments, of which two localities are briefly presented here. The section at Haldorbu in the Fjelldokka valley (Fig. 4) is 2–3 m high and 10 m wide, and is oriented almost perpendicular to the ridge at its proximal side. Numerous cobbles and boulders are found scattered in compact, massive matrix-supported sandy diamicton in the uppermost 1 m. Some of the larger clasts, as well as lenses of massive silty sand and gravelly sand are tilted towards W. The diamicton is set through by several shear planes, also dipping towards W. The lower part of the exposed section is dominated by layers of massive sand and planar cross-laminated sand and gravelly sand. These sorted sediments are partly deformed by shear planes and flame structures, and by bifurcating intrusions of massive, matrix-supported sandy silty diamicton. At the second site, the uppermost 1 m of the proximal side of a ridge at Trollåsen (Fig. 5) is dominated by compact, massive matrix-supported sandy and silty sandy diamicton, slightly coarser and more consolidated than the diamicton at Haldorbu. Close to the surface, stratified matrix-supported gravelly sandy diamicton is common. Many of the abundant cobbles and boulders are orientated parallel with the ridge surface (tilted towards W), a similar orientation that is also displayed by the numerous shear planes cutting the diamicton and some few lenses of massive silty sand.

The diamicton at both Haldorbu and Trollåsen is interpreted as a subglacial till based on its compactness and glaciotectonic structures as shear planes (Evans et al., 2006). The sorted sediments at Haldorbu must have another origin as e.g. lacustrine or fluvial before being deformed, likely by an overriding glacier. The intrusions at Haldorbu are interpreted as clastic dykes suggesting, together with the presence of flame structures, depositional conditions with a high water saturation and overloading (Damsgaard et al., 2015; Le Heron and Etienne, 2005; van der Meer et al., 2009).

4.1.3. Spatial relations of glacial landforms

The mapping of glacial landforms in Gausdal Vestfjell suggests

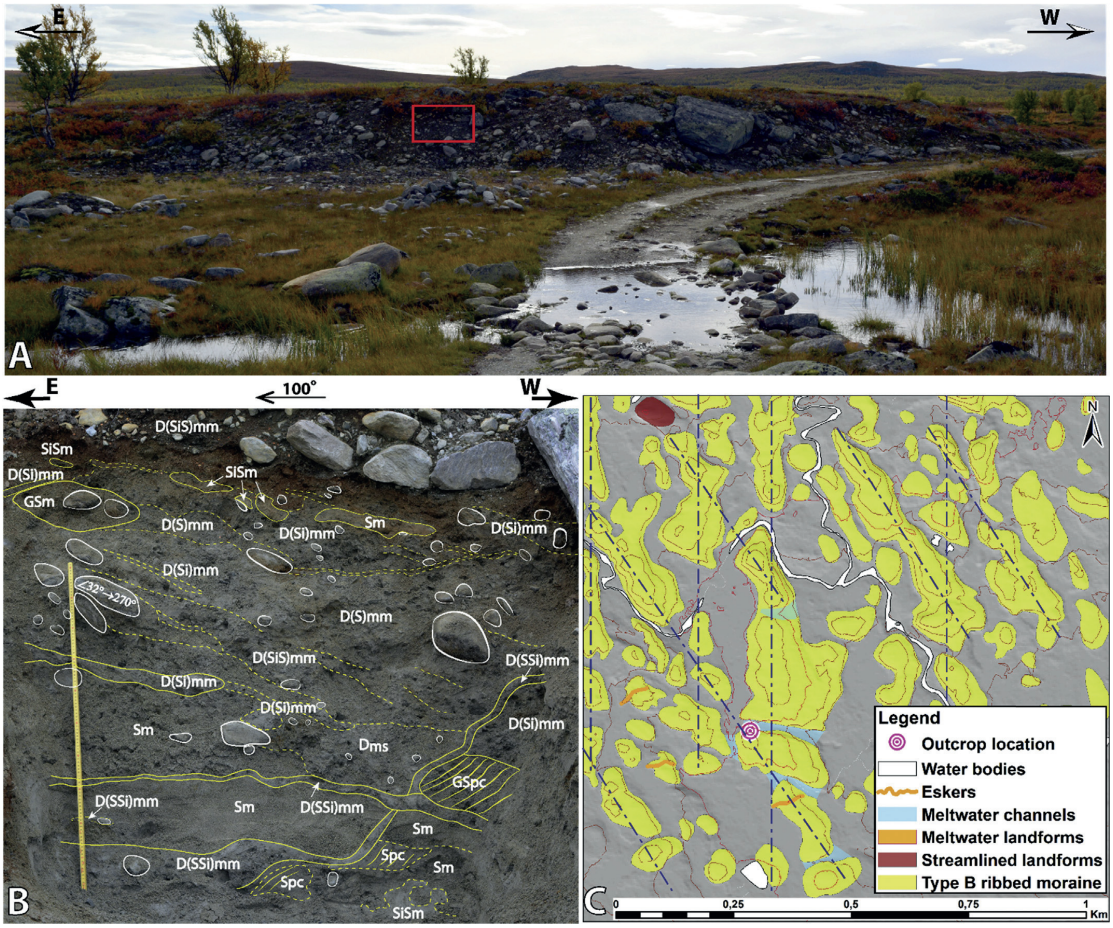

Fig. 4. Sediment outcrop at the proximal side of a moraine ridge near Haldorbu, in the Fjelldokka ribbed moraine belt. **A.** Overview photo of the outcrop. The outcrop is partly natural, located on the side of a meltwater channel. **B.** Close-up photo (scale 1 m) of investigated part of the outcrop (red box in A) with lithofacies (see Table 2). Stippled lines mark sediment boundaries and glaciotectonic features. Note the cross-cutting clastic dykes filled with sandy silty diamicton. **C.** Glacial landform map from the nearby area of the outcrop (2.5 m contour intervals). Note the eskers on top of and meltwater channels cross-cutting the identified ribbed moraine. Stippled lines mark the two orientations of the ribbed moraine ridges; see Fig. 2C for larger coverage area. (For interpretation of the references to colour in this figure legend, the reader is referred to the web version of this article.)

some correlations between identified landforms regarding the size, morphology and their overall location in the terrain, as well as spatial relations between streamlined landforms and ribbed moraine ridges. Both types of landforms indicate a dominant ice movement towards the SE at their formation.

There are two spatial distribution types of ribbed moraine (see also 4.1.2), broad fields (type A) and elongated ribbed moraine belts (type B). Type A ribbed moraine (broad fields) are occurring more sparsely and are generally located in open areas not constrained by the topographical conditions (Fig. 2D). Ribbed moraine of this type occurs at the same topographical level as the surrounding streamlined landforms. Type B ribbed moraine (belts) areas host the most pronounced ridges and are mainly found at lower hypsometric levels than the surrounding streamlined landforms (Fig. 2B and C, supplement no. 3). Ribbed moraines of this type are usually located in confined elevation lows (narrow valleys) that are often followed by an increasing slope gradient in ice flow direction. Ribbed moraine areas of both types are often followed by distinct and well-elongated (L/W ratio >3) streamlined landforms further down-flow (as seen distinctly in Fig. 2B). As noted in 4.1.1, the size and shape of streamlined landforms varies regarding their elevation in the terrain, and their divergence in orientation occurs at varying elevation heights (Fig. 2, supplement no. 2 and 3).

Both ribbed moraine ridges and streamlined landforms are often found in superposition, in some cases with diverging orientations and sometimes showing signs of re-molding. Found within the whole study area, although more abundant in the eastern part, are smaller streamlined landforms overlying other streamlined landforms with a different orientation indicating a change in ice flow direction (Figs. 2D and 3C). Some moraine ridges within type B areas are similarly found with diverging orientations (Fig. 4C). The streamlined landforms are often located in close association with ribbed moraines of both types, being more abundant within the ribbed moraine belts (type B). In these cases, the streamlined

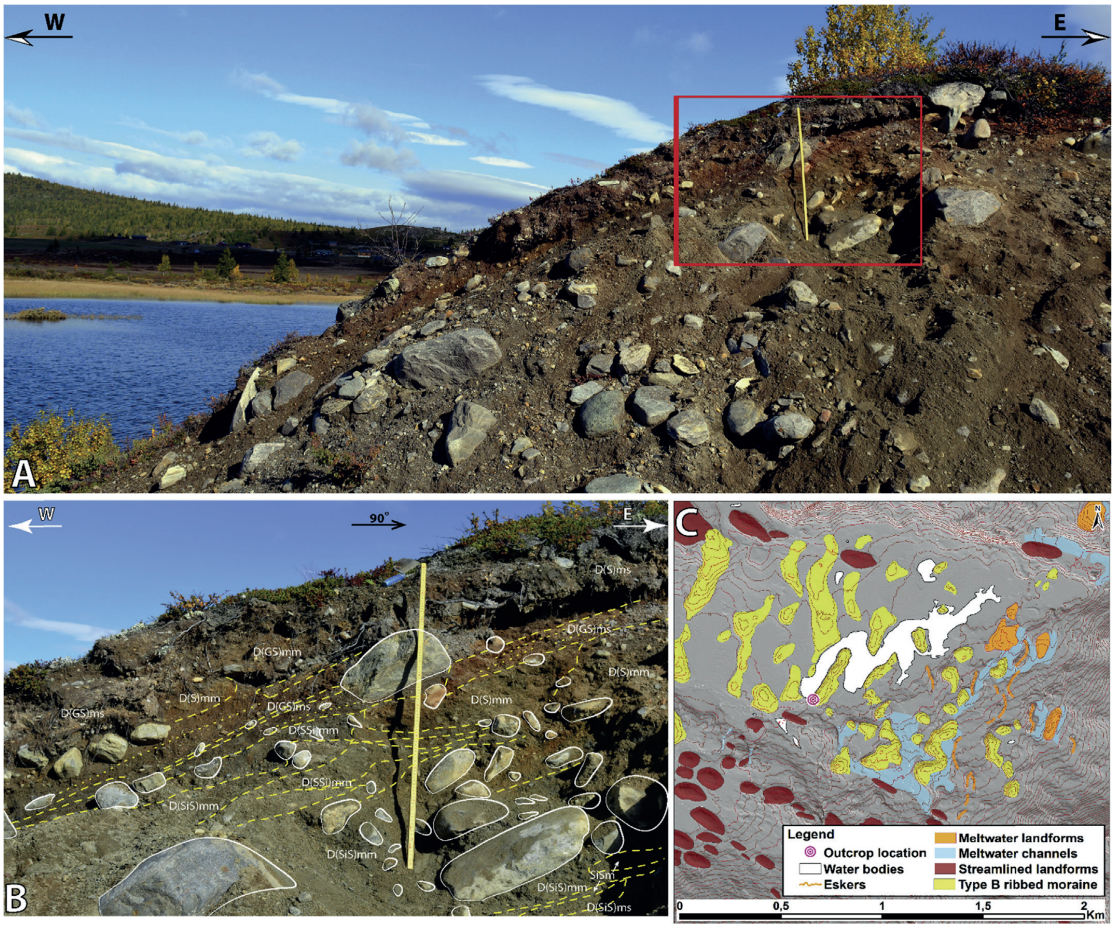

Fig. 5. Ribbed moraine ridge in the Trollåsen area. **A.** Overview photo of outcrop (scale 1 m), situated in proximal side of the landform. **B**. Close-up of investigated part (box in A) with identified lithofacies (see Table 2). Stippled lines mark sediment boundaries and glaciotectonic features. **C**. Glacial landform map of the nearby area (2.5 m contour intervals). Note the spatial relation between and orientation of identified ribbed moraine ridges and meltwater landforms, orientation of these ridges are similar indicating perpendicular direction of respectively ice flow and meltwater flow.

landforms are located either on top of the ribbed moraine ridge crests or in between them, and are usually small in size (IV in Fig. 2). We suggest that this morphostratigraphical relation shows a transition in landform build-up from transverse-to parallel-to-ice-flow as a continuous change with time at the same glacial events. In addition, we have also noticed the reverse – a transition from streamlined landforms into ribbed moraines at several localities, mainly within the broad fields of ribbed moraine (type A). Two types of morphostratigraphical relations are observed, deposition of moraine ridges on top of streamlined landforms (Figs. 2D and 3C) and a distinct fragmentation of streamlined landforms where the landform is converted into moraine ridge by re-shaping the bulk of landform (Fig. 2D close-up).

4.2. Meltwater landforms

Several meltwater landforms like meltwater channels, eskers, kames, deltas, and outwash fans (Table 1) are identified within the study area. Although this genetic group of landforms is not in the primary scope of this study, it is an important source of additional information in regards to deglaciation patterns of the study area. Identified meltwater landforms are often found on top of (eskers) or cross-cutting (meltwater channels) both ribbed moraine ridges and streamlined landforms (Figs. 2, 3C, 4C and 5C) suggesting that they were formed at a later stage than the glacial landforms, likely during the deglaciation of the area.

Two groups of distributional pattern of eskers are recognized, parallel (III(a) in Fig. 2) and transverse (III(b) in Fig. 2) to the general ice flow direction. Eskers of the first group usually form longer and more distinct systems, thus suggesting they evolved over a longer period of time, while the others form shorter systems and have more fragmented characteristics indicating shorter time of development. Judging from the morphology and location on the valley slopes, it is reasonable to assume that the transverse eskers (III(b) in Fig. 2A and D) were formed at the very last stages of deglaciation when dead ice was heavily crevassed, meltwater fluxes were high, and plenty of sediments were accessible (c.f. Garnes and Bergersen, 1980). Field observations suggest that some of these features (II in

Fig. 2C and D) formed in open supraglacial channels as crevasse fill as areal down wasting of the ice occurred.

Numerous eskers and meltwater channels have close spatial relations with each other (Fig. 2) suggesting a highly connected meltwater drainage system, and that there was a spatial evolution from a subglacial to proglacial environment. Most of the identified meltwater channels are lateral channels and reveal complex development during the deglaciation (Fig. 2, especially close-up Cii). When in close proximity to eskers, some of the meltwater channels have been found to be (a) continued by an esker (NW in Fig. 2B), (b) located downstream from an esker (N in Fig. 2A), or (c) contain esker features within the channel (Fig. 2D), thus having a clear subglacial origin at least for the initial part of the landform formation.

Often meltwater channels and eskers are in their distal downflow direction connected with deltas, outwash fans, or kames of various shapes and sizes. In some cases, like in the Fjelldokka valley, deltaic and outwash fan features are found close to the valley sides where their morphology appears similar to the nearby ribbed moraine (Figs. 2C and 5C). This suggests that these outwash fans were accumulated in ice crevasses in a very late phase, burying the underlying ribbed moraines. In other cases, as for Etne valley, outwash fans are deposited partly over and in between several ribbed moraine ridges (Fig. 2B and C), suggesting at least partly ice-free conditions.

4.3. Bedrock influence and striations

Bedrock topography has evidently a large influence on the depositional pattern of glacial sediments as a majority of the observed subglacial landforms and meltwater features in the study area are located either (sub-) parallel or transverse to the valley trends, that follow the structures and weakness zones of the bedrock. Hilltops have often acted as obstacles. Several locations of glacial striated bedrock are found in the study area. Although the direction of the measured striations varies locally, the ice flow direction dominantly indicated from striae is towards the SE and E. This is a general directional trend throughout the whole study area. Often the measured azimuths coincide with the orientation of the crests of streamlined landforms on which the striations are found (Fig. 6).

5. Flow patterns

In the study area, the orientation of identified streamlined landforms and ribbed moraine ridges (Fig. 7A) are the main indicators of former ice-flow direction, and therefore the primary basis for differentiating changes in the ice flow over time. The spatial and morphostratigraphical relations between these landforms, such as cross-cutting, overlying and reworked landforms (as seen in e.g. Figs. 2D, 3C and 4C), are subsequently used to reconstruct a sequence of flow patterns. For the latter we also used the altitudinal occurrence of these landforms in the terrain, as we consider landforms at higher altitudes to be older than those at the lower positions. This is based on that south-central Norway, including Gausdal Vestfjell, underwent a vertical thinning of the ice sheet during the deglaciation (Garnes and Bergersen, 1980; Sollid and Sørbel, 1994). Meltwater channels and eskers are here used as an additional information source for flow pattern reconstruction, especially for the later stages of flow prior to the deglaciation. The identified flow pattern within the study area (Fig. 7, supplement no. 2) is characterized by an overall tendency of diverting a general SSE oriented flow (phase I) into a more localized (phase II) flow towards the SE, which is then developed further into several superimposed channelized flows (phase III).

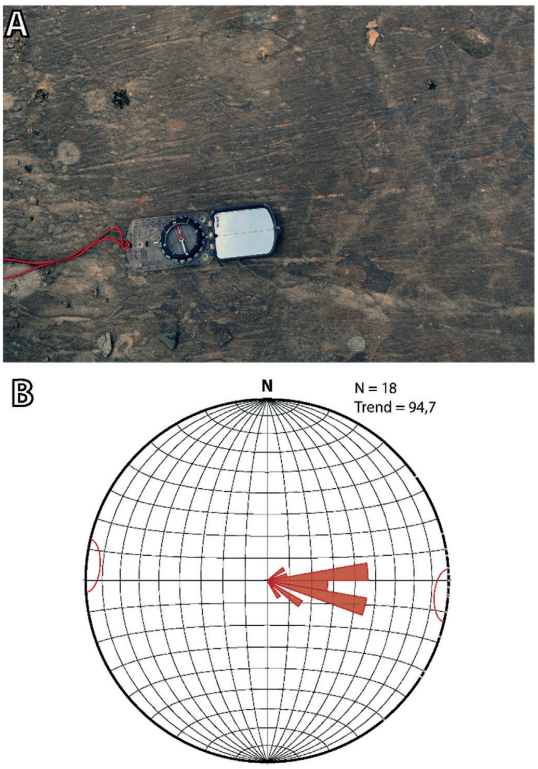

Fig. 6. Overview of bedrock striations within the study area. **A.** Striations on metasandstone outcrop from valley N of Synnfjell. **B.** Rose diagram of measured striation azimuths. See Fig. 2 for striae measurement locations.

Phase I or *the topographically independent phase* is the earliest glacial phase that is identified within the study area (Fig. 7B, supplement no. 2). It is represented by the streamlined landforms that are found at high elevation levels, on the erosional plateau hilltops as well as the hilltops on the northern border of the study area. This phase has a distinct signature of SSE ice flow direction.

The following phase – phase II, is called *the regional flow phase* due to its well-developed flow pattern (Fig. 7B, supplement no. 2). Most of the identified streamlined landforms represent this phase, and come in a large range of sizes. Broad fields of ribbed moraine (type A) are characteristic to this phase, and are overlying phase II streamlined landforms. Phase II has a very distinct SE flow direction pattern that coincides with the general elevation slope in the area.

The youngest identified phase is phase III, called *the channelized flow phase*, displaying an increased topography control over the ice flow (Fig. 7C, supplement no. 2). It is characterized by a landform-complex of ribbed moraines (type B), streamlined landforms and meltwater features. The ribbed moraine tends to cluster in belts, while other areas are dominated by distinctly elongated streamlined landforms as well as smaller streamlined landforms overlying ribbed moraine ridges (Figs. 2 and 7C, supplements no. 2 and 3). Parallel esker system are commonly found close to the onset of phase III flow sets. The geological record shows a complex sequence of events, where several substages are distinguished (Fig. 7C). We have to note that it is difficult to estimate the relative age relations between the different flow sets of phase III as overlying relation do

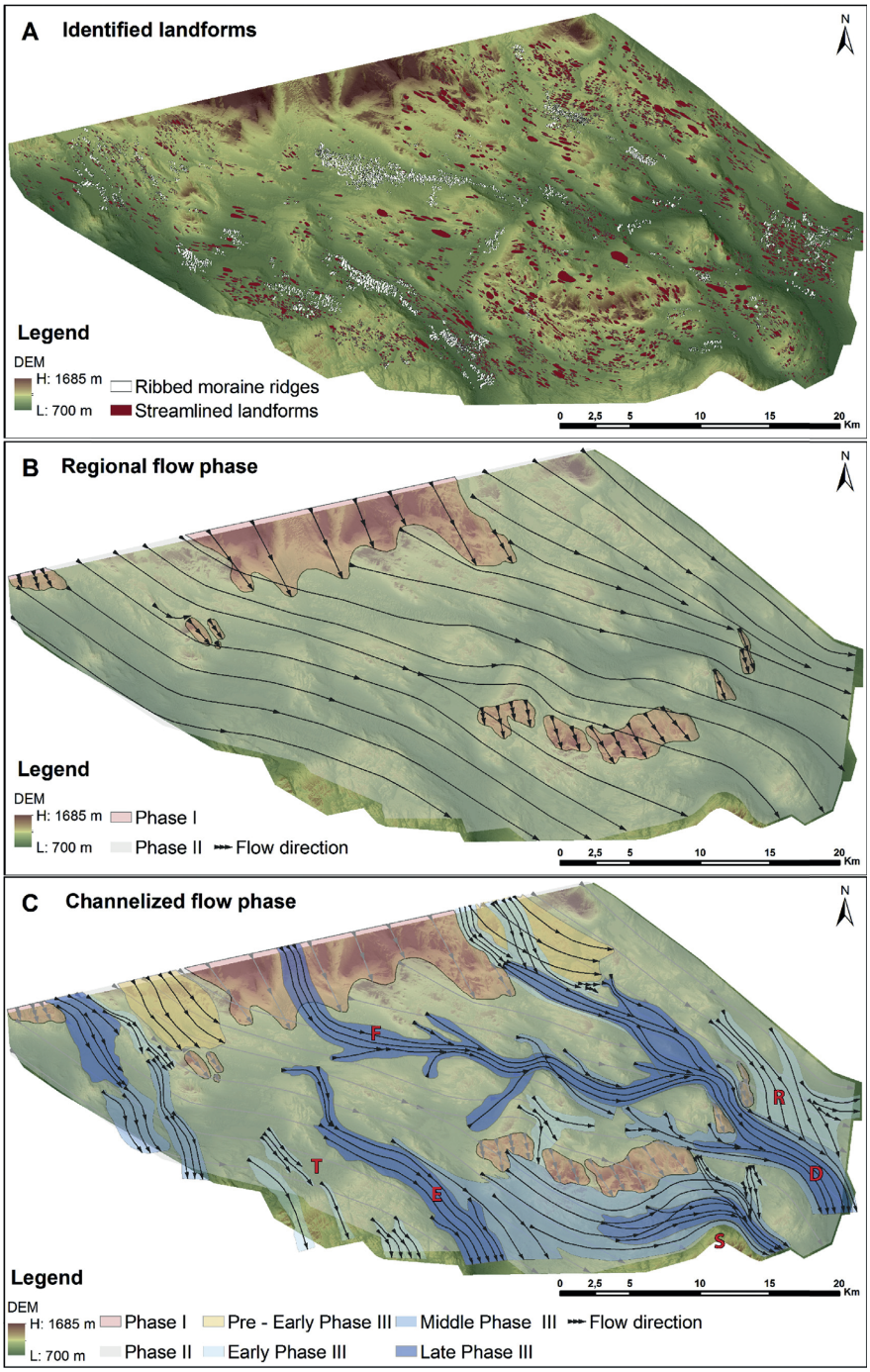

Fig. 7. Reconstructed ice flow pattern. **A.** Identified glacial landforms used for the flow pattern reconstructions. **B.** The early development of flow patterns (phase I and phase II) dominated by regional, topography-independent ice flow. **C.** Late-stage flow pattern (phase III and its substages) with channelized ice flow characteristics. For explanation, see text. Letters indicating place names mentioned in text: T – Trollåsen, F – Fjelldokka valley, E – Etne valley, S – Synnfjell, R – Reinsåsen, D – Dokka valley. See supplement no. 2 for a detailed map.

not exist in or between some areas. This is especially true for the western part of the study area as the flow pattern here belonged to the system in the Øystre Slidre valley (Figs. 1C and 7C), which is only partly covered in this study. Therefore, the distinguished substages of phase III are mainly based on observations from central and eastern part of the study area. In some areas, the flow sets are parallel and overlapping each other, making it hard to distinguishing them. Here we only mark the latest imprint of flow that are identified (Fig. 7C).

Streamlined landforms representing the pre-early phase III are identified in the northern part of the study area (Fig. 7C). From the mountain ridge, the flow sets widen and display a slightly divergent flow. These landforms are found in a close relation to landforms of phase II, but must be younger as they are overriding phase II landforms and have an offset in the flow direction with a more easterly orientation. The relative age estimation is further constrained as early phase III ice flow is found cross-cutting the pre-early phase III flow set located to the NE.

The flow patterns of early phase III are distinguished in several places and mainly at high elevations within the study area (Fig. 7C, supplement no. 2). The streamlined landforms found there are often small and less elongated, and tend to be directed downwards into the valleys where a distinct flow pattern of a younger age (middle phase III) is found, and partly cross-cutting. This suggests a continuous transition into flow pattern of the younger middle phase III.

The middle phase III flow sets are found at lower elevation levels than the features of the early phase III flow, and are characterized by streamlined landforms of various sizes with a few narrow ribbed moraine ridges that are overridden by smaller streamlined landforms. During the middle phase III substage, the main ice flow drainage in the eastern part occurred through the valley N of Synnfjell and the Fjelldokka – Dokka valley and its tributaries (Fig. 7C, supplement no. 2). The flow diverted into the deepest part of the valley, however, as the same route was also used after a gradual transition into the late phase III, it is difficult to differentiate between the middle and late substages in these areas. In the Fjelldokka – Dokka valley system, two ice flow patterns of middle phase III age are distinguished in different hypsometric levels, representing the early (wider flow set located higher up and is overriding the topographic obstacles) and late (flow set located lower in terrain and in lee side of topographic obstacles) parts of this substage. The flow system from Etne valley to the valley N of Synnfjell likely commenced at this substage, partly cross-cutting early phase III flow diverting into the valley.

The flow pattern of late phase III age is represented by the variety of streamlined landforms, ribbed moraine ridges and smaller streamlined landforms overlapping the ribbed moraine. These landforms are found in the lowest areas of the terrain, the valley floors, and it can be traced extensively through the whole study area (Fig. 7C, supplement no. 2). This includes the Fjelldokka – Dokka valley and its tributaries where it can be traced up to the northern mountain ridge, and the valley N of Synnfjell and Etne valley in southern part.

6. Discussion

6.1. Glacial development

The reconstructed ice flow sets in Gausdal Vestfjell show a general SE orientation of ice flow. Phases II and III (including all substages) display an increasing dependence on topography, becoming more and more confined to lower elevated areas as well as an increased interaction with meltwater features. None of the ice flow phases are dated, but due to the relatively fresh appearance and extensive preservations of the identified glacial landforms as well as the gradual transition development of phases II and III and the following deglaciation, we assume they are from Late Weichselian and the following deglaciation by down wasting. However, an older age of phase I cannot be excluded.

Phase I. Our phase I with topographically independent ice movement towards SSE is previously described as *the main phase* by Bergersen and Garnes (1972), and noted by Sollid and Sørbel (1994). It is a prerequisite to have had warm-based and sliding ice conditions under which the streamlined landforms formed. The ice sheet thickness must have been considerable to overcome the topographic obstacles as ice flowed over the mountain Skaget at an altitude of 1685 m a.s.l. This is in accordance with Mangerud (2004) and Olsen et al. (2013), reasoning that the ice thickness was >2000 m a.s.l. The FIS surface probably covered all the peaks in southern Norway (Goehring et al., 2008; Mangerud et al., 2011), although this has been debated (Mangerud et al., 2011; Nesje, 1992; Nesje et al., 1988). Olsen et al. (2013) argue that the LGM maximum ice thickness of western FIS was reached prior to 26 ka (LGM 1) when the ice divide was located at its western position (Fig. 1B). As phase I indicates the thickest ice over Gausdal Vestfjell and with an ice divide to the NW, it may represent this western FIS maximum. However, it is also possible that phase I is from a previous glaciation, at least some of the more bedrock-dominated landforms could have been formed cumulatively over several glaciations (cf. Fig. 3 in Fredin et al., 2013).

Phase II. The morphological features of Phase II (regional ice flow) consist of the majority of all identified streamlined landforms, including some of the largest and most elongated landforms. Their spatial orientations suggest a well-developed flow pattern following the general topography towards SE with some deflection around the higher mountain ridges (Fig. 7B). This points towards a relatively long-existing phase of warm-based ice as the most pronounced and elongated subglacial landforms are considered to have been formed during a longer period than smaller features (Fowler et al., 2013) and to a thinner ice, slightly more affected in its flow pattern by the underlying landscape. The onset of the vertical thinning in the Gausdal Vestfjell area may have occurred at the same time as at the mountain Blåhø (1617 m a.s.l.), situated ca. 70 km N of the study area, soon after 25.1 ± 1.0 ^{10}Be ka (Goehring et al., 2008). Several authors (e.g. Dahl et al., 2010; Mangerud, 2004; Olsen et al., 2013) have suggested that the ice surface lowering may have had a significant contribution of an active operating NCIS, effectively removing ice from the interior areas. If this is correct, then the lowering seen in phase II must have happened before ca. 17 ka at which time the Norwegian Channel was completely deglaciated (Sejrup et al., 2009).

Phase II with its abundance of streamlined landforms can be correlated to Phase 3 by Vorren (1977) and (together with phase III) to the *later inland phase* by Bergersen and Garnes (1972), characterized by its continuous shift of flow directions. Vorren (1977) suggested his Phase 3 represented the FIS maximum extent with an ice divide at its easternmost position (Fig. 2B). We consider a LGM age of phase II as plausible, however, there may have been (periods of) prevailing cold-based conditions beneath the ice divide during the LGM, similar to the cold-based preservation zones in central Sweden (e.g. Kleman et al., 1997). No positive indicators, such as block fields, are found in the study area although there are several nearby, slightly N and W of the late ice divide (Olsen et al., 2013). Phase II can possibly represent a later stage of the LGM, perhaps even closer in age to the deglaciation, in line with the apparently gradual transition from phases II to III and to the following down-wasting (Garnes and Bergersen, 1980). Irrespective of age, as phase II in Gausdal Vestfjell displays an unambiguous ice flow towards SE, the ice divide must have been to the NW. This

suggest that close to the study area, the ice divide was located at a more westerly position, at least as far W and N as possible within the late ice divide zone by Vorren (1977) (Fig. 1B). At some locations, the phase II streamlined landforms are overlaid by broad field type A ribbed moraines with the similar regional flow pattern (Figs. 2 and 3C). This depositional shift from streamlined landforms to ribbed moraine suggest that the ice velocity slowed down at the late part of phase II (Hall and Glasser, 2003).

Phase III. Many of the flow sets belonging to the channelized flow of phase III do not have a spatial overlap making it difficult to evaluate their temporal relation. Nevertheless, they have been divided into temporal substages (Fig. 7C) based on the criteria listed in Ch. 5. Those flow sets that do have overlapping features show a distinct development of being increasingly dependent on underlying topography as they become more and more constrained in low-lying areas and the deeper parts of the valleys. They also show an increasing diversion from a SE directed flow, probably draining a remaining ice dome in Jotunheimen. These changes are most likely due to the vertical thinning of ice. Some of the flow directions of phase III, as well as phase II, are confirmed by the observed trend of bedrock striations (Fig. 2). Phase III with channelized ice flow with its substages can also be correlated to the *later inland phase* by Bergersen and Garnes (1972) as well to Vorren's (1977) Phase 4 of Preboreal (Early Holocene) age. Vorren (1977) states that transition from his Phase 3 to Phase 4 was gradual, although with some definite halts (sub-phases), representing periods of stagnation and/or readvance during deglaciation. This corresponds well with our observations of the transitional evolution of our phase III and its substages.

The flow sets of pre-early and early phase III were probably active for only a relatively short time as they are characterized by relatively small streamlined landforms (Fowler et al., 2013) and are overlain by younger flow sets. The pre-early phase III flow sets show ice flowing from mountain passes in the N continuing on the flatter plateau with slight diverging directions. Most likely, these flow sets represent local changes in ice dynamics. Several of the early phase III flow sets indicate ice flowing from upland areas following the local topography downward to the larger valley systems. Such local changes characteristic for both pre-early and early phase III correspond well to the flow mode of the Nunatak phase by Garnes and Bergersen (1980). During this phase the ice surface is estimated to be at ca. 1500 m a.s.l. (Garnes and Bergersen, 1980), indicating a ca. 300 m thick ice flowing over the topographic highs within the study area. At some locations (e.g. Reinsåsen, Fig. 4C), the flow has partly modified the type A ribbed moraine from late phase II by depositing streamlined landforms on top. This suggest an increase ice velocity from late phase II to early phase III (c.f. Hättestrand and Kleman, 1999). The preservation of these early phase III flow sets where no traces of re-shaping are present indicates cold-based or at least less active ice existed in these areas afterwards, while the lower parts of the terrain served to accelerate ice flow and promote frictional heating beneath the ice (Hall and Glasser, 2003).

Similar to early phase III, the unambiguous features of middle phase III are only preserved in areas without younger ice flow. These are found along the valley sides at elevations higher than the late substage flow sets and in higher elevated SE-trending valleys. Some flow sets indicate that the ice at this time was thick enough to flow up-hill where the difference in altitude is ca. 90 m. In the late substage, ice must have been thinner as it was flowing around obstacles, following the underlying topography. Ice flow in the larger valleys occurred both during the middle and late substages (likely started already during the early substage), providing long enough time for formation of the large glacial bedforms found on the valley floors. In the Fjelldokka – Dokka valley and the Etne – Synnfjell area, the ice flow sets of middle and late substages reveal cross-cutting flow in the middle part and similar flow direction in the lower part of the valleys, supporting the idea of an inward migrating onset of ice flow. We correlate our middle and late substages with the Krusgrav deglacial phase by Garnes and Bergersen (1980) with flow following the Fjelldokka – Dokka valley system. At this phase, ice surface was ca. 1100 m a.s.l. (Garnes and Bergersen, 1980), indicating a ca. 200 m thick ice for the up-hill flow of middle substage.

The largest belts of ribbed moraine (type B) are located in the upstream part of the phase III flow sets, while the downstream parts are dominated by streamlined landforms (Fig. 7). Variations of thermal conditions within the same flow set may be the reason for this uneven distribution, possibly reflecting different periods from onset to ceasing of an active flow. The type B ribbed moraines are at several places overlain by small streamlined landforms, often displaying same flow direction. This suggests close temporal relations between the landforms, as well as a transition from sluggish to fast-flow conditions (Hättestrand and Kleman, 1999). As mentioned above, the higher elevated areas surrounding these flow sets where likely covered by cold-based or less active ice, with no significant deposition of subglacial bedforms. Probably the higher peaks were ice-free as the ice surface lowered (c.f. Garnes and Bergersen, 1980).

Esker systems parallel to ice flow (III(a) in Figs. 2 and 8B, supplement no. 2 and 3) are mainly found on the valley sides and close to the onset zones of phase III flow. This indicates that they acted as conduits feeding subglacial meltwater into the valleys where ice flow occurred, affecting the ice flow dynamics. Such spatial relations are in an accordance with the inwards migrating thermal boundary described by Hättestrand and Kleman (1999). They also point to close association to the deglaciation, althougth it cannot be excluded that the eskers might have formed later. The substages of phase III, especially the late phase III substage, indicate that the ice flow was active for the last time prior to the switch to stagnant conditions and the following deglaciation by vertical down-melting of the ice (Garnes and Bergersen, 1980). The latter is identified by the abundances of lateral meltwater channels and other meltwater features as transverse eskers (Fig. 2), interpreted as indicative of crevassed, stagnant ice from the last stages of deglaciation. Such meltwater features are occasionally found in close spatial relations to ribbed moraines of the phase III flow pattern. The distribution pattern of meltwater channels confirms the down-wasting mode of the deglaciation, as described by Garnes and Bergersen (1980) and Sollid and Sørbel (1994). Garnes and Bergersen (1980) suggested a deglaciation occurred around 9000 ^{14}C years ago (ca. 10 ka) in the neighboring valleys Espedalen and Vestre Gausdal, and similar ages can be expected for Gausdal Vestfjell area.

General development. The abundance of soft-sediment bedforms, points to widespread warm-based conditions for at least at some stages during the last glacial period. This do not exclude periods with cold-based ice as warm-based conditions may have large landscape imprint (cf. Landvik et al., 2014). The observed spatial relations between the glacial landforms in our study area support the suggestion that streamlined landforms and ribbed moraine represent a continuum of landform formation process along the ice-bed interface (e.g. Aario, 1977; Rose, 1987; Everest et al., 2005; Stokes et al., 2013; Ely et al., 2016), and thus a bedform system (Stokes and Clark, 1999, 2001; Clark and Stokes, 2003).

Development of the ice flow phases and their associated landforms, suggests a gradual lowering of the ice surface with increased topographical control. Transition from phases II to III was gradual, as seen by the configuration of flows and the difference between types of ribbed moraine characteristics for phase II and phase III (discussed below). This suggests that the regional ice flow became

slower (Hättestrand and Kleman, 1999) and then reorganized into faster, active flow in the valleys during phase III (Fig. 7C), probably an effect of the transition to channelized flow. This topographically constrained ice-flow of phase III corresponds well with the concept of a 'local flow style' as described by Landvik et al. (2014). At the same time, higher elevated areas became increasingly less active, probably with cold ice preserving older flow set, and eventually ice free (Garnes and Bergersen, 1980). Close spatial distribution of meltwater features with phase III landforms suggest a gradual transition to the deglaciation.

6.2. Ribbed moraines - implications on glacial dynamics

The ribbed moraines identified in this study are assigned to type A (broad fields) ribbed moraine from regional flow phase II and to type B (belts) ribbed moraine from the channelized flow phase III. The reason for this division is probably only related to the topography and the vertical thinning of ice. Type A ribbed moraine is typically only found on plateaus yielding enough space for a wide distribution of moraine ridges and limiting the active ice flow to phase III. Whereas, type B is scattered throughout the whole study area, although commonly found in topographic lows, i.e. in areas with less space and active phase III ice flow. It cannot be excluded that some of the type B ribbed moraine ridges may have initiated during phase II or at the transition to phase III. The varying locations of the ribbed moraine, from high plateaus to low-lying valleys, connect these to different phases and substages (Fig. 7). Thus, suggest that the formation of ribbed moraine ridges occurred at different times, probably at the transition from phase II to III and at the late substage of phase III.

The formation of ribbed moraine is widely discussed, and numerous theories exist. Important factors proposed for the formation includes substrate characteristics, subglacial hydrology, ice velocity and flow conditions, and transition from cold-to warm-based conditions (Trommelen et al., 2014, and references therein). Dunlop and Clark (2006b) propose a single unifying theory should be sought to explain their genesis, whereas others (e.g. Kurimo, 1980; Finleyson and Bradwell, 2008; Möller, 2005; Möller and Dowling, 2015; Möller et al., 2016) suggest that ribbed moraine as geomorphic term should be seen as a polygenetic landform group. Though the formation mechanisms of ribbed moraine are uncertain, it is commonly agreed that they are formed subglacially under slow and sluggish ice-flow conditions (e.g. Aario, 1977; Dunlop et al., 2008; Hättestrand, 1997; Hättestrand and Kleman, 1999; Lindén et al., 2008; Möller, 2005; Sollid and Sørbel, 1994; Sarala, 2006; Stokes et al., 2008; Trommelen et al., 2014).

Within the framework of this paper, the question is whether the occurrence of ribbed moraine represents an ice-flow stage of acceleration or deceleration in ice. Hättestrand and Kleman (1999) suggested that as cold-to warm-based conditions migrated inwards, ribbed moraine formed during ice-flow acceleration. Observations in line with this are (a) distinctly elongated streamlined

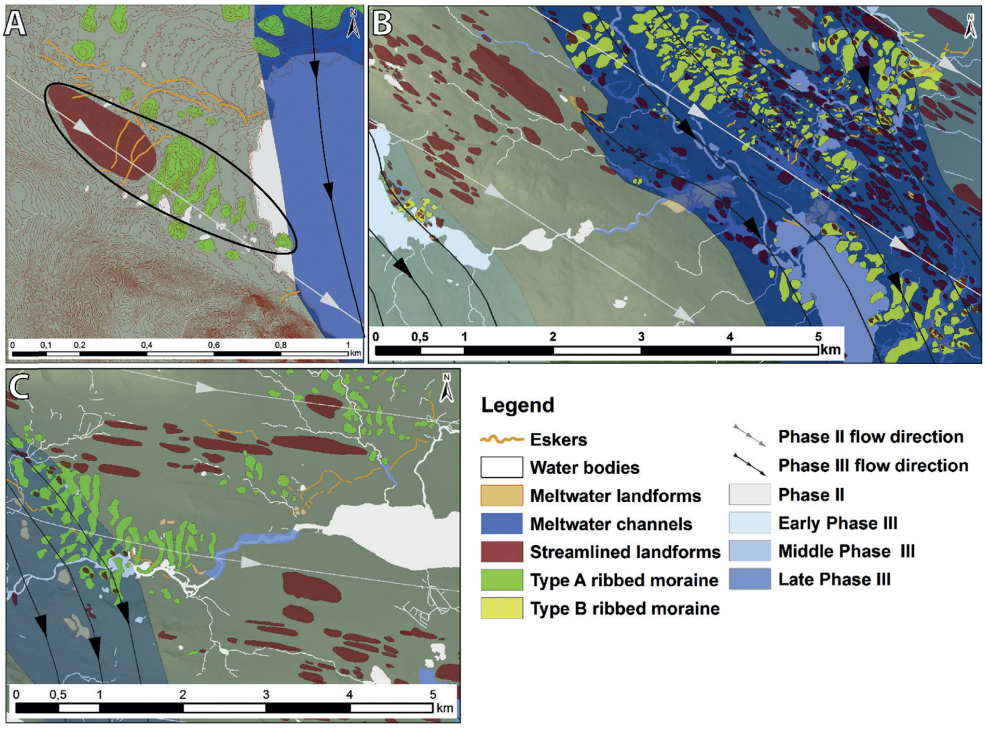

Fig. 8. Glacial landforms plotted on reconstructed ice flow sets (details from Fig. 7), showing examples of ribbed moraine formation in connection to the slowdown of the regional ice flow (phase II). **A.** Previous streamlined landform (outlined in black) reworked into ribbed moraines in downstream (eastern) part. Both bedforms belong to phase II. Map excerpt from the western part of study area (0.5 m contour intervals). **B.** Ribbed moraine overlain by streamlined landforms in Etne valley. Small overlying streamlined landforms are of late phase III age. **C.** Streamlined terrain and ribbed moraine fields of phase II located close to Lake Yddin. They are partly affected by the younger phase III flow as seen by overlying small streamlined landforms and re-orientation of some ribbed moraine ridges.

landforms accompanying the ribbed moraine ridges in the down-flow direction (Fig. 2B), (b) streamlined landforms on top of ribbed moraine ridges (Figs. 2, 3C and 8) and (c) rotation of ridge-crest to subparallel alignment to the latest flow direction (Figs. 4C and 8C). Such relations are commonly found in our study area, more often within ribbed moraine belts (type B) in the low-lying valleys sloping in same direction as the ice flow. This morphological setting may have contributed to the increase in flow velocity (Dunlop et al., 2008).

Observations supporting a decelerating ice flow are (a) re-worked streamlined landforms into ribbed moraine ridges (Fig. 2D close-up and 8A) and (b) ribbed moraine ridges on top of streamlined landforms (Fig. 2D close-up and 3C) ice flow (Dunlop et al., 2008). These observations are all found within phase II flow, including the streamlined terrain and ribbed moraines in the Reinsåsen area (Fig. 2D close-up, 3C and 7C). Here, the ribbed moraine ridges lie on top of streamlined landforms or are reworked from original streamlined landforms. Deposited on top of these two bedforms are small-scale streamlined landforms belonging to phase III. From this spatial pattern at Reinsåsen, it is evident that the ribbed moraine ridges could have formed close to or during the final stage of phase II. At this time the regional ice flow must have gradually slowed down, possibly due to the stiffening of the bed, either through meltwater drainage or change in thermal regime (c.f. Stokes et al., 2013).

In the Trollåsen area (Figs. 2C and 5), ice was flowing uphill in the narrow, confined valley, crossing over a pass into the lower-lying Etne valley during phase II. Similar constrained and uphill flow of ice is observed in other parts of the study area (e.g. in W of Fig. 8C). These topographical conditions are favorable for compressional (and decelerating) ice flow with shear and stack processes (e.g. Lindén et al., 2008; Stokes et al., 2008), and was probably the driving mechanism for formation of the ribbed moraine field here. Such compressional conditions must have produced excess of subglacial meltwater that likely drained through a meltwater channel, initially subglacial, from Trollåsen to Etne valley (close-up in Fig. 2C), and as elsewhere feeding the subglacial drainage system. This provided additional meltwater input to Etne valley, and such water-rich conditions must have affected the formation of ribbed moraines here. Moreover, the spatial distribution of parallel esker systems in the whole study area suggests high input of subglacial meltwater close to type B ribbed moraines. Therefore, we admit the connection between ribbed moraine formation and meltwater occurrence, and to some limited extent, agree on Sollid and Sørbel's (1994) interpretations that ribbed moraines are formed in areas with isolated patches of subglacial water bodies.

7. Conclusions

The extensive mapping of spatial distribution pattern of glacial landforms carried out during this study, has revealed new insight on the development of ice flow pattern and ice flow dynamics during the Late Weichselian within the inner areas of the Fenno-scandian Ice Sheet.

- The reconstructed flow pattern reveals a stepwise evolution where the *topographically independent flow (phase I)* with the maximum ice sheet thickness succeeded by the *regional flow (phase II)*.
- Following a gradual transition is the *channelized flow (phase III)* with several substages, prior to the complete deglaciation by a vertical wastage meltdown. The flow sets in phase III reflect gradually stronger dependence on topography. Cold-based or less active ice conditions prevailed between the flow sets.
- Esker systems parallel to ice flow likely fed the subglacial drainage network within the valleys during phase III, while transverse esker systems probably formed in crevasses of dead ice during the late stages of deglaciation.
- All of the identified flow phases show unambiguous ice flow towards the SE, thus the ice divide must have been to the NW. This suggests that close to the study area, the ice divide was located at a more westerly position, at least as far W and N as possible within the late ice divide zone by Vorren (1977).
- Ribbed moraine formation can occur both when the ice flow slows down (identified by various re-worked streamlined landforms and ribbed moraine ridges on top of streamlined landforms) and speeds up (ribbed moraine ridges overlaid by streamlined landforms, both belonging to phase III). This implies that the 'ribbed moraine' should be regarded as a geomorphic term used for a polygenetic landform group (identifying transverse-to-ice-flow ridges), and the landforms of this group are a subject to the principles of equifinality. Further, ribbed moraine formation seems to have occurred prior to the latest stages of phase II (by deceleration) and of phase III (by acceleration).

Acknowledgements

The authors would like to thank Jon Landvik for valuable input and discussion, Leif Vidar Jakobsen, Håvard Tveite and Sverre Anmarkrud for the technical support, the Norwegian Mapping Authority (Kartverket) for providing the LiDAR data set and Renata Lapinska-Viola (NGU) for helping on acquiring additional data sets of the study area. Thanks to the reviewers Sarah Greenwood and Per Möller for their constructive comments. The fieldwork was funded by NMBU-project TverrForsk.

Appendix A. Supplementary data

Supplementary data related to this article can be found at http://dx.doi.org/10.1016/j.quascirev.2017.03.008.

References

Aario, R., 1977. Classification and terminology of morainic landforms in Finland. Boreas 6, 87–100.
Bergersen, O.F., Garnes, K., 1971. Evidence of sub-till sediments from a Weichselian interstadial in the Gudbransdalen valley, central East Norway. Nor. Geol. Tidsskr. 25, 99–108.
Bergersen, O.F., Garnes, K., 1972. Ice movements and till stratigraphy in the Gudbransdal area. Preliminary results. Nor. Geol. Tidsskr. 26, 1–16.
Bergersen, O.F., Garnes, K., 1981. Weichselian in central South-Norway - the Gudbransdal interstadial and the following glaciation. Boreas 10, 315–322.
Bergersen, O.F., Garnes, K., 1983. Glacial deposits in the culmination zone of the Scandinavian ice sheet. In: Ehlers, J. (Ed.), Glacial deposits in North-West Europe. Balkema, Rotterdam, pp. 29–40.
Böse, M., Luthgens, C., Lee, J.R., Rose, J., 2012. Quaternary glaciations of northern Europe. Quat. Sci. Rev. 44, 1–25.
Boulton, G., Hagdorn, M., 2006. Glaciology of the British Isles Ice Sheet during the last glacial cycle: form, flow, streams and lobes. Quat. Sci. Rev. 25, 3359–3390.
Briner, J.P., 2007. Supporting evidence from the New York drumlin field that elongate subglacial bedforms indicate fast ice flow. Boreas 36, 143–147.
Carlson, A.B., Sollid, J.L., 1979. Fullsenn, kvartærgeologisk kart 1717 III - 1:50 000. Norges geologiske undersøkelse, Trondheim.
Carlson, A.B., Sollid, J.L., 1983. Fullsenn. Beskrivelse til kvartærgeologisk kart 1717 III – M 1:50 000 Norges geologiske undersøkelse, vol. 390, pp. 1–35. Trondheim.
Clark, C.D., 1993. Mega-scale glacial lineations and cross-cutting ice-flow landforms. Earth Surf. Process. Landf. 18, 1–29.
Clark, C.D., 1997. Reconstructing the evolutionary dynamics of former ice sheets using multi-temporal evidence, remote sensing and GIS. Quat. Sci. Rev. 16, 1067–1092.
Clark, C.D., Hughes, A.L.C., Greenwood, S.L., Jordan, C., Sejrup, H.P., 2012. Pattern and timing of retreat of the last British-Irish ice sheet. Quat. Sci. Rev. 44, 112–146.
Clark, C.D., Stokes, C.R., 2003. Palaeo-ice stream landsystem. In: Evans, D.J.A. (Ed.), Glacial Landsystems. Hodder Arnold, London.
Dahl, S.O., Linge, H., Fabel, D., Murray, A.S., 2010. Extent and timing of the

scandinavian ice sheet during late Weichselian (MIS3/2) glacier maximum in central southern Norway—link to the Norwegian Channel Ice stream? Abstr. Proc. Geol. Soc. Nor. 1–2010, 37–38.
Damsgaard, A., Egholm, D.L., Piotrowski, J.A., Tulaczyk, S., Larsen, N.K., Brædstrup, C.F., 2015. A new methodology to simulate subglacial deformation of water-saturated granular material. Cryosphere 9, 2183–2200.
Dunlop, P., Clark, C.D., 2006a. Distribution of ribbed moraine in the Lac Naococane region, central Québec, Canada. J. Maps 2, 59–70.
Dunlop, P., Clark, C.D., 2006b. The morphological characteristics of ribbed moraine. Quat. Sci. Rev. 25, 1668–1691.
Dunlop, P., Clark, C.D., Hindmarsh, R.C.A., 2008. Bed ribbing instability explanation: testing a numerical model of ribbed moraine formation arising from coupled flow of ice and subglacial sediment. J. Geophys. Res. Earth Surf. 113.
Ely, J.C., Clark, C.D., Spagnolo, M., Stokes, C.R., Greenwood, S.L., Hughes, A.L.C., Dunlop, P., Hess, D., 2016. Do subglacial bedforms comprise a size and shape continuum? Geomorphology 257, 108–119.
Evans, D.J.A., Phillips, E.R., Hiemstra, J.F., Auton, C.A., 2006. Subglacial till: formation, sedimentary characteristics and classifications. Earth Sci. Rev. 78, 115–176.
Everest, J., Bradwell, T., Golledge, N., 2005. Subglacial landforms of the Tweed palaeo-ice stream. Scott. Geogr. J. 121, 163–173.
Eyles, N., Eyles, C.H., Miall, A.D., 1983. Lithofacies types and vertical profile models - an alternative approach to the description and environmental interpretation of glacial diamict and diamictite sequences. Sedimentology 30, 393–410.
Finlayson, A.G., Bradwell, T., 2008. Morphological characteristics, formation and glaciological significance of Rogen moraine in northern Scotland. Geomorphology 101, 607–617.
Fowler, A.C., Spagnolo, M., Clark, C.D., Stokes, C.R., Hughes, A.L.C., Dunlop, P., 2013. On the size and shape of drumlins. Int. J. Geomath. 4, 155–165. http://dx.doi.org/10.1007/s13137-013-0050-0.
Fredin, O., Bergstrøm, B., Eilertsen, R., Hansen, L., Longva, O., Nesje, A., Sveian, H., 2013. Glacial landforms and Quaternary landscape development in Norway. In: Olsen, L., Fredin, O., Olesen, O. (Eds.), Quaternary Geology of Norway, vol. 13. Geological Survey of Norway Special Publication, pp. 5–25.
Garnes, K., Bergersen, O.F., 1977. Distribution and genesis of tills in central South Norway. Boreas 6, 135–147.
Garnes, K., Bergersen, O.F., 1980. Wastage features of the inland ice sheet in central South Norway. Boreas 9, 251–269.
Goehring, B.M., Brook, E.J., Linge, H., Ralsbeck, G.M., Yiou, F., 2008. Beryllium-10 exposure ages of erratic boulders in southern Norway and implications for the history of the Fennoscandian Ice Sheet. Quat. Sci. Rev. 27, 320–336.
Greenwood, S.L., Clark, C.D., 2009a. Reconstructing the last Irish Ice Sheet 1: changing flow geometries and ice flow dynamics deciphered from the glacial landform record. Quat. Sci. Rev. 28, 3085–3100.
Greenwood, S.L., Clark, C.D., 2009b. Reconstructing the last Irish Ice Sheet 2: a geomorphologically-driven model of ice sheet growth, retreat and dynamics. Quat. Sci. Rev. 28, 3101–3123.
Greenwood, S.L., Clark, C.D., Hughes, A.L.C., 2007. Formalising an inversion methodology for reconstructing ice-sheet retreat patterns from meltwater channels: application to the British Ice Sheet. J. Quat. Sci. 22, 637–645.
Hall, A.M., Glasser, N.F., 2003. Reconstructing the basal thermal regime of an ice stream in a landscape of selective linear erosion: glen Avon, Cairngorm Mountains, Scotland. Boreas 32, 191–207.
Hättestrand, C., 1997. Ribbed moraines in Sweden - distribution pattern and palaeoglaciological implications. Sediment. Geol. 111, 41–56.
Hättestrand, C., Kleman, J., 1999. Ribbed moraine formation. Quat. Sci. Rev. 18, 43–61.
Heim, M., Schärer, U., LMilnes, G., 1977. The nappe complex in the Tyin-Bygdin-Vang region, central southern Norway. Nor. Geol. Tidsskr. 57, 171–181. Oslo.
Hubbard, A., Bradwell, T., Golledge, N., Hall, A., Patton, H., Sugden, D., Cooper, R., Stoker, M., 2009. Dynamic cycles, ice streams and their impact on the extent, chronology and deglaciation of the British-Irish ice sheet. Quat. Sci. Rev. 28, 758–776.
Hughes, A.L.C., Clark, C.D., Jordan, C.J., 2014. Flow-pattern evolution of the last British ice sheet. Quat. Sci. Rev. 89, 148–168.
Hughes, A.L.C., Gyllencreutz, R., Lohne, Ø.S., Mangerud, J., Svendsen, J.I., 2016. The last Eurasian ice sheets – a chronological database and time-slice reconstruction, DATED-1. Boreas 45, 1–45.
Kleman, J., Glasser, N.F., 2007. The subglacial thermal organisation (STO) of ice sheets. Quat. Sci. Rev. 26, 585–597.
Kleman, J., Hättestrand, C., Borgstrom, I., Stroeven, A., 1997. Fennoscandian palaeoglaciology reconstructed using a glacial geological inversion model. J. Glaciol. 43, 283–299.
Knight, J., 2010. Basin-scale patterns of subglacial sediment mobility: implications for glaciological inversion modelling. Sediment. Geol. 232, 145–160.
Knight, J., 2011. Subglacial processes and drumlin formation in a confined bedrock valley, northwest Ireland. Boreas 40, 289–302.
Kurimo, H., 1980. Depositional deglaciation forms as indicators of different glacial and glaciomarginal environments. Boreas 9, 179–191.
Landvik, J.Y., Alexanderson, H., Henriksen, M., Ingólfsson, Ó., 2014. Landscape imprints of changing glacial regimes during ice-sheet build-up and decay: a conceptual model from Svalbard. Quat. Sci. Rev. 92, 258–268.
Larsen, N.K., Piotrowski, J.A., 2003. Fabric pattern in a basal till succession and its significance for reconstructing subglacial processes. J. Sediment. Res. 73, 725–734.
Le Heron, D.P., Etienne, J.L., 2005. A complex subglacial clastic dyke swarm, Sólheimajökull, southern Iceland. Sediment. Geol. 181, 25–37.
Lindén, M., Möller, P., Adrielsson, L., 2008. Ribbed moraine formed by subglacial folding, thrust stacking and lee-side cavity infill. Boreas 37/1, 102–131.
Mangerud, J., 2004. Ice Sheet Limits on Norway and the Norwegian Continental Shelf, Developments in Quaternary Science. Elsevier, pp. 271–294.
Mangerud, J., Gyllencreutz, R., Lohne, Ø., Svendsen, J.I., 2011. Glacial history of Norway. In: Ehlers, J., Gibbard, P.L., Hughes, P.D. (Eds.), Developments in Quaternary Sciences. Elsevier, pp. 279–298.
Mangerud, J., Larsen, E., Longva, O., Sønstegaard, E., 1979. Glacial history of western Norway 15,000-10,000 BP. Boreas 8, 179–187.
Möller, P., 2005. Rogen moraine: an example of glacial reshaping of pre-existing landforms. Quat. Sci. Rev. 25, 362–389.
Möller, P., Dowling, T.P.F., 2015. The importance of thermal boundary transitions on glacial geomorphology; mapping of ribbed/hummocky moraine and streamlined terrain from LiDAR, over Småland, South Sweden. GFF 137 (4), 452–283.
Möller, P., Dowling, T.P.F., Cleland, C., Johnson, M.D., 2016. On the issue of equifinality in glacial geomorphology. Geophys. Res. Abstr. 18, EGU2016–13626. EGU General Assembly 2016.
Nesje, A., 1992. Geometry, thickness and isostatic loading of the Late Weichselian Scandinavian ice sheet. Nor. Geol. Tidsskr. 72, 271–273.
Nesje, A., Dahl, S.O., Anda, E., Rye, N., 1988. Block fields in southern Norway: Significance for the Late Weichselian ice sheet. Nor. Geol. Tidsskr. 68, 149–169.
Nickelsen, R.P., 1988. Fullsenn 1717 III, berggrunnskart M 1:50 000. Norges Geol. Unders.
Olsen, L., 1985. Weichselian till stratigraphy in the Lillehammer area, southeast Norway. Nor. Geol. Unders. 401, 59–81.
Olsen, L., Sveian, H., Bergstrøm, B., Ottesen, D., Rise, L., 2013. Quaternary glaciations and their variations in Norway and on the Norwegian continental shelf. In: Olsen, L., Fredin, O., Olesen, O. (Eds.), Quaternary Geology of Norway, vol. 13. Geological Survey of Norway Special Publication, pp. 27–78.
Ottesen, D., Dowdeswell, J.A., Rise, L., 2005. Submarine landforms and the reconstruction of fast-flowing ice streams within a large Quaternary ice sheet: the 2500-km-long Norwegian-Svalbard margin (57°–80°N). Geol. Soc. Am. Bull. 117, 1033–1050.
Roberts, D.H., Long, A.J., 2005. Streamlined bedrock terrain and fast ice flow, Jakobshavns Isbrae, West Greenland: implications for ice stream and ice sheet dynamics. Boreas 34, 25–42.
Rose, J., 1987. Drumlins as part of a glacier bedform continuum. In: Menzies, J., Rose, J. (Eds.), Drumlin Symposium. Balkema, Rotterdam, pp. 103–116.
Ross, M., Campbell, J.E., Parent, M., Adams, R.S., 2009. Palaeo-ice streams and the subglacial landscape mosaic of the North American mid-continental prairies. Boreas 38, 421–439.
Sarala, P., 2006. Ribbed moraine stratigraphy and formation in southern Finnish Lapland. J. Quat. Sci. 21, 387–398.
Sejrup, H.H., Nygård, A., Hall, A.M., Haflidason, H., 2009. Middle and late Weichselian (Devensian) glaciation history of south-western Norway, North sea and eastern UK. Quat. Sci. Rev. 28, 370–380.
Siedlecka, A., Nystuen, J.P., Englund, J.O., Hossack, J., 1987. Lillehammer- Berggrunnskart M. 1:250 000. Norges geologiske undersøkelse, Trondheim.
Sollid, J.L., Sørbel, L., 1994. Distribution of glacial landforms in southern Norway in relation to the thermal regime of the last continental ice sheet. Geogr. Ann. Ser. A Phys. Geogr. 76, 25–35.
Spagnolo, M., Clark, C.D., Ely, J.C., Stokes, C.R., Anderson, J.B., Andreassen, K., Graham, A.G.C., King, E.C., 2014. Size, shape and spatial arrangement of mega-scale glacial lineations from a large and diverse dataset. Earth Surf. Process. Landf. 39, 1432–1448.
Spagnolo, M., Clark, C.D., Hughes, A.L.C., 2012. Drumlin relief. Geomorphology 153–154, 179–191.
Stokes, C.R., Clark, C.D., 1999. Geomorphological criteria for identifying Pleistocene ice streams. Ann. Glaciol. 28, 67–75.
Stokes, C.R., Clark, C.D., 2001. Palaeo-ice streams. Quat. Sci. Rev. 20, 1437–1457.
Stokes, C.R., Lian, O.B., Tulaczyk, S., Clark, C.D., 2008. Superimposition of ribbed moraines on a palaeo-ice-stream bed: implications for ice stream dynamics and shutdown. Earth Surf. Process. Landf. 33, 593–609.
Stokes, C.R., Spagnolo, M., Clark, C.D., 2011. The composition and internal structure of drumlins: complexity, commonality, and implications for a unifying theory of their formation. Earth Sci. Rev. 107, 398–422.
Stokes, C.R., Spagnolo, M., Clark, C.D., Ó Cofaigh, C., Lian, O.B., Dunstone, R.B., 2013. Formation of mega-scale glacial lineations on the Dubawnt Lake Ice Stream bed: 1. size, shape and spacing from a large remote sensing dataset. Quat. Sci. Rev. 77, 190–209.
Svendsen, J.I., Alexanderson, H., Astakhov, V.I., Demidov, I., Dowdeswell, J.A., Funder, S., Gataullin, V., Henriksen, M., Hjort, C., Houmark-Nielsen, M., Hubberten, H.W., Ingolfsson, O., Jakobsson, M., Kjaer, K.H., Larsen, E., Lokrantz, H., Lunkka, J.P., Lysa, A., Mangerud, J., Matiouchkov, A., Murray, A., Moller, P., Niessen, F., Nikolskaya, O., Polyak, L., Saarnisto, M., Siegert, C., Siegert, M.J., Spielhagen, R.F., Stein, R., 2004. Late Quaternary ice sheet history of northern Eurasia. Quat. Sci. Rev. 23, 1229–1271.
Svendsen, J.I., Briner, J.P., Mangerud, J., Young, N.E., 2015. Early break-up of the Norwegian Channel Ice stream during the last glacial maximum. Quat. Sci. Rev. 107, 231–242.
Trommelen, M., Ross, M., 2010. Subglacial landforms in northern Manitoba, Canada,

based on remote sensing data. J. Maps 6, 618–638.
Trommelen, M.S., Ross, M., Ismail, A., 2014. Ribbed moraines in northern Manitoba, Canada: characteristics and preservation as part of a subglacial bed mosaic near the core regions of ice sheets. Quat. Sci. Rev. 87, 135–155.
van der Meer, J.J.M., Kjær, K.H., Krüger, J., Rabassa, J., Kilfeather, A.A., 2009. Under pressure: clastic dykes in glacial settings. Quat. Sci. Rev. 28, 708–720.
Vorren, T.O., 1977. Weichselian ice movement in south-Norway and adjacent areas. Boreas 6, 248–257.

Supplement 1

Statistics for identified glacial landforms within the study from Gausdal Vestfjell area.

Streamlined landforms

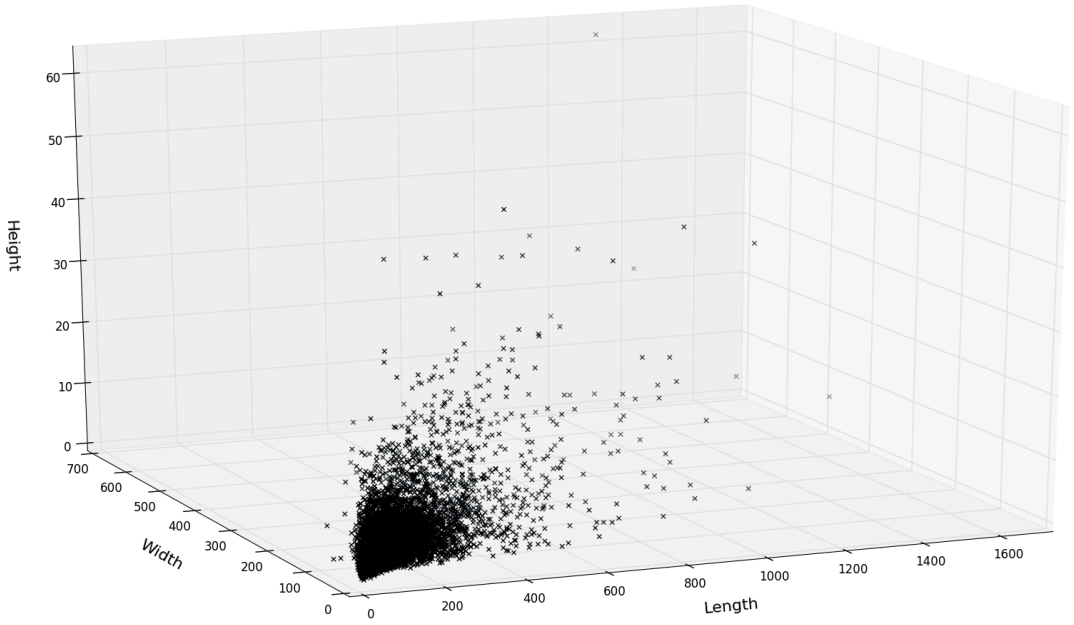

Parameter:	Length	Width	Height
Min	12.66	4.15	0.19
Max	1687.81	666.19	62.20
Mean	140.81	57.71	4.07
Variance	15402.83	2040.54	12.74
Skewness	3.21	3.06	4.08
Kurtosis	17.08	17.50	30.33
N = 8145			

Ribbed moraine

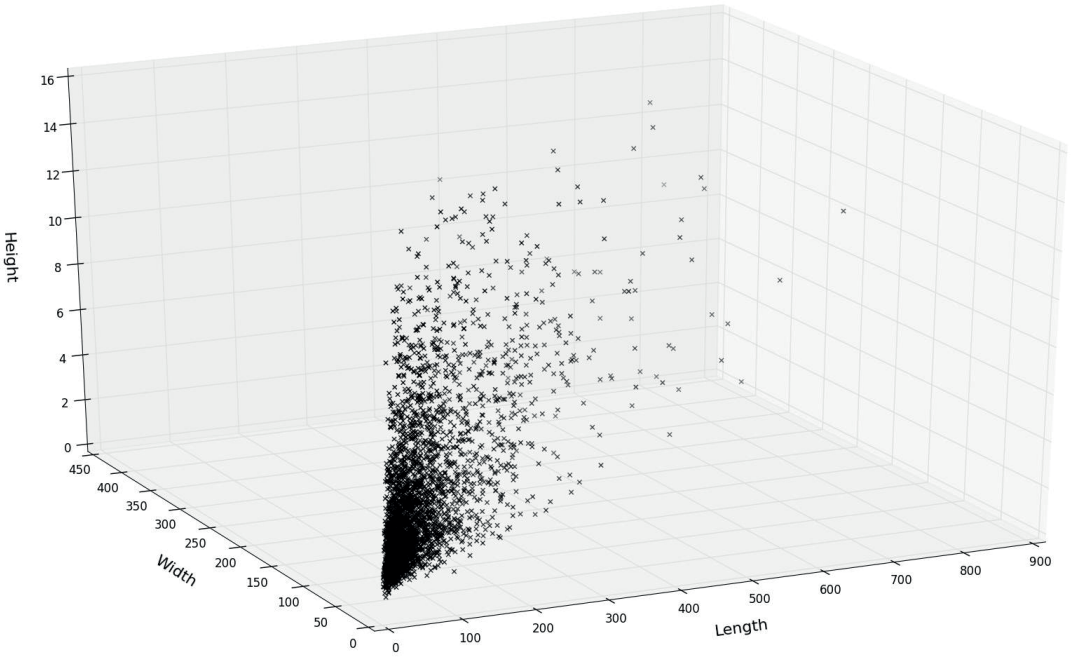

Parameter:	Length	Width	Height
Min	12.84	9.12	0.47
Max	766.64	354.42	14.67
Mean	118.18	64.17	3.84
Variance	8602.88	1675.54	6.82
Skewness	2.26	1.79	1.44
Kurtosis	7.21	4.92	1.81
N = 3105			

Supplement 2

The evolution of ice flow pattern at an inner region of the Fennoscandian Ice Sheet

Reconstructed by glacial landforms from Gausdal Vestfjell area, south-central Norway

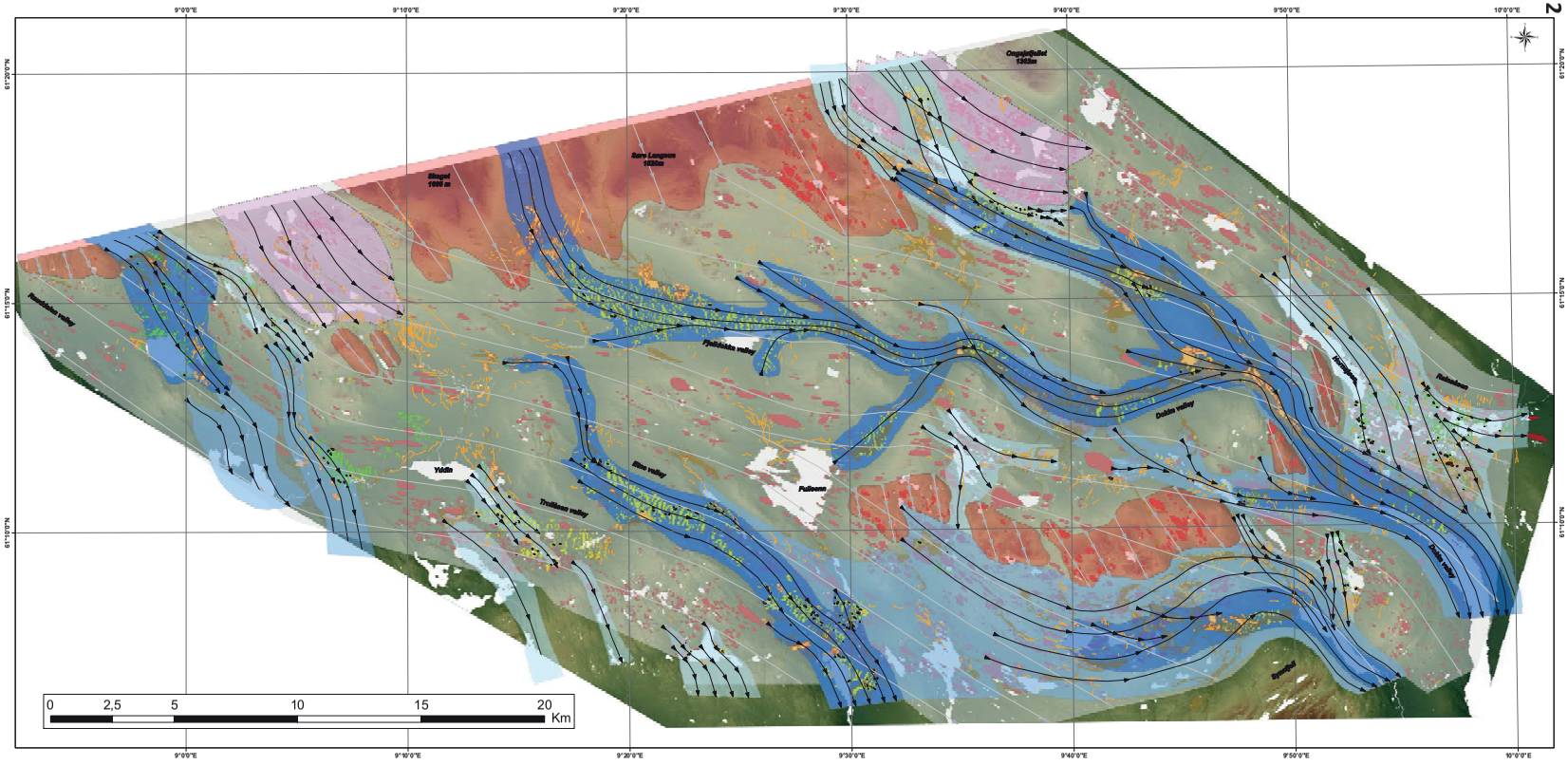

Legend

Identified landforms:

- Eskers
- Meltwater channels
- Meltwater landforms
- Streamlined landforms
- Type A ribbed moraine (broad fields)
- Type B ribbed moraine (belts)

Reconstructed flow pattern:

- Phase I
- Phase II
- Pre - Early Phase III
- Early Phase III
- Middle Phase III
- Late Phase III
- Fow direction

Terrain:

- Water bodies
- DEM
- 1685 m asl
- 711 m

Norwegian University of Life Sciences

© Artūrs Putniņš *,*, Mona Henriksen *
* Faculty of Environmental Sciences and Natural Resource Management, Norwegian University of Life Sciences, P.O. Box 5003, 1432 Ås, Norway
* Corresponding author. Tel. +47 67231815. E-mail address: arturs.putnins@nmbu.no

Supplement 3

Supplement. no 3. Relative height distribution of streamlined landforms and ribbed moraine ridges within the study area

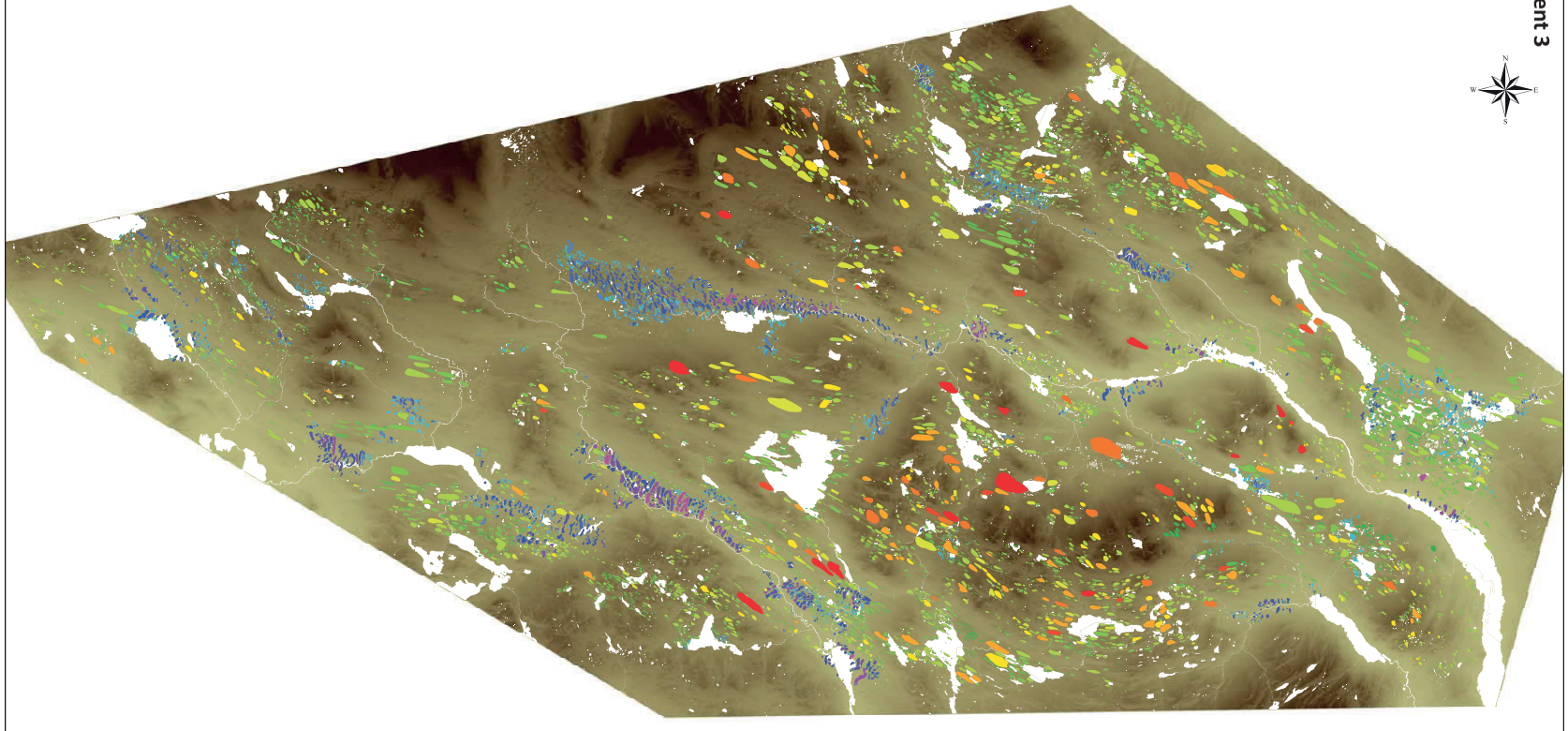

0 5 10 15 20 25 Km

Legend

Ribbed moraine ridges (m)

0,47 - 1,89 | 1,90 - 3,31 | 3,32 - 4,73 | 4,74 - 6,15 | 6,16 - 7,57 | 7,58 - 8,99 | 9,00 - 10,41 | 10,42 - 11,83 | 11,84 - 13,25 | 13,26 - 14,67

Glacial lineations (m)

0,19 - 1,50 | 1,51 - 2,50 | 2,51 - 5,00 | 5,01 - 10,00 | 10,01 - 12,50 | 12,51 - 15,00 | 15,01 - 20,00 | 20,01 - 25,00 | 25,01 - 35,00 | 35,01 - 62,20

DEM

1685 m

711 m

Paper II

Putniņš, A., Tveite, H. Extracting and visualising glacial ice flow directions from Digital Elevation Models using Grayscale Thinning and directional trend analyses. *Submitted to Computers and Geosciences.*

Extracting and visualising glacial ice flow directions from Digital Elevation Models using Grayscale Thinning and directional trend analyses

Artūrs Putniņš [a, *], Håvard Tveite [b]
[a] Faculty of Environmental Sciences and Natural Resource Management, Norwegian University of Life Sciences
[b] Faculty of Science and Technology, Norwegian University of Life Sciences, P.O. Box 5003, 1432, Ås, Norway

Corresponding author. Tel. +47 67231815. E-mail address: arturs.putnins@nmbu.no

Abstract

Flow pattern reconstructions for past glaciations are mostly based on the analysis of the spatial distribution of subglacial landforms. Streamlined subglacial landforms (oriented parallel, sub-parallel to the ice flow) are regarded as the main indicators of the previous ice flow. Manual mapping of these landforms is a time consuming and subjective process, therefore, semi-automated mapping (SAM) methods are becoming increasingly attractive. We present a fairly simple method for extracting mean directional trends from a DEM, based on grayscale thinning of slope rasters.

The paper presents preliminary results of the application of grayscale thinning for extracting the mean directional trends of both artificial (synthetically generated) and real terrain surfaces. The tests carried out on the artificial surfaces reveal that a landform feature has to be at least six (raster) cells wide to be properly detected by the method. The application of the method on real-world terrain data illustrates the robustness of the approach and indicates that the method is a promising tool for reconstructing glacial flow patterns.

Keywords
Grayscale thinning, DEM, Directional trends, Glacial landforms.

1. Introduction

Analysing the spatial distribution of subglacial landforms is a well-known tool for reconstructing the flow patterns of previous ice sheets (Boulton and Hagdorn, 2006; Clark et al., 2012; Greenwood and Clark, 2009a,b; Hubbard et al., 2009; Hughes et al., 2014; Kleman et al., 1997; Putniņš and Henriksen, 2017; Ross et al., 2009). Studies like these rely on manual mapping of landforms that for large areal extents is a time consuming and often subjective process (Smith, 2011). Therefore, there has been an increasing interest in the applications of (semi-)automated mapping (SAM) techniques within the geomorphology and Quaternary geology field (Sărășan et al., 2018; Jorge and Brennand, 2017; Saha et al., 2011; Smith

et al., 2009; Yu et al., 2015). Although SAMs for analysis and classification of Digital Elevation Models (DEMs) into simple units have been proposed (Drăguţ and Blaschke, 2006; Jasiewicz and Stepinski, 2013; Minár and Evans, 2008), methods for delineating genetic landforms are generally less successful (Jorge and Brennand, 2017). Moreover, SAMs for subglacial streamlined landforms are rather recent (d'Oleire-Oltmanns et al., 2013; Hillier et al., 2015; Jorge and Brennand, 2017; Saha et al., 2011; Yu et al., 2015). They are based on object-based image analysis (OBIA) (Baatz and Schape, 2000). OBIA either **(a)** segments the image based on homogeneity criteria (region-based segmentation) or outlines (edge-based segmentation), or **(b)** classifies the image into meaningful objects based on candidate objects (Blaschke, 2010; Blaschke et al., 2000).

Although OBIA based SAM techniques are regarded as objective and fast (Jorge and Brennand, 2017; Saha et al., 2011), they are often applied to relatively small (a few sq.km) areas, that contain well pronounced streamlined glacial landforms without 'noise' in the form of other glacial landforms (ribbed moraine ridges, eskers etc.), inherited bedrock topography or man-made artefacts (roads, ditches, and others). This is often far from the geomorphological settings in the central parts of the Scandinavian Mountains. SAM methods also often require rather complex raster pre-processing to mask out objects that introduce noise (Hillier et al., 2015; Jorge and Brennand, 2017). This introduces bias (Piégay, 2017) when the overall goal is to extract directional trends. Finally, OBIA based SAM techniques often require a pre-existing dataset of manually mapped landforms as input (Saha et al., 2011).

We present an approach for extracting directional trends based on grayscale thinning of slope rasters. The tool does not require extensive DEM pre-processing, and provides quantitative assessments that are less biased than visual observations (eye-bailing) (Piégay, 2017). It may be used for site selection for detailed studies. Here the tool is used and validated in the context of glacial flow pattern reconstructions (Putniņš and Henriksen, 2017), however it could have potential for a wide range of geomorphological studies (seafloor analyses, dune and other landform morphology).

2. Method description

Extracting directional tendencies for streamlined landforms is achieved either by using the concave breaks in the slope (landform outlines) or ridge crests (Evans, 2012; Saha et al., 2011). To identify glacial lineations (streamlined glacial landforms) one should search for linearly shaped areas with slope values exceeding their surroundings or for areas with a certain curvature (Evans, 2012).

We present an approach where the input slope raster is processed in a step-wise manner: a certain search range (slope level) is selected, thinned to skeletons, converted to vector lines and then analysed. To increase flexibility, a grayscale skeletonisation method (Biagioni and Eriksson, 2012) was used instead of traditional binary thinning (Marchand-Maillet and Sharaiha, 2000). The grayscale thinning approach respects variations in steepness by using several intervals simultaneously. The general processing scheme is shown in figure 1. The processing can be divided into: 1) DEM preparation (Input), 2) Processing and optional Optimisation, 3) Analysis. Each step is discussed further below.

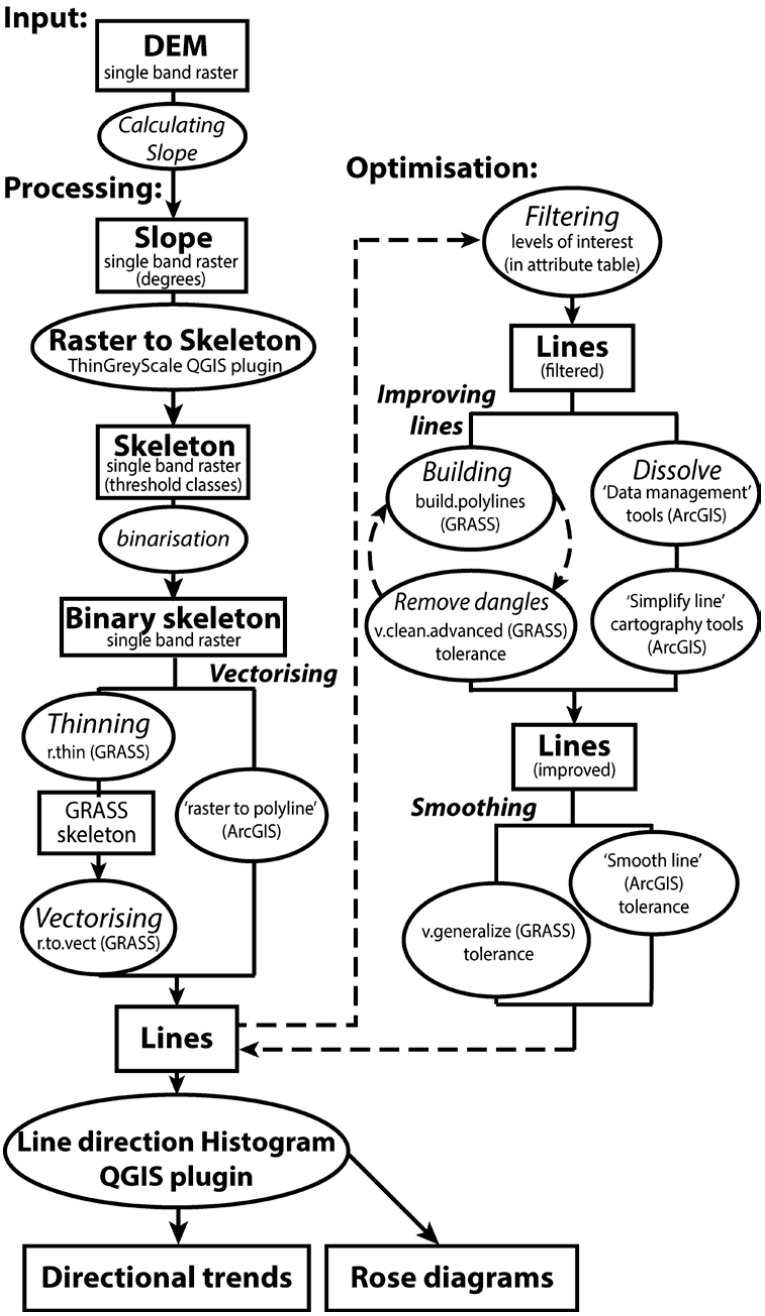

Figure 1. Method overview.

Input

A raster Digital Elevation Model (DEM) is created and a slope raster is calculated from it. This slope calculation is the only required processing of the DEM, but other types of processing (i.e. applying filters and masks to increase the overall data quality) may be included. We generated DEMs from synthetic surfaces and from a LiDAR dataset covering the case study site in Gausdal Vestfjell, in south central Norway.

Processing

The slope raster is processed using the Thin Greyscale Image to Skeleton QGIS plugin (Tveite, 2017a), that implements a skeletonisation algorithm (Biagioni and Eriksson, 2012) which works on density maps in the form of grayscale raster images. A grayscale raster is thinned to a skeleton based on a set of threshold values. The raster image is thinned considering the highest slope values first, and then, in a stepwise manner, the skeletonisation switches to the next level (with lower slope values), building on the skeleton extracted from the higher levels. The number of thresholds (and thus, slope levels) used in the skeletonisation will depend on user preferences. Threshold values can be selected, either **(a)** mathematically (using equal intervals – a function built into the plugin), **(b)** statistically (based on the raster image statistics), or **(c)** manually. Regardless of the thresholding method applied, the minimum value for the lowest level must always be significantly greater than zero to avoid computational problems during the skeletonisation. The minimum value should be chosen according to the answer to the question - *at which point does the slope become significant for the landforms to be recognized*? This will depend on **(a)** the target landform (i.e. type of landform and minimum size) and **(b)** the smoothing effect of the input resolution.

When applying the grayscale skeletonisation on real-world terrain data, the use of thresholds allows us to ignore the steepest parts, excluding some of the directional trend signals caused by the (inherited)

bedrock topography. Therefore, choosing the upper and lower limits for thresholding is an important aspect of the application of this algorithm, possibly, more significant than the number of thresholds (levels). The use of thresholds also allows us to analyse the directional trends within the different slope levels (the output data can be treated as a united skeleton or as separated skeletons for each level).

After the skeletonisation (and the optional removal of the steepest level) the output grayscale skeleton raster is binarised before being vectorised to a line dataset using for instance the GRASS function *r.to.vect*[1] or the ArcGIS *'Raster to Polyline'* tool. If slope levels are to be considered in the further analysis, the binarisation step is skipped. Removing the highest slope level may be desired to reduce the influence of bedrock topography and man-made features.

For simplicity reasons, we have used the 'Raster to Polyline' tool, adding the possibility to use the 'simplify lines' option and specify 'minimum dangle length' (see the 'Optimisation' step). After the vectorisation of the skeleton (Fig. 1), the dataset can either be analysed as is (if the present outcome is satisfying) or be subjected to further processing (to increase the signal to noise ratio of the outcome) as described below.

Optimisation

The line segments that result from the vectorisation of the slope skeleton (Fig. 1) follow the one pixel wide raster skeleton, and the line directions will reflect that. Thus, horizontal and vertical line segments will be over-represented, as will diagonal segments (45° and 135° angles). In the analysis phase, this can make the identification of directional trends more difficult. This over-representation can be reduced by

[1] r.to.vect expects input on the GRASS skeleton format, and that can be produced using the r.thin (GRASS) function.

smoothing the resulting lines, as is done by the 'Raster to Polyline' (ArcGIS) tool with the 'simplify lines' option.

Thinning produces some noise. For example short (one or a few pixels long) lines connected to the skeleton through only one of its ends (type I in Fig. 2, also called "dangles"); so called 'salt and pepper-like' noise (Blaschke et al., 2000; Wang et al., 2017; Wang et al., 2016) (type II in Fig. 2); and pseudo nodes (unnecessary splitting of lines, type III in Fig. 2). A problem with short lines is that the effect of smoothing is limited, contributing to the over-representation of the raster angles. Pseudo nodes (nodes with degree two) may result when the raster skeleton has not been binarised (nodes will appear between lines from different skeleton levels) and when lines have been removed. To avoid some of these effects, very short isolated and "dangle" lines can be removed, and degree two nodes eliminated before the smoothing.

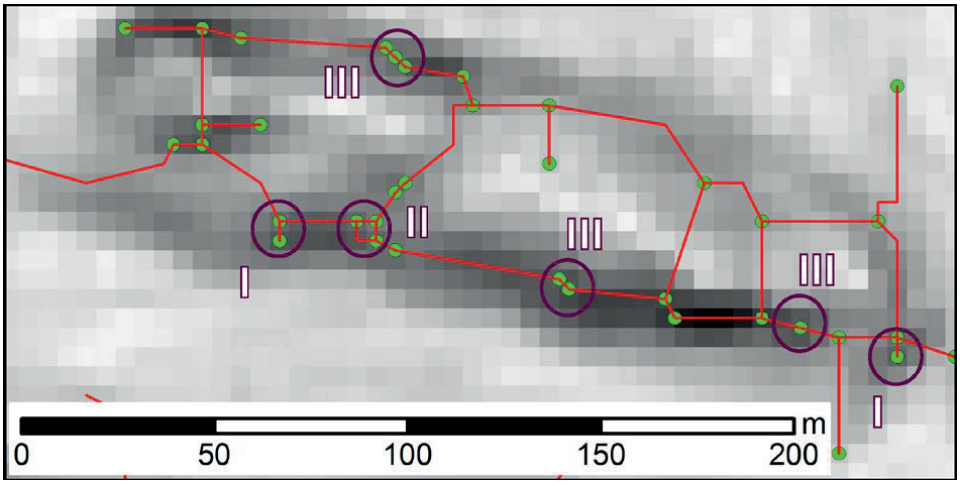

Figure 2. Examples of noise introduced by raster effects. Red lines indicate extracted features, small green dots show nodes, roman numbers show examples of different types of noise: I – dangles, II – rectangular formation, presumably caused by a cell with a lower value (i.e. 'salt and pepper –like' noise), III – pseudo nodes.

The operations described below are considered supplementary but with a potential to increase the quality of the outcome:

1) Clip the line dataset to exclude possible edge effects.

2) Remove dangles and pseudo nodes. Pseudo nodes can be removed (merging connected lines into longer lines) using 'v.build.polylines' (GRASS function). In ArcGIS, the 'Dissolve' tool can be used. The dangles (short line segments connected at one end only) can be removed using 'v.clean.advanced' (GRASS function) with the 'rmdangle' option and a given tolerance (length). New pseudo nodes may result when dangles are removed, so this process is repeated with larger tolerances for dangle length until a satisfactory result is reached.

3) Smoothing the lines using, for instance, the GRASS tool 'v.generalize'[2]. In ArcGIS, the 'Simplify Line' and 'Smooth Line' tools may be used. The tolerance value should be larger than the raster resolution, but within the same order of magnitude. There must be a rational reasoning behind the choice of tolerances. It should be based on the cell size of the input raster, as well as the expected dimensions of the landforms of interest.

Conducted experiments show that smoothing, after removing dangles and pseudo-nodes, may improve the results, while removing the highest slope level is useful for areas with bedrock and man-made features. Edge effects decrease when the amount of extracted lines increase.

Analysing the Output

The line dataset is analysed using the Line direction histogram QGIS plugin (Tveite, 2017b), that visualises the distribution of line directions as rose diagrams. The plugin has a number of options:

1) '0-180 ('orientation' neutral)' must be selected.

[2] v.generalize provides several smoothing algorithms. We chose 'chaiken' with tolerance=2*raster cell size after also testing 'snakes' with alpha=1 and beta=1 (see supplement 1 for comparison).

2) ‘No weighting on length’ must not be selected.
3) Around 30 bins with an ‘Angle offset’ of 2-3 degrees, and ‘Area proportional’ sector sizes produced good visual results - the exact number of bins did not turn out to be very important.
4) The mean direction option was used to include the directional trend according to circular statistics (Jammalamadaka & Sengupta, 2001).
5) The tiling option was used to partition the area and generate one diagram per tile. Tiles are taken from a polygon layer, and the tiling could for instance be based on landform outlines (as used in s. 3.1.) or be a regular grid of squares (e.g. 1x1 km). For the study area (s. 3.2) we used a regular grid of squares. The size of the squares should reflect the resolution of the dataset, the size of the real-world features and the expected frequency of the phenomenon to be analysed. For the analysis to provide meaningful results, it is important that the total length of lines per tile is not too small.

3. Results

3.1. Artificial surface tests

The method was first tested on artificial surfaces (Fig. 3) with varying parameters, to test the skeletonising process in a controlled environment. Two artificial surfaces were generated with Blender, a freeware software for 3D modelling and rendering, using combinations of planar shapes (two), elongation ratios (two), orientations (three) and scales/resolutions (five). See table 1 and Figs. 4, 5. The width of the base (scale 1) shapes were set to three (cells) and the height to 0.6 giving a maximum slope of 36 to 38 degrees – which slightly exceeds the average angle of repose for various types (sand, silt, clay) of unconsolidated sediments (Culshaw et al., 1991). The shapes used were ‘egg’ and ‘ellipses’. The *egg-shape* was chosen because, in the literature, it is often referred to as the *‘classic’* drumlin shape outline (Clark et al., 2009). The *ellipse-shape* was chosen because it has proven to be a more common

drumlin shape outline (Spagnolo et al., 2010). Elongation ratios of 2 ('LW 2') and 6 ('LW 6') were selected based on the literature (Clark et al., 2009; Hess and Briner, 2009; Spagnolo et al., 2012), where elongation ratios between 2 and 3 are reported as being the most common for streamlined landforms. 'LW 2' therefore represents a common elongation ratio, while 'LW 6' represents a less common, but still realistic ratio. Three angles (0, 20 and 45 degrees) were used to test the effects of orientation relative to the raster cell structure. The 0 degree axis orientation illustrates the 'neutral' landform position when the landform is oriented parallel to one of the raster axis. 45 degrees is presumably much affected by the orthogonal nature of rasters. 20 degrees represents a case that is not aligned with typical raster angles (0, 11.25, 22.5, 33.75, 45, ...). A cell size of one was used, and the shapes were scaled using the factors *1, 1.5, 2, 5* and *8* to simulate the effects of resolution.

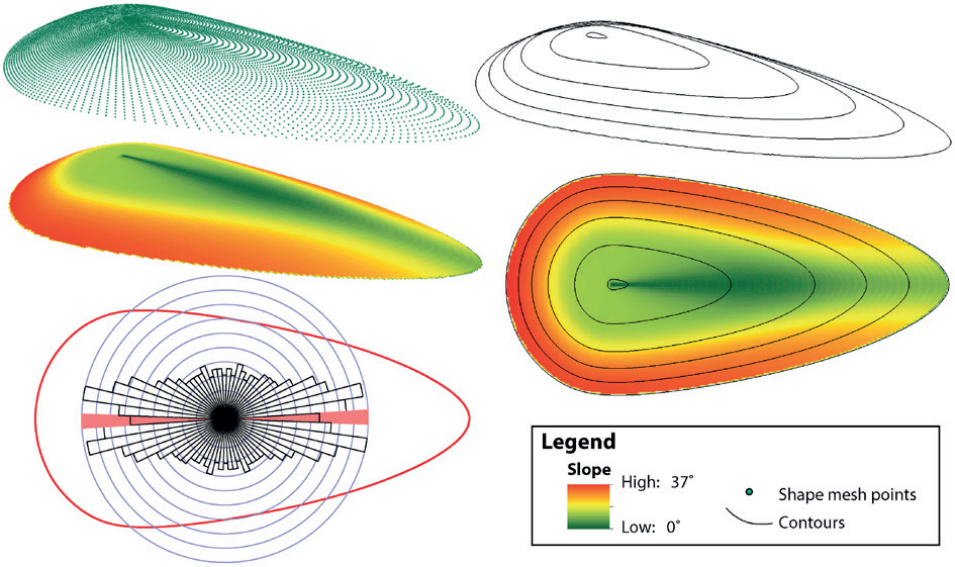

Figure 3. An example of a generated streamlined landform (egg shaped) and the representation of its outline *(the 'ideal' histogram outcome)* as a directional histogram using the settings described above.

The generated shapes, extracted lines and direction trends (30 bins, 3 degrees offset) for the shape combinations of Table 1 are presented in figure 4 and figure 5, including effects of simplification and

smoothing. Figure 6 illustrates the 'noise' introduced by the thinning process in the lowest levels and its effect on over-representing certain (orthogonal) raster angles in the rose diagrams.

Table 1. Landform dimensions (width, length and height) in cells for the chosen scales.

Scale	Width (cells)	Length 'LW 2', (cells)	Length 'LW 6', (cells)	Height
1	3	6	18	0.6
1.5	4.5	9	27	0.9
2	6	12	36	1.2
5	15	30	90	3
8	2.5	48	144	4.8

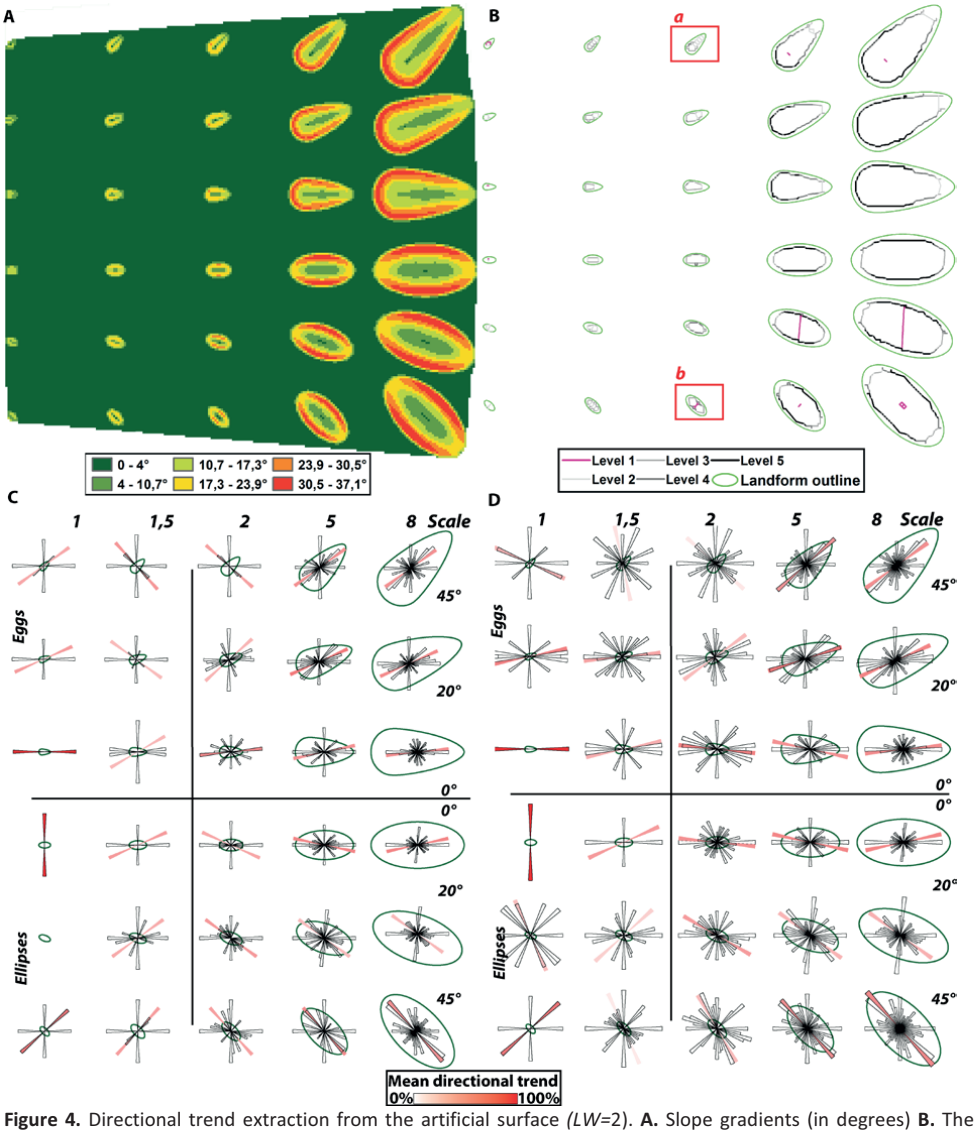

Figure 4. Directional trend extraction from the artificial surface *(LW*=2). **A.** Slope gradients (in degrees) **B.** The skeletonisation outcome – vectorised lines sorted by skeleton levels. Red boxes indicate chosen landforms seen in close-ups in Fig. 6. **C.** Line direction histograms (with mean directional trend) before optimisation (outlines as background). **D.** Line direction histograms with mean directional trend - simplification and smoothing applied (outlines as background).

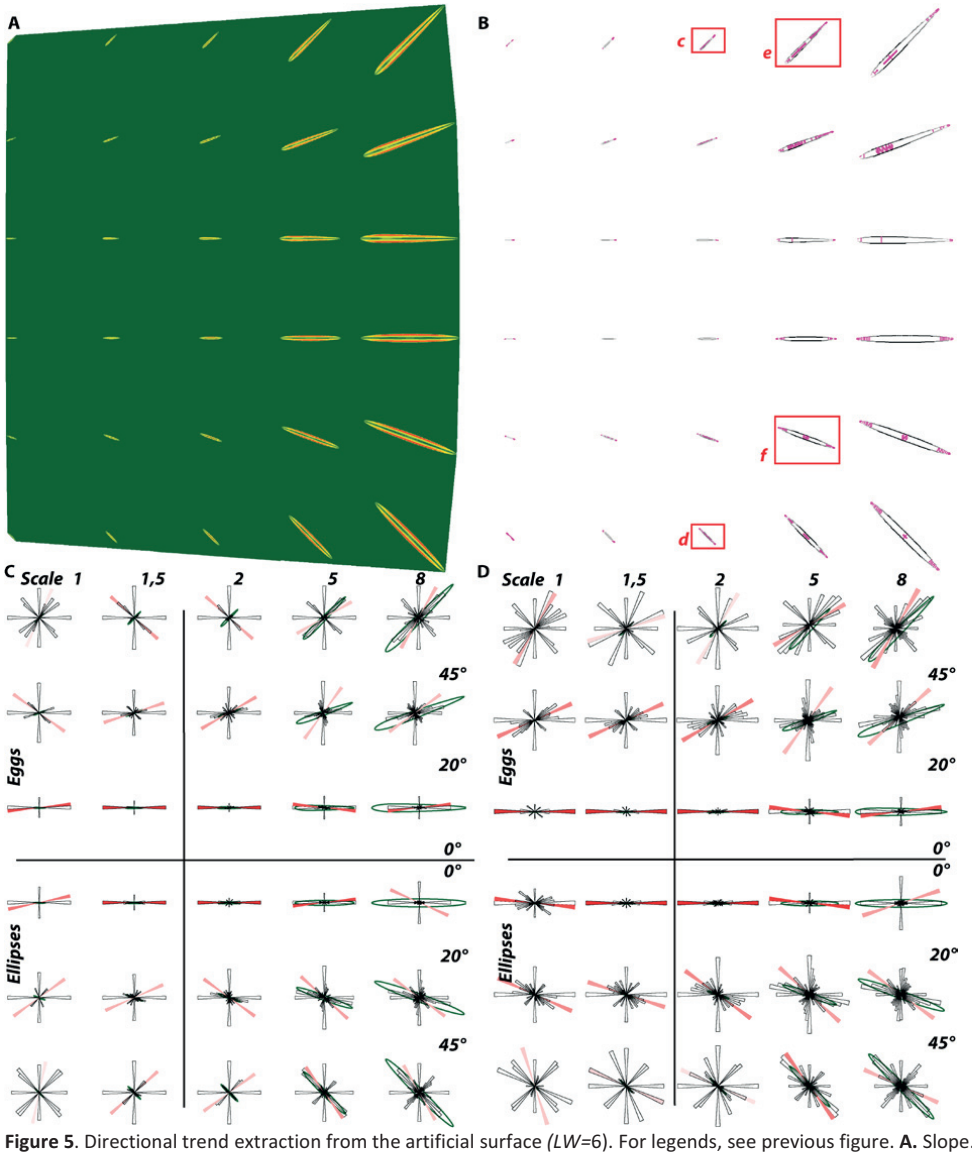

Figure 5. Directional trend extraction from the artificial surface *(LW*=6). For legends, see previous figure. **A.** Slope. **B.** The outcome of the skeletonisation – vectorised lines sorted by skeleton. **C.** Line direction histograms (with mean directional trend) before optimisation (outlines as background). **D.** Line direction histograms with mean directional trend - simplification and smoothing applied (outlines as background).

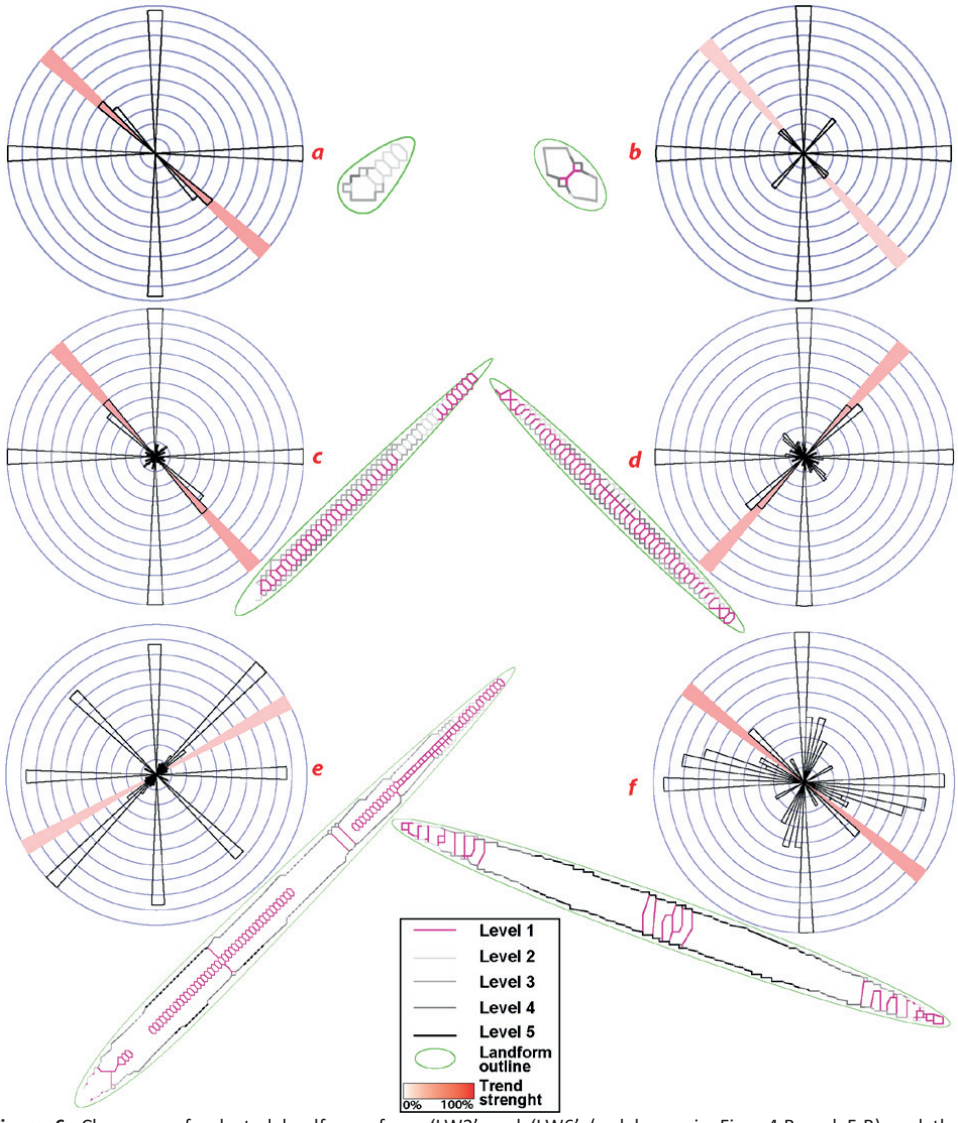

Figure 6. Close-ups of selected landforms from 'LW2' and 'LW6' (red boxes in Figs. 4.B and 5.B) and the corresponding directional histograms. Multi-level lines. Various scales used. Note the overall raster effect in the histograms and the 'noise' introduced by level 1 lines (4 to 10.6°).

3.2. Real-world terrain data

The grayscale thinning method was applied on a real-world terrain in Gausdal Vestfjell, south central Norway. This area contains important paleo-geographic and morphological records from the last ice age for the inner regions of the Fennoscandian Ice Sheet (Putniņš and Henriksen, 2017). The case-study area is 200 km^2 large and contains rather complex geomorphology (Fig. 7).The terrain consists of numerous valleys, lake depressions, local elevation highs and several mountain peaks and passes. Streamlined glacial landforms are abundant, as well as 'noise' in the form of other glacial and glacifluvial landforms (e.g. ribbed moraine ridges and eskers), fluvial landforms (lakeshores, riverbanks and smaller streams), inherited bedrock topography, and some man-made artefacts (e.g. roads and ditches).

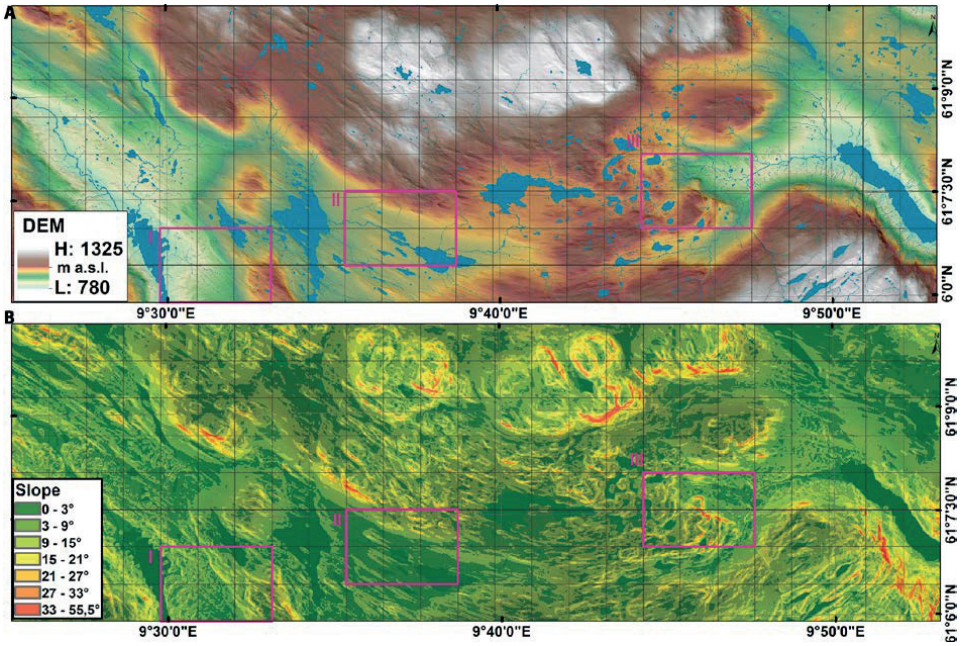

Figure 7. The real-world terrain data used for testing the method. **A.** DEM (20m resolution) calculated from *LiDAR* data with water features (in blue). Data provided by the Norwegian mapping authority *(Kartverket)*. **B.** Slope raster (20m resolution) calculated from the DEM. Red boxes and Roman numbers indicate the areas used for close-up examples. Location coordinates (degrees, minutes, seconds) given in accordance to WGS84.

The raster resolution has effects on the landform appearance (i.e. loss of detail with increasing cell sizes (Deng et al., 2007; Napieralski and Nalepa, 2010)). Therefore, the resolution of the raster DEM should be chosen based on the scale of the features of interest. Here, two resolutions (5 and 20 meters - based on suggestions by Napieralski and Nalepa, 2010) were chosen to test the performance and assess the outcome.

Through trial and error, it was found that streamlined landform features become detectable in the slope gradient range of 1 to 2 degrees. However, the lowest threshold value was set to 3 degrees to reduce the noise effects of micro-relief. By doing so, less distinct streamlined landforms might be lost, but the glacial flow directions should still be represented by more prominent (steeper) terrain features. The highest threshold value was set to 33 degrees – corresponding to the angle of repose of unconsolidated sediments (Culshaw et al., 1991). Everything steeper than this is considered as bedrock features.

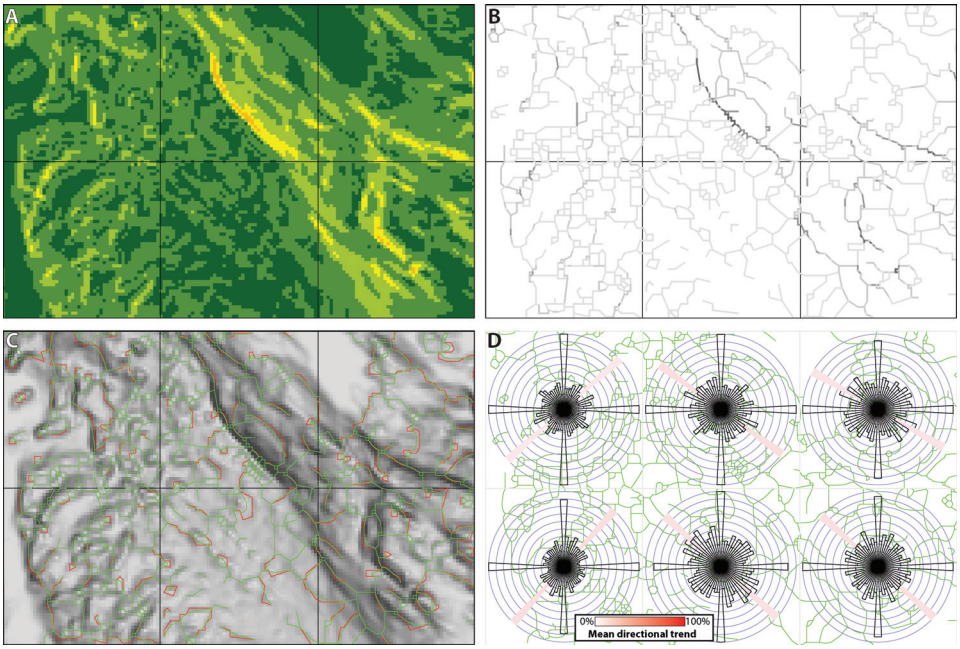

Figure 8. Skeletonisation outcome and the full line direction histograms with mean directional trends for Close-up I (20m resolution). **A.** Slope raster (for slope level legend, see Fig. 7). **B.** Skeletonisation outcome with slope levels

(vector lines). **C.** Smoothing result (in green) overlaid on slope raster – red lines are "raw" lines affected by optimisations. **D.** Line directional histograms generated from the smoothed lines (in green).

Different thresholding approaches (five or ten levels; equal interval or quantile) were tested during the development stage (see supplement 2), and it was found that they all performed reasonably well. The further tests were performed using a slope raster resolution of 20 meters and with equal interval (five levels) thresholding. The slope gradient range (3° to 33°) was split into the following (five) intervals: 3° to 9° (level 1); 9° to 15° (level 2); 15° to 21° (level 3); 21° to 27° (level 4); 27° to 33° (level 5) (Fig.7). 33° and above (level 6) was excluded from further processing. Figures 8A, 8B and 9A show the slope raster and the result of the skeletonisation. Further processing was carried out following the steps described in section 2 (without binarising the skeleton). The output was vectorised using the ArcGIS 'Raster to Polyline' tool with the 'simplify lines' option selected and 'minimum dangle length' set to 30 (to only remove the shortest dangles, including diagonals – 1.5 * resolution). The line features belonging to the steepest class (level 6) were removed. The rest of the line features (belonging to level 1 to 5) were combined (ignoring level 6) and smoothed (Fig. 8C) using the GRASS functions described in section 2. Then, the extracted line dataset was analysed with the Line direction histogram tool using a grid of 1x1 km tiles and the 'Mean direction' option. Figures 8D and 9B show the resulting histogram for each tile whereas 9C shows only the extracted mean directional trends.

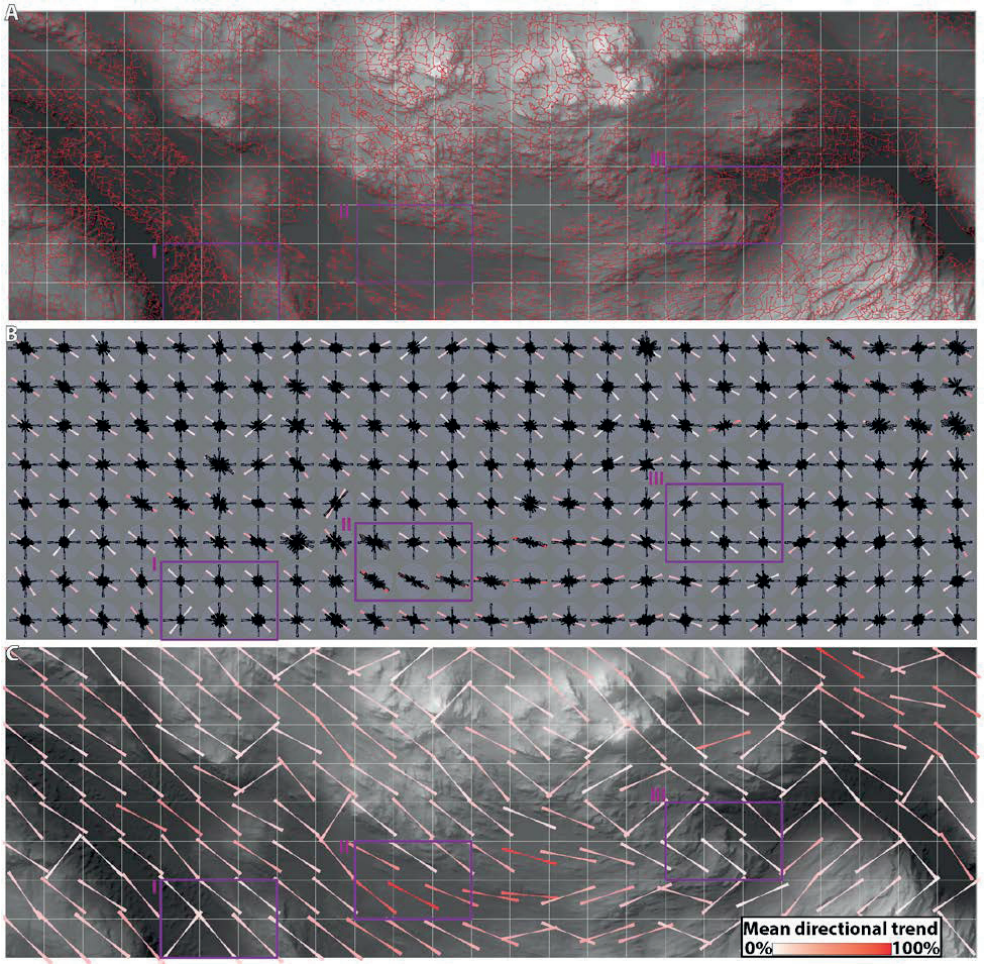

Figure 9. Extracted mean directional trends from real terrain (20m DEM). **A**. Skeletonisation outcome (filtered and smoothed lines) dataset overlaid a hillshaded DEM (with tiles). Purple boxes show areas of close-ups illustrated in other figures. **B**. Rose diagrams with mean directional trends. **C**. Mean directional trends (generated per tile) overlaid on the DEM (with hillshading).

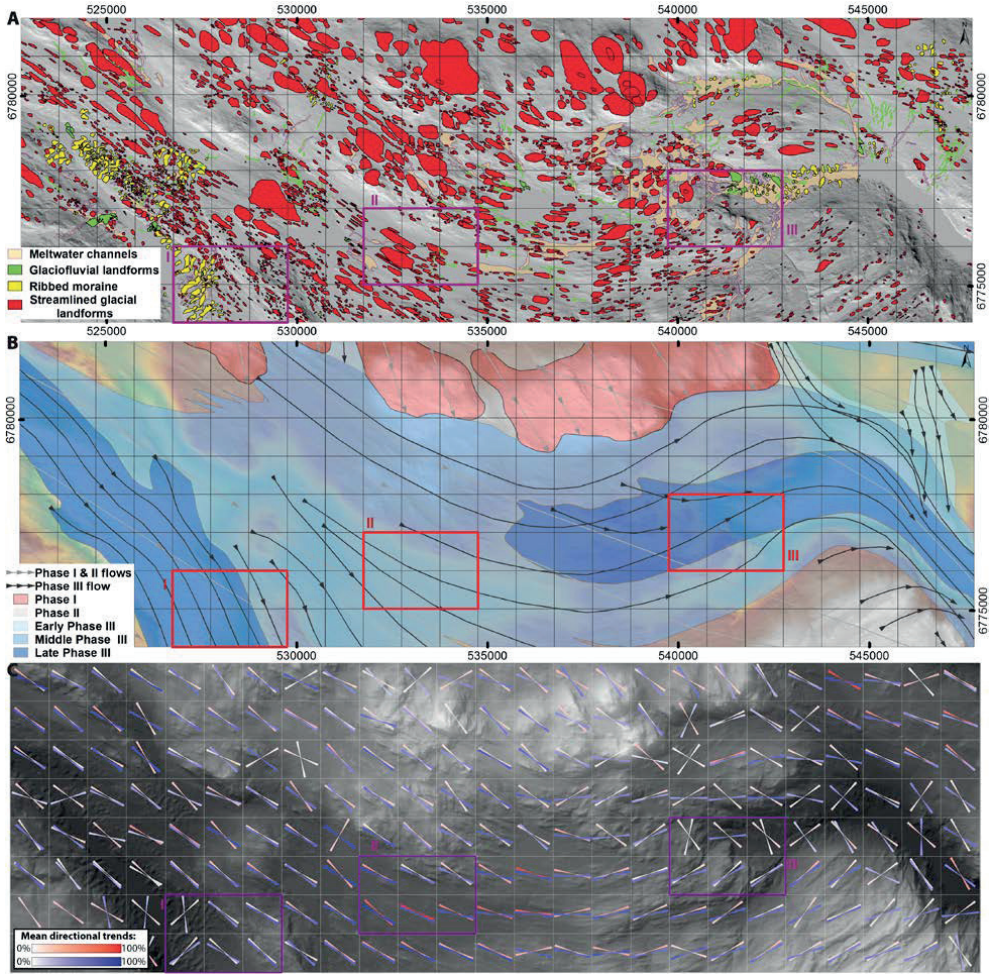

Figure 10. A. Mapped landforms (modified from Putniņš and Henriksen (2017))**. B.** Reconstructed flow pattern evolution of previous Fennoscandian Ice sheet (modified from Putniņš and Henriksen (2017)). **C.** Extracted mean directional trends of mapped landforms (in blue) overlaid with extracted trends from 'the 20m, 5 equal intervals' example presented earlier (Fig. 9). DEM (enhanced by hillshading) used as background. Coordinate reference system WGS 1984, UTM Zone 32N.

Validation

The extracted mean directional trends were compared with the mean directional trends for manually mapped landforms (Fig. 10A) and existing ice flow reconstructions (Fig. 10B) within the area (reported

by Putniņš and Henriksen, 2017). Figure 10C shows the mean directional trends for both the manually mapped landforms and the extracted lines (See supplement for the comparison with the other thresholding approaches). Further, the signal strength and the deviations of the mean directional trends (within each tile) of the datasets were compared (Fig.11). When comparing the signal strengths for each tile, it is evident that the manually mapped landform dataset produces stronger signals (Figs 10C; 11A) than the ones extracted from the slope raster (Figs 9C, 10C and 11A). The distribution of the absolute values of the directional deviations (Figs 10C, 11C) has mode = 5.625° (one sector) and median = 11.25° (two sectors). The majority of the deviations (ca 112 of 194) are less than equal to 11.25°.

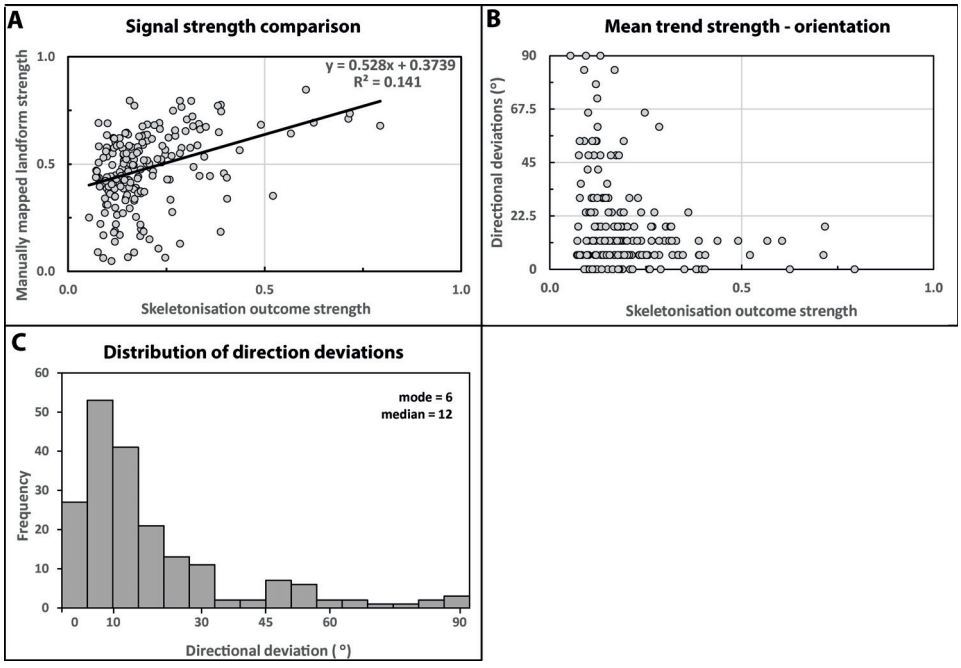

Figure 11. A. Comparison of extracted signal strengths extracted from both datasets. **B.** Signal strength of the DEM derived dataset related to absolute value of the deviations of the mean directional trends. **C.** Frequency distribution of directional deviations (in absolute values).

Later, several areas with varying mean directional trends (close ups I, II and III in Figs 7, 9 & 10) were subjected to a detailed investigation. For these areas, a higher resolution (5m) slope raster was used.

Although the LiDAR point cloud resolution (2 points per m^2) would allow a smaller cell size, 5m was chosen based on the landform dimensions and available computing power. For the skeletonisation the same thresholding approach was used (the 3 to 33 degree gradient range was split into five equal intervals) and the same processing steps were applied. A 0.5x0.5 km tiling grid was used when extracting the mean directional trends (for a 1x1 km tiling with 5m resolution data for the whole area please see supplement 2). The aim of this was to validate the strength and the accuracy of the mean directional trends (extracted from the 20 m resolution dataset) within the selected areas by comparing them to a more detailed (5m) dataset. Close-up examples (Fig. 12) illustrate the resolution effects on the skeletonisation as well as the difference in mean directional trends for different tile sizes. In addition, in figure 13, the 5m dataset was used to illustrate the mean directional trends generated for each separate threshold levels for Close-up III (Figs. 7, 9 & 10).

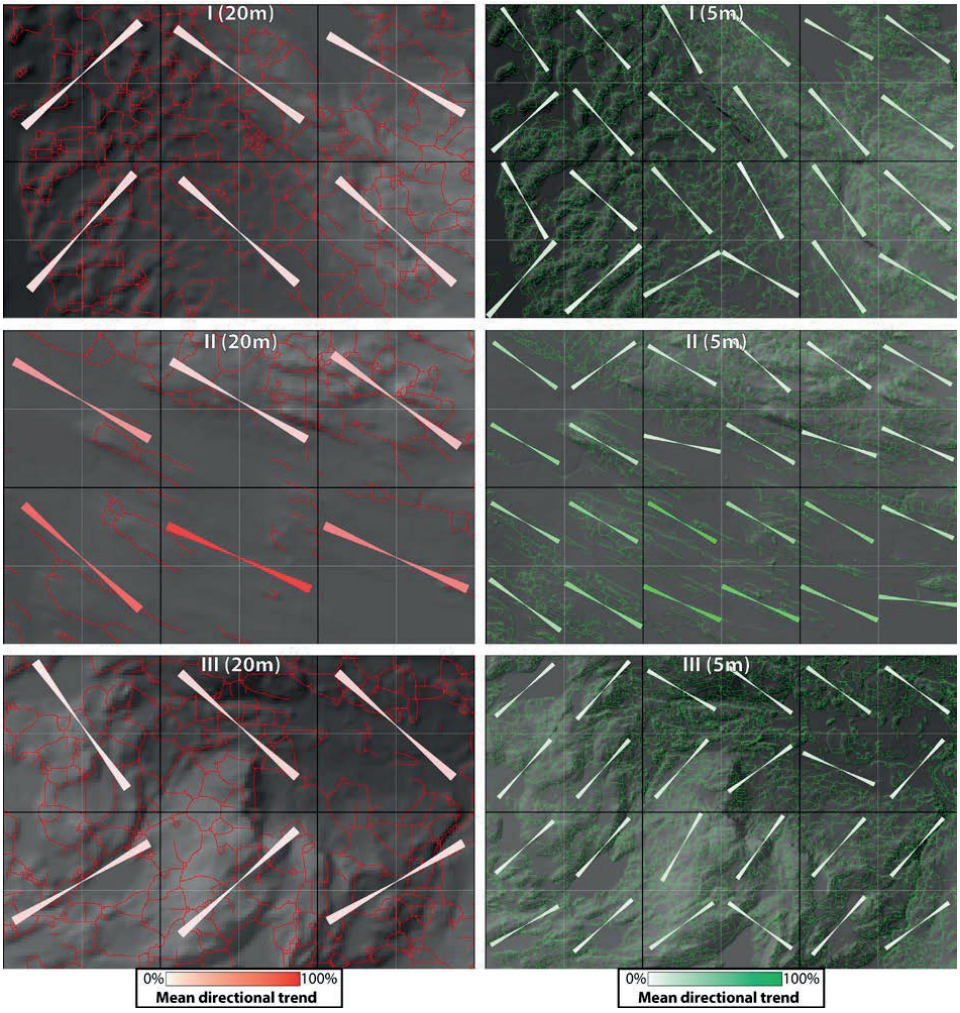

Figure 12. Close-ups (I, II and III from Fig 7). 20 m resolution on the left and 5m resolution on the right.

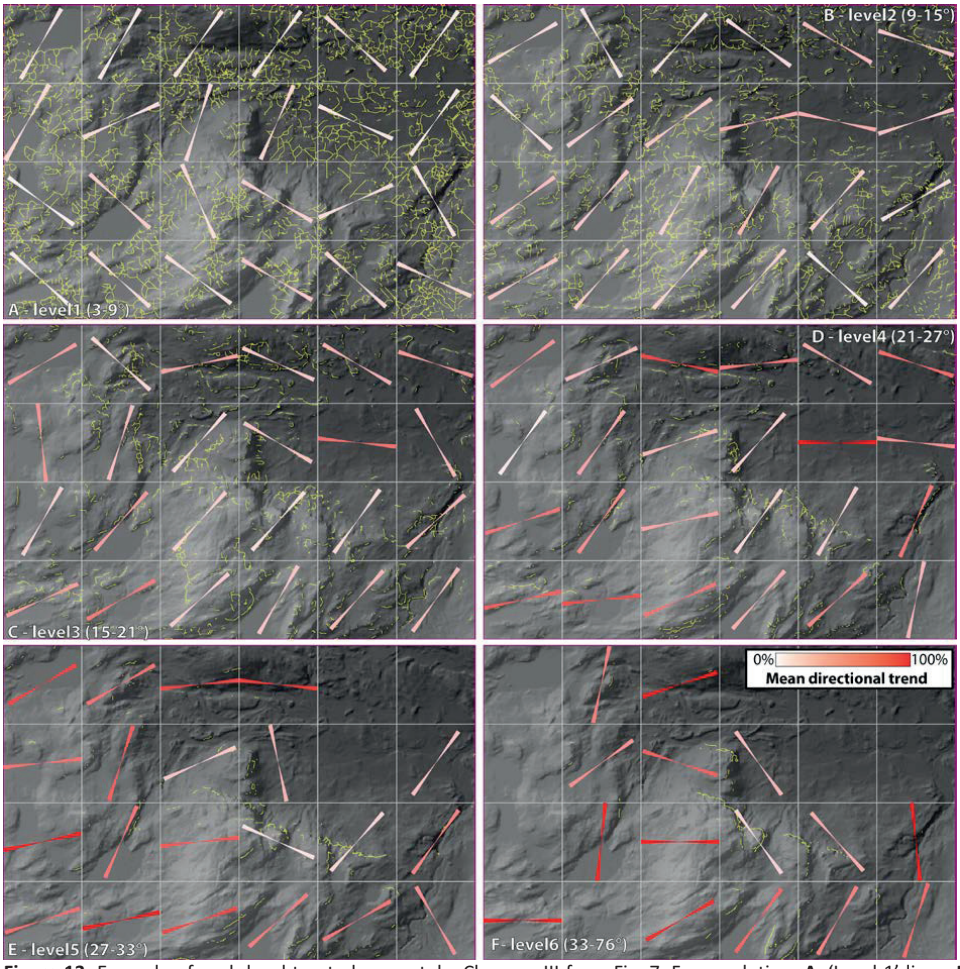

Figure 13. Example of each level treated separately. Close-up III from Fig. 7, 5m resolution. **A**. 'Level 1' lines. **B**. 'Level 2'. **C**. 'Level 3' lines. **D**. 'Level 4' lines. **E**. 'Level 5' lines. **F**. 'Level 6' lines – '33° and above' (bedrock) excluded from the dataset.

4. Discussion

Existing SAMs for streamlined landform mapping (d'Oleire-Oltmanns et al., 2013; Hillier et al., 2015; Jorge and Brennand, 2017; Saha et al., 2011; Yu et al., 2015) have been relatively successful within small areas (a few sq.km). However, we do not consider them optimal for terrains with complex geomorphological and geological settings (as within the highest parts of the Scandinavian mountains)

that are often influenced by the inherited bedrock topography; have large differences in elevation; or contain other glacial landforms and man-made infrastructure.

Here we have presented a method for extracting and visualising directional trends based on grayscale thinning of slope rasters. Extracting directional trends in this manner provides quantitative assessments that should be preferred over visual observations (eye-bailing) to prevent biases (Piégay, 2017). In contrast to binary thinning, grayscale thinning (Biagioni and Eriksson, 2012) takes advantage of intensity (Marchand-Maillet and Sharaiha, 2000), and should therefore be well suited for slope rasters when used for extracting directional trends. Grayscale thinning considers the values (intensities) of the raster by grouping them into a number of intervals and constraining the thinning at lower intensities by the results from higher intensities.

The output of all thinning methods will have raster effects resulting from the vectorisation of the one pixel wide skeleton. The resulting line dataset will have a limited number of line directions represented. As observed for both the artificial surfaces and real terrain, the impact of such artefacts is higher when the total line length is small. Noise reduction by filtering has been advocated by several researchers (Eisank et al., 2014; Hillier and Smith, 2012; Hillier et al., 2015; Jorge and Brennand, 2017; Sofia et al., 2013), but all manipulations introduce some degree of bias. Therefore, in order to keep the method simple, we have focused on post processing for noise reduction.

4.1. Artificial surface findings

Two artificial surfaces with variations in size, direction and elongation ratio were used to test grayscale thinning for extracting directional trends in a controlled environment. The tests illustrate the importance of post-processing to reduce the over-representation of the raster angles (Figs. 3, 4, 5 and 6). Directional trends for both surfaces (egg and ellipse) are recognized equally well (Fig. 4C, D; Fig. 5D). For the 'LW 2'

surface, the directional trends appear stronger for the eggs (Fig.4D), whereas for 'LW 6' the trends are stronger for the ellipse (Fig. 5D). All the variations of surfaces (except the 0° orientation for 'LW6') of scale 1 and 1.5 (table 1) are considered unrecognizable. The scale 2 surfaces are the first to be reasonably recognizable; however, the 45° orientation produces a perpendicular-to-the-crest mean direction for both elongation ratios (Figs. 4, 5 and 6), presumably caused by raster. This indicates that landforms with a width of six cells are the first that can be regarded as recognizable.

Although the chosen skeletonisation thresholds and post-processing operations were similar for both cases, there are some differences between the identified mean direction and the actual orientation of the shape (Figs 4, 5 and 6). Since the total length of lines is larger for LW6 than LW2, the signals should be stronger. However, in particular for the 20° orientation, the direction trends are more accurate for LW 2(Fig. 4D) than for LW 6 (Fig. 5D). This can be explained by less noise in the LW 2 skeletonisation outcome (Fig. 4B) than the LW 6 case (Fig. 5B).

As illustrated in the figures (Figs. 4C, 5C and 6) this noise is picked up by the lowest skeletonisation level (level 1), indicating that the lowest threshold value chosen (4°) may be too low. In addition, tests show that the smoother and flatter the surface is (particularly the LW6 surface, which becomes very flat along the longest axis for the largest landforms), the more pronounced is the noise introduced by the thinning algorithm (Figs. 4C, 5C and D). Increasing the lowest threshold could improve the results.

4.2. Tests on real-world terrain

When grayscale thinning is applied on real-world terrain data, the noise pattern is less regular, as expected. The noise in the real-world terrain examples differs somehow from the noise in the artificial surfaces. The stand-alone short line segments oriented perpendicular to the crests of narrow landforms (Fig. 12) resemble the noise found at the smallest scales (1.5 and 2) for the LW2 surface (Fig. 4) and are

similar to noise at 'scale 5' for LW6 (Fig. 5C, D). Such noise tends to disappear on wider landforms (and higher thresholding levels) in the real-world terrain examples (Figs.9, 12). Other types of noise, such as one pixel wide squares (caused by single pixel peaks/pits, see II in Fig.2) and straight lines parallel to the slope direction occurring on wide, gentle slopes are more common for the real-world terrain (Fig.12) than the artificial surfaces. Although all of the noise sources affect the results, we have found that their main effect is only to reduce the strength of the resulting directional trends.

Comparing the skeletonisation outcome to manually mapped landforms (Fig.10C), the extracted trends show reasonable resemblance in orientation. However, other glacial landforms like ribbed moraine ridges (broadly used as previous ice flow indicators (Dunlop and Clark, 2006) - oriented perpendicular to the ice flow) contribute to reducing the overall signal strength within some tiles (close-up I in Figs 7, 9, 10 and 11). Therefore, further investigation of areas (tiles) with weak directional trends is suggested. Regardless of the parameters used in the method, expert knowledge in combination with additional data (like aerial imagery or fieldwork) should be used to validate the findings and to give an assessment of the overall effect of noise.

Different DEM resolutions and Tile sizes

The effects of spatial resolution are illustrated in Figure 12 where the 20m resolution outcome is compared to 5m resolution in combination with variation in tile size. As expected, more and smaller landform features are reflected when using a higher resolution. However, there is also more noise (in particular, the straight, parallel-to-the slope lines occurring on wide, gentle slopes (Fig.12). Moreover, higher resolution also means that more non-glacial landforms (river and stream banks, lakeshores and fragments of valley footslopes) or man-made artefacts (roads, ditches and artificial embankments) are

reflected in the results (Fig. 12). Coarser resolution (Napieralski and Nalepa, 2010) mask out most man-made artefacts.

Higher spatial resolution means longer processing time, and this is a drawback for large datasets. The choice of resolution should be based on the phenomena that are being investigated. Higher resolution could be helpful in some cases, particularly for smaller areas, but coarser resolution could be better for cases with a large areal coverage.

As illustrated in figure 12, the tile size may affect the results. With smaller tiles, the total length of lines within each tile is reduced, making the statistics less reliable, while for larger tiles, high frequency directional trends may be lost (as illustrated in supplement 2 – where 1x1km tiles are used for 5m resolution data on the whole area). The tile size should reflect the expected frequency of the directional trends in the landscape and the spatial resolution of the input DEM, while respecting the size of the particular phenomena that are expected to expose the directional trends. A certain minimum number of features-per-tile is required to get 'valid' results (as illustrated by figs 12 and 13). When analysing large datasets, one also has to consider that smaller tiles will increase the running time of the Line direction histogram plugin.

Treating extracted levels separately

Treating the levels separately as illustrated by Example 4 has *pros and cons*. Analysing data separately allows comparison of the resulting trends (Fig. 13) for the different slope levels. This can be used to identify areas where the directional trend is significantly affected by the (inherited) bedrock topography. The main disadvantage of treating the levels separately is that due to the splitting of lines where there is a change in steepness level, the line segments will be shorter (complicating smoothing). And the potential for improvement through optimisation is less for shorter lines. As illustrated in figure 13,

another limitation is that splitting into levels may make the total amount of lines for some levels very small, making the mean directional trend less reliable.

4.3. Future work

The tests presented here, using slope gradient (measured in degrees) is used as input, have produced satisfactory results. Future work should focus on reducing noise and raster effects, but also explore the method using other DEM derivatives, such as profile curvature, as input. Using more sophisticated rasters (combinations of several parameters/rasters within a single dataset) could also to be interesting. Yet, curvature is regarded as more scale dependent than slope (Evans, 2013; Evans, 2012; Evans and Cox, 1999). Further, as pointed out by Evans (2013), the distributions of curvature values (measured in degrees per unit length) has a tendency to strongly peak at zero. And the presence of such extreme positive and negative values can greatly bias the calculation of product-moment correlations. Therefore, some pre-processing transformations (like the normalisation procedure proposed by Csillik and others (2015)) is required to overcome sensitivity issues (Evans, 2013) for curvature.

The problem of over-representation of raster angles could be reduced by using a hexagonal grid instead of the 'classic' square grid (de Sousa et al., 2006; de Sousa and Leitão, 2017). However, the methodology (and software) for hexagonal raster implementation is still at the development stage (de Sousa and Leitão, 2017), and most software cannot handle hexagonal rasters yet.

5. Conclusions

Grayscale thinning of slope rasters for extracting directional trends from terrains have shown promising results for obtaining information on former glacial ice flow directions of the past glaciations. When compared to other SAM techniques, advantages of this approach are simplicity and robustness. Such characteristics are important when working with large (in terms of areal extent and file-size) datasets.

Therefore, the method has the potential to become a useful tool for regional scale applications in geomorphology.

Further development should focused on pre-processing and filtering techniques to minimize noise and raster effects, in order to better handle complex terrains as found in the central parts of the Scandinavian Mountains.

The method should also be tested on other previously glaciated landscapes (in Northern America, British Isles or Central and Eastern Europe) to demonstrate its capabilities within less complex geomorphological settings.

Acknowledgements

The authors would like to thank Sverre Anmarkrud for help with creating artificial surfaces, Jan Vermaat for valuable input on the manuscript, the Norwegian Mapping Authority (Kartverket) for providing the LiDAR dataset and Renata Lapinska-Viola (NGU) for help with acquiring additional datasets for the study area. We would also like to thank the anonymous reviewers of an earlier version of the manuscript for valuable comments

References

Baatz, M., Schape, A., 2000. Multiresolution segmentation: an optimization approach for high quality multi-scale image segmentation. Multiresolution Segmentation: An Optimization Approach for High Quality Multi-scale Image Segmentation, 12-23.

Biagioni, J., Eriksson, J., 2012. Map inference in the face of noise and disparity, Proceedings of the 20th International Conference on Advances in Geographic Information Systems. ACM, Redondo Beach, California, pp. 79-88.

Blaschke, T., 2010. Object based image analysis for remote sensing. ISPRS Journal of Photogrammetry and Remote Sensing, 65(1), 2-16.

Blaschke, T., Lang, S., Lorup, E., Strobl, J., Zeil, P., 2000. Object-oriented image processing in an integrated GIS/remote sensing environment and perspectives for environmental applications. Environmental Information for Planning, Politics and the Public, 555-570.

Boulton, G., Hagdorn, M., 2006. Glaciology of the British Isles Ice Sheet during the last glacial cycle: form, flow, streams and lobes. Quaternary Science Reviews, 25(23-24), 3359-3390.

Clark, C.D., Hughes, A.L.C., Greenwood, S.L., Jordan, C., Sejrup, H.P., 2012. Pattern and timing of retreat of the last British-Irish Ice Sheet. Quaternary Science Reviews, 44, 112-146.

Clark, C.D., Hughes, A.L.C., Greenwood, S.L., Spagnolo, M., Ng, F.S.L., 2009. Size and shape characteristics of drumlins, derived from a large sample, and associated scaling laws. Quaternary Science Reviews, 28(7), 677-692.

Csillik, O., Evans, I.S., Drăguţ, L., 2015. Transformation (normalization) of slope gradient and surface curvatures, automated for statistical analyses from DEMs. Geomorphology, 232, 65-77.

Culshaw, M.G., Cripps, J.C., Bell, F.G., Moon, C.F., 1991. Engineering geology of Quaternary soils: I. Processes and properties. Geological Society, London, Engineering Geology Special Publications, 7(1), 3.

d'Oleire-Oltmanns, S., Eisank, C., Drăgut, L., Blaschke, T., 2013. An Object-Based Workflow to Extract Landforms at Multiple Scales From Two Distinct Data Types. IEEE Geoscience and Remote Sensing Letters, 10(4), 947-951.

de Sousa, L., Nery, F., Sousa, R., Matos, J., 2006. Assessing the accuracy of hexagonal versus square tiled grids in preserving DEM surface flow directions. In: Caetano, M., Painho, M. (Eds.), Proceedings of the 7th International Symposium on Spatial Accuracy Assessment in Natural Resources and Environmental Sciences (Accuracy 2006). Instituto Geográphico Português, Lisbon, pp. 191–200.

de Sousa, L.M., Leitão, J.P., 2017. HexASCII: A file format for cartographical hexagonal rasters. Transactions in GIS, n/a-n/a.

Deng, Y., Wilson, J.P., Bauer, B.O., 2007. DEM resolution dependencies of terrain attributes across a landscape. International Journal of Geographical Information Science, 21(2), 187-213.

Drăguţ, L., Blaschke, T., 2006. Automated classification of landform elements using object-based image analysis. Geomorphology, 81(3), 330-344.

Dunlop, P., Clark, C.D., 2006. The morphological characteristics of ribbed moraine. Quaternary Science Reviews, 25(13-14), 1668-1691.

Eisank, C., Smith, M., Hillier, J., 2014. Assessment of multiresolution segmentation for delimiting drumlins in digital elevation models. Geomorphology, 214, 452-464.

Evans I. S. 2013 Land surface derivatives. Proceedings of Geomorphometry 2013: Nanjing Conference, 5-8.[Extended abstract]http://geomorphometry.org/Evans2013 http://geomorphometry.org/content/geomorphometry-2013-programme

Evans, I.S., 2012. Geomorphometry and landform mapping: What is a landform? Geomorphology, 137(1), 94-106.

Evans, I.S., Cox, N.J., 1999. Relations between land surface properties: Altitude, slope and curvature. In: S. Hergarten, H.J. Neugebauer (Eds.), Process Modelling and Landform Evolution. Springer Berlin Heidelberg, Berlin, Heidelberg, pp. 13-45.

Greenwood, S.L., Clark, C.D., 2009a. Reconstructing the last Irish Ice Sheet 1: changing flow geometries and ice flow dynamics deciphered from the glacial landform record. Quaternary Science Reviews, 28(27–28), 3085-3100.

Greenwood, S.L., Clark, C.D., 2009b. Reconstructing the last Irish Ice Sheet 2: a geomorphologically-driven model of ice sheet growth, retreat and dynamics. Quaternary Science Reviews, 28(27–28), 3101-3123.

Hess, D.P., Briner, J.P., 2009. Geospatial analysis of controls on subglacial bedform morphometry in the New York Drumlin Field – implications for Laurentide Ice Sheet dynamics. Earth Surface Processes and Landforms, 34(8), 1126-1135.

Hillier, J.K., Smith, M.J., 2012. Testing 3D landform quantification methods with synthetic drumlins in a real digital elevation model. Geomorphology, 153-154, 61-73.

Hillier, J.K., Sofia, G., Conway, S.J., 2015. Perspective – synthetic DEMs: A vital underpinning for the quantitative future of landform analysis? Earth Surf. Dynam., 3(4), 587-598.

Hubbard, A., Bradwell, T., Golledge, N., Hall, A., Patton, H., Sugden, D., Cooper, R., Stoker, M., 2009. Dynamic cycles, ice streams and their impact on the extent, chronology and deglaciation of the British-Irish ice sheet. Quaternary Science Reviews, 28(7-8), 758-776.

Hughes, A.L.C., Clark, C.D., Jordan, C.J., 2014. Flow-pattern evolution of the last British Ice Sheet. Quaternary Science Reviews, 89, 148-168.

Jammalamadaka, S. R., & Sengupta, A. 2001. Topics In Circular Statistics-vol 5. River Edge, N.J.: World Scientific.

Jasiewicz, J., Stepinski, T.F., 2013. Geomorphons — a pattern recognition approach to classification and mapping of landforms. Geomorphology, 182, 147-156.

Jorge, M.G., Brennand, T.A., 2017. Semi-automated extraction of longitudinal subglacial bedforms from digital terrain models – Two new methods. Geomorphology, 288, 148-163.

Kleman, J., Hattestrand, C., Borgstrom, I., Stroeven, A., 1997. Fennoscandian palaeoglaciology reconstructed using a glacial geological inversion model. J. Glaciol., 43(144), 283-299.

Marchand-Maillet, S.p., Sharaiha, Y.M., 2000. Binary Digital Image Processing : A Discrete Approas. Academic Press, San Diego.

Minár, J., Evans, I.S., 2008. Elementary forms for land surface segmentation: The theoretical basis of terrain analysis and geomorphological mapping. Geomorphology, 95(3), 236-259.

Napieralski, J., Nalepa, N., 2010. The application of control charts to determine the effect of grid cell size on landform morphometry. Computers & Geosciences, 36(2), 222-230.

Piégay, H. (2017). Quantitative Geomorphology. In International Encyclopedia of Geography: People, the Earth, Environment and Technology (eds D. Richardson, N. Castree, M. F. Goodchild, A. Kobayashi, W. Liu and R. A. Marston). doi:10.1002/9781118786352.wbieg0417

Putniņš, A., Henriksen, M., 2017. Reconstructing the flow pattern evolution in inner region of the Fennoscandian Ice Sheet by glacial landforms from Gausdal Vestfjell area, south-central Norway. Quaternary Science Reviews, 163, 56-71.

Ross, M., Campbell, J.E., Parent, M., Adams, R.S., 2009. Palaeo-ice streams and the subglacial landscape mosaic of the North American mid-continental prairies. Boreas, 38(3), 421-439.

Saha, K., Wells, N.A., Munro-Stasiuk, M., 2011. An object-oriented approach to automated landform mapping: A case study of drumlins. Computers & Geosciences, 37(9), 1324-1336.

Smith, M.J., 2011. Chapter Eight - Digital Mapping: Visualisation, Interpretation and Quantification of Landforms. In: M.J. Smith, P. Paron, J.S. Griffiths (Eds.), Developments in Earth Surface Processes. Elsevier, pp. 225-251.

Smith, M.J., Rose, J., Gousie, M.B., 2009. The Cookie Cutter: A method for obtaining a quantitative 3D description of glacial bedforms. Geomorphology, 108(3), 209-218.

Sofia, G., Pirotti, F., Tarolli, P., 2013. Variations in multiscale curvature distribution and signatures of LiDAR DTM errors. Earth Surface Processes and Landforms, 38(10), 1116-1134.

Spagnolo, M., Clark, C.D., Hughes, A.L.C., 2012. Drumlin relief. Geomorphology, 153-154, 179-191.

Spagnolo, M., Clark, C.D., Hughes, A.L.C., Dunlop, P., Stokes, C.R., 2010. The planar shape of drumlins. Sedimentary Geology, 232(3), 119-129.

Sărășan, A., Józsa, E., Ardelean, A.C., Drăguț, L., 2018. Sensitivity of geomorphons to mapping specific landforms from a digital elevation model: A case study of drumlins. Area, 0(0).

Tveite, H. 2017a. The QGIS Thin grayscale image to skeleton Plugin, version 0.3. March 2017. URL: http://plugins.qgis.org/plugins/ThinGreyscale/

Tveite, H. 2017b. The QGIS Line Direction Histogram Plugin, version 2.4. October 2017. URL: http://plugins.qgis.org/plugins/LineDirectionHistogram/

Wang, Y., Han, L., Xiao, S., Wang, J., Zhai, X., 2017. A novel statistical approach to remove salt-and-pepper noise. Journal of Statistical Computation and Simulation, 87(13), 2538-2548.

Wang, Y., Wang, J., Song, X., Han, L., 2016. An Efficient Adaptive Fuzzy Switching Weighted Mean Filter for Salt-and-Pepper Noise Removal. IEEE Signal Processing Letters, 23(11), 1582-1586.

Yu, P., Eyles, N., Sookhan, S., 2015. Automated drumlin shape and volume estimation using high resolution LiDAR imagery (Curvature Based Relief Separation): A test from the Wadena Drumlin Field, Minnesota. Geomorphology, 246, 589-601.

Supplement 1. Comparison of smoothing algorithms (GRASS) tested for skeletonisation outcome of real-world terrain (20 m resolution) from Close-up I presented in the paper.

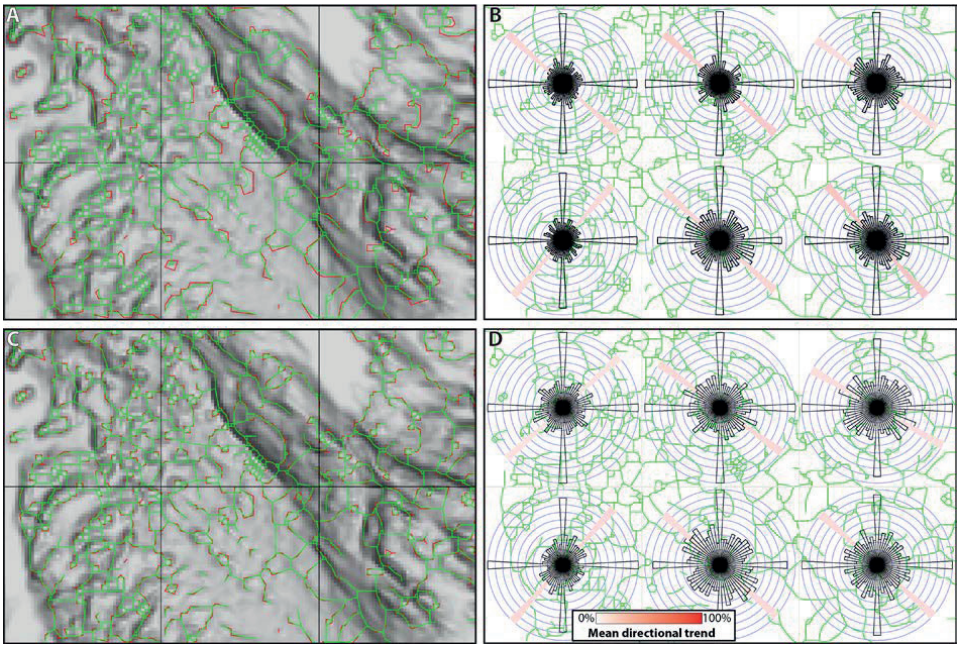

A. Result of 'snakes' with alpha=1 and beta=1 (in green) overlaid on slope raster and "raw" lines (in red) used as input for smoothing. **B.** Corresponding line directional histograms (for 'snakes') generated from the smoothed lines (in green). **C.** Result of 'chaiken' with tolerance=2*raster cell size (in green) overlaid on slope raster and "raw" lines (in red) used as input for smoothing. **D.** Corresponding line directional histograms (for 'chaiken') generated from the smoothed lines (in green).

Supplement 2. Skeletonisation outcome of various other thresholding approaches compared to the five equal interval approach:

20 m resolution, Quantile distribution, five thresholds.

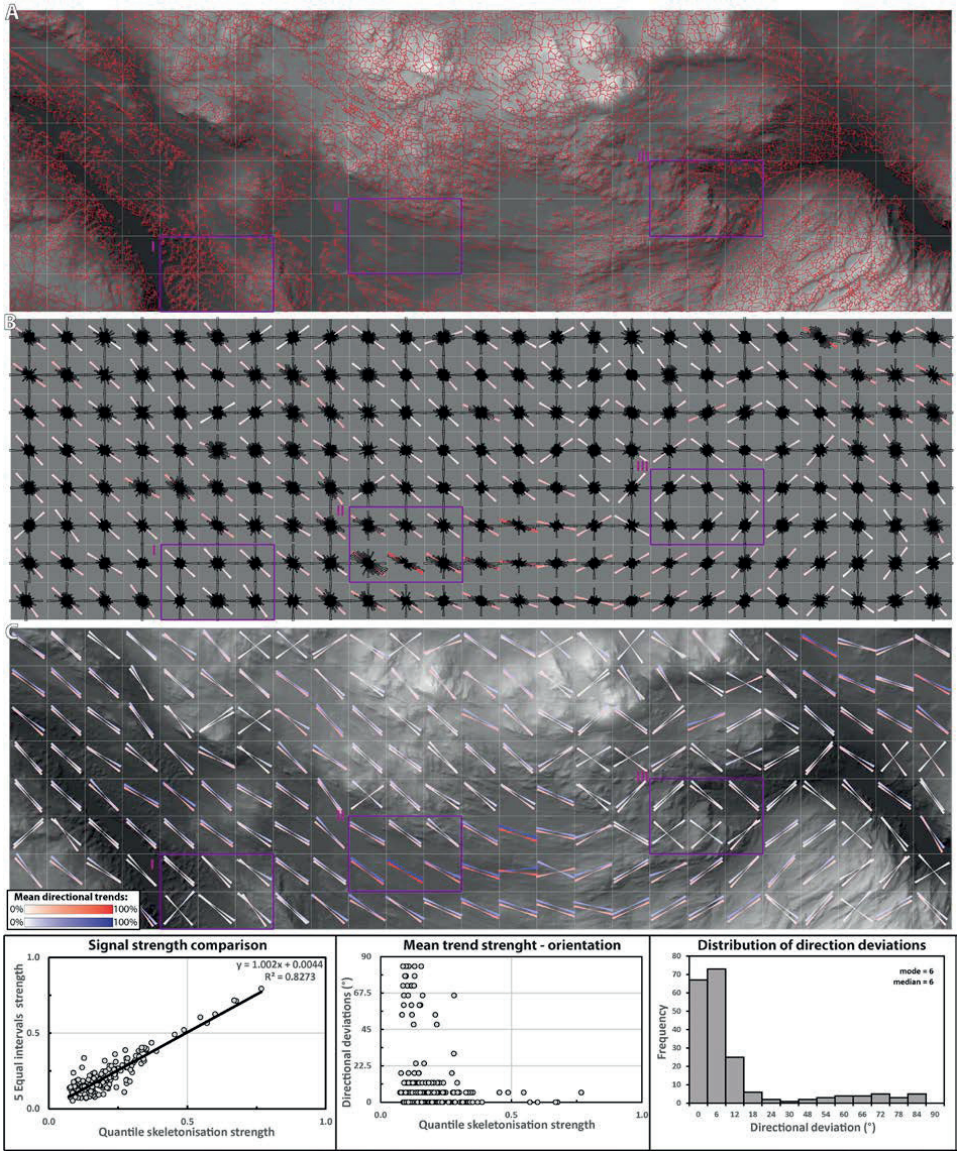

A. Skeletonisation outcome (filtered and smoothened lines) over DEM (hillshaded). **B.** Rose diagrams with mean directional trends. **C.** Mean directional trends extracted by using the Quantile distribution thresholding (in red) compared to mean directional trends extracted using Equal intervals (in blue). Statistical comparison between mean directional trends at the bottom of the figure.

20 m resolution, ten equal thresholding intervals.

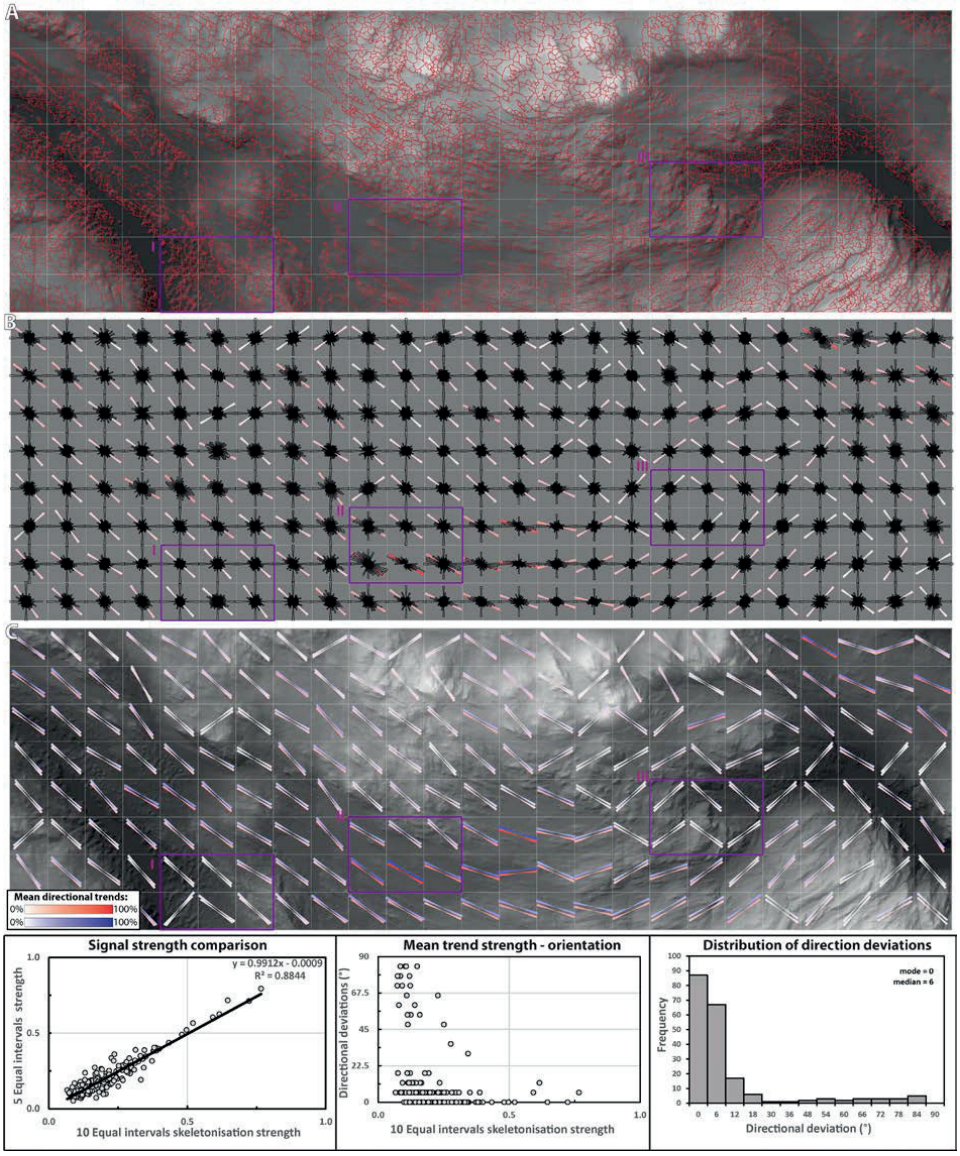

A. skeletonisation outcome (filtered and smoothened lines) over DEM (hillshaded). **B.** Rose diagrams with mean directional trends. **C.** Mean directional trends extracted by using the Ten Equal intervals' distribution thresholding (in red) compared to mean directional trends extracted using Equal intervals (in blue). Statistical comparison between mean directional trends at the bottom of the figure.

5 m resolution, five equal thresholding intervals.

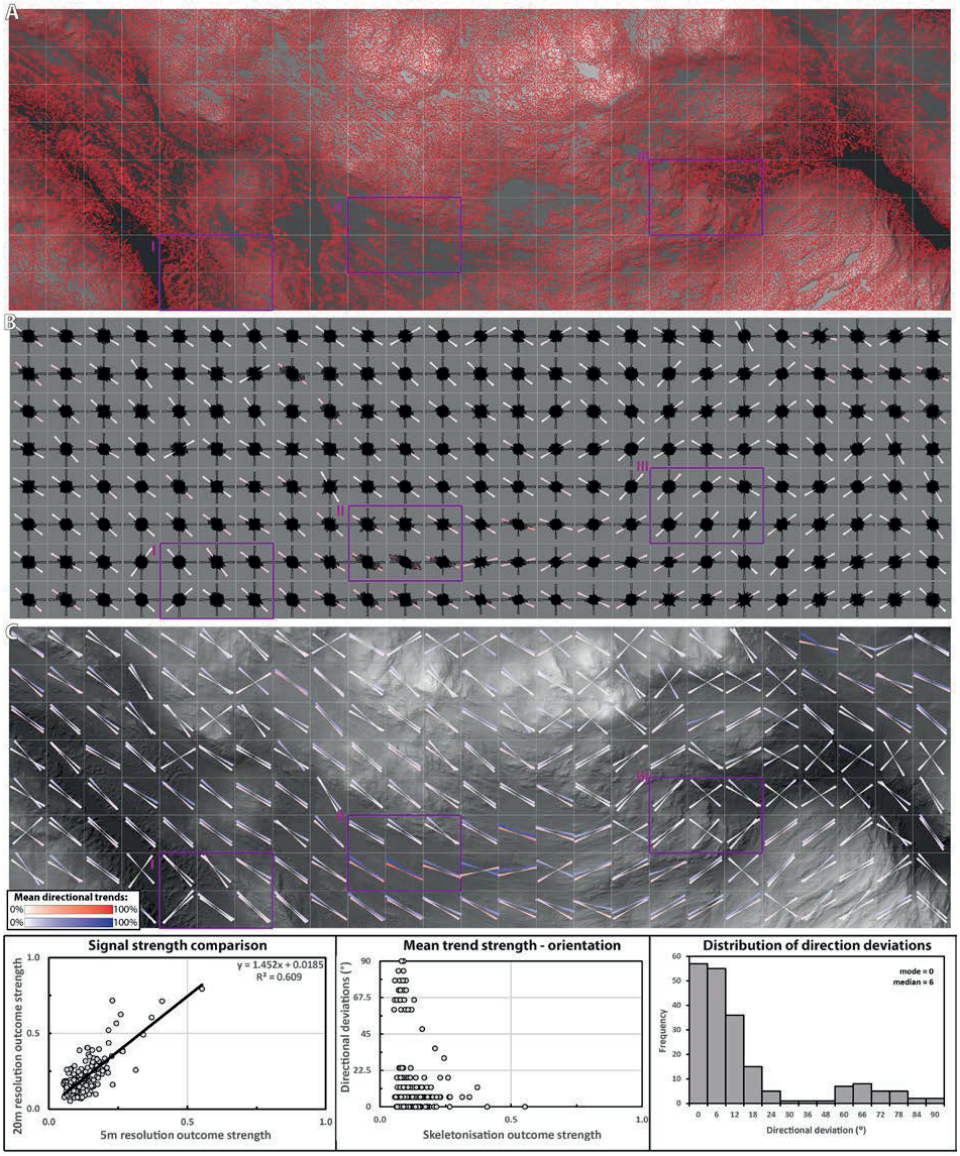

A. skeletonisation outcome (filtered and smoothened lines) over DEM (hillshaded). **B.** Rose diagrams with mean directional trends. **C.** Mean directional trends extracted by using the 5 Equal intervals, 5 m resolution (in red) compared to mean directional trends extracted using 5 Equal intervals, 20 m resolution (in blue). Statistical comparison between mean directional trends at the bottom of the figure.

Paper III

Putniņš, A., Henriksen, M. Final stages of deglaciation reconstructed from meltwater landforms in the Upper Etne valley, south-central Norway. *Manuscript. Prepared for submission to Boreas.*

Final stages of deglaciation reconstructed from meltwater landforms in the Upper Etne valley, south-central Norway

Artūrs Putniņš [a], *, Mona Henriksen [a]

[a] Faculty of Environmental Sciences and Natural Resource Management**, Norwegian University of Life Sciences, P.O. Box 5003, 1432 Ås, Norway**

* Corresponding author. Tel. +47 67231815. E-mail address: arturs.putnins@nmbu.no

Abstract

The meltwater landform domain contains valuable information on the dynamics of past ice sheets and their deglaciation. However, establishing the retreat patterns based on correlations of spatial and temporal relations of meltwater landforms can be difficult and lead to large uncertainties. Located in the inner area of the former Fennoscandian Ice Sheet, the upper Etne valley in south-central Norway contains numerous meltwater landforms. In order to use these landforms to reconstruct the deglaciation in detail, a simple reference surface gradient was implemented. By vertical sliding downwards this 'virtual ice surface' it represents the vertical down-wasting of ice. Delineations, where reference surfaces intersected with the terrain, where compared with the distribution pattern of meltwater landform to identify several important ice marginal positions and significant events of the meltwater drainage. This have revealed a reasonable sequence of events at the final stages of the deglaciation illustrating changes in ice dynamics, disintegration of ice, existence and drainage of local ice-dammed lakes in greater detail than described before. The reconstructed down-wasting of ice indicates that at the final stages of deglaciation the north–northwest inflow of ice shifted to being more from the west.

Keywords: Fennoscandian Ice Sheet, Deglaciation, Meltwater landforms, Down-wasting of ice, Virtual ice surface, Retreat patterns,

Introduction

The analysis of spatial distribution pattern of glacial landforms is a widely used tool in palaeoglaciological reconstructions of Pleistocene ice sheets (Livingstone *et al.* 2012; Clark *et al.* 2012; Margold *et al.* 2013a; Finlayson *et al.* 2014; Hughes *et al.* 2014; Margold *et al.* 2015; Putniņš & Henriksen 2017). The majority of studies have focused on the fluctuations of ice margins, ice thickness and ice volume (Mangerud 2004; Hughes *et al.* 2014; Stroeven *et al.* 2016) as well as in large-scale ice sheet reorganisations including the activity of the ice streams (e.g. Clark *et al.* 2012, 2017; Margold *et al.* 2015). Sequences of deglacial events are reconstructed by correlating certain mapped landform types with ice marginal positions (e.g. Clark *et al.* 2012). For example, sequent end-moraines indicates ice retreat (e.g. Clark *et al.* 2012, 2017) whereas trimlines can show the maximum thickness or different ice thermal conditions (Briner *et al*., 2006; Fabel *et al.* 2012). Meltwater landforms (and processes) have often played a minor role in such palaeogeological reconstructions leading to reduced meltwater involvement on governing and modulation ice sheet

dynamics (Greenwood *et al.* 2007; Storrar & Livingstone 2017). A recent conceptual development (Greenwood *et al.* 2016) emphasize the need to incorporate the records of meltwater landforms more thoroughly, since the 'deglacial envelope' of Kleman *et al*. (2006) provides a potential to reconstruct ice dynamics through space and time during the last deglaciation (Margold *et al.* 2011; Storrar & Livingstone, 2017). The need of understanding the meltwater drainage systems and their effect on the ice dynamics has particularly high importance within the context of the present-day warming climate (Greenwood *et al.* 2016). However, analysing the spatial distribution and temporal relations of marginal meltwater landforms is a relatively complex process (Ng *et al.* 2010; Margold *et al.* 2011, 2013 a, b; 2015) where uncertainties in the correlations between landforms lead to uncertainties in the established retreat patterns (Clark *et al*. 2012).

Reconstructions by Putniņš & Henriksen (2017) provide detailed insight on the distribution of different thermal conditions and the evolution of the retreat pattern within the inner sector of the Fennoscandian Ice Sheet (FIS), however, the development towards the complete deglaciation remains unreported. They have also mapped various types of meltwater landforms including two distinct distributional patterns of eskers – parallel and transverse to the ice flow (Putniņš & Henriksen 2017). Here we will pursue the final deglaciation by further investigate the complex development of flow pattern of the channelized flow phase (Phase III) (ibid) by utilizing the meltwater geomorphological domain and link it to the vertical down-wasting of the ice sheet (Garnes & Bergersen 1980). In order to gain more reliability of the findings we introduce a reference surface gradient based on the Krusgrav phase of Garnes & Bergersen (1980). Here the spatial and temporal relations of meltwater landforms from two nearby valleys, Fjelldokka and upper Etne and their adjacent areas are presented.

Regional setting

The study area (Fig. 1) is located in the mountain plateau of Gausdal Vestfjell in Oppland County, south-central Norway, c. 60 km west of Lillehammer and roughly 50 km southeast of Jotunheimen. The latter area is the highest part of the Scandinavian Mountains, an inner region of the former FIS (Mangerud *et al.* 2011). The study presented here particularly focuses on the upper part of Etne river valley and the adjacent areas; Lake Fullsenn, Fjelldokka and Trollåsen valleys and the valley north of Synnfjell.

The Upper Etne river valley area consists of metamorphosed sedimentary rocks of Precambrian to Ordovician age composed in series of thrust sheets (nappes) emplaced during the Caledonian orogeny (Heim *et al.* 1977). In the north of the study area, the Jotun-Valdres Nappe complex consists of metamorphosed arkose, greywacke sandstone, conglomerate and quartzite whereas slate, sandstone and limestone form the Synnfjell Nappe in the south. The rocks of the latter are highly deformed by faulting, thrusting, and stacking in NE-SW direction and have a high degree of schistosity (Heim *et al.* 1977).

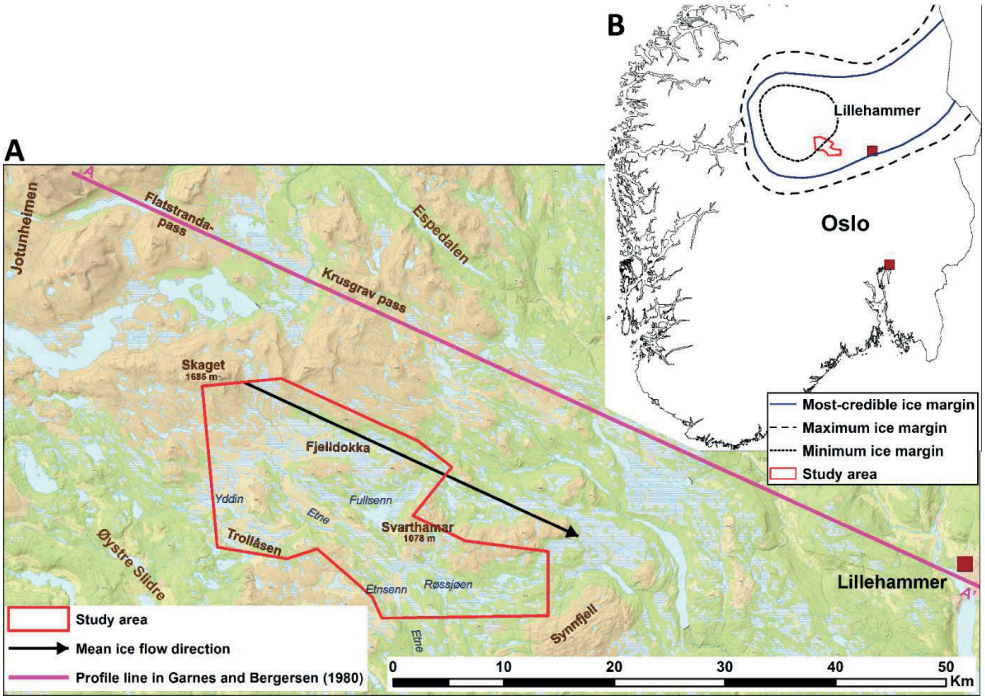

Figure 1. Location maps. **A.** Map of the study area with the approximate location of the profile line (A–A') used for the reference gradient surface generation, the Krusgrav phase by Garnes & Bergersen (1980). **B.** Overview map of southern Norway with minimum, maximum and most-credible ice margin locations at 10 ka (according to Hughes *et al.* 2016).

The study area is encountered with several mountain ridges, most notable are the ridge in the north with the highest peak Skaget (1685 m a.s.l.) and Synnfjell ridge (1415 m a.s.l.) in the southeast (Fig. 1). Separating the valleys and lake basins are several local elevated areas, typically around 1000 m a.s.l. whereas the valleys are mainly located between 920 and 800 m a.s.l. In general, the mountain plateau and the valleys are gently sloping towards southeast. Main drainage flow is in the same direction, including the two largest rivers, Fjelldokka and Etne, both emerging from the foothill of Skaget. Etne river runs into the lake Etnsenn, and continues downstream as Etna. In this study we use upper and lower Etne valley only for the stretch upstream Etnsenn, i.e. within the study area.

Two exceptions from the generally southeast sloping terrain are Trollåsen valley draining towards the northwest and the SW-NE oriented valley north of Synnfjell, following the bedrock structure (Fig. 1).

The sediment cover varies spatially throughout the study area depending mainly on the terrain topography. Till deposits of continuous cover and considerable thickness are mainly found on the valley floors, whereas the valley sides and hilltops either contain discontinuous thin glacial deposits or have exposed bedrock (Carlson & Sollid 1979). Glacifluvial deposits are abundant within the study area (Carlson & Sollid 1979, 1983; Putniņš & Henriksen 2017), associated with various landforms like eskers, kames, outwash fans and deltas or in form of sheet covers associated with ice dammed lakes. Also common are erosional landforms like various meltwater channels and over-washed surfaces. Peat and fluvial sediments from the Holocene are present throughout the study area (Carlson & Sollid 1979, 1983; Garnes & Bergersen 1980).

Until recently, the previous glacial reconstructions were mainly based on the investigations of till deposits and glacial striations at Gudbrandsdalen (roughly 50 km east of the study area) and its tributary valleys (Bergersen & Garnes 1972, 1983; Garnes & Bergersen 1980; Olsen 1985). Putniņš & Henriksen (2017) presented an extensive data set of the geomorphological mapping of glacial landforms (derived from the LiDAR data) providing insight on the development of ice flow pattern and ice dynamics during the Late Weichselian in the study area. The identified flow pattern evolution consists of three main phases; Phase I – topography-independent ice flow, a regional Phase II, and Phase III – a strongly channelized, topography driven ice flow, including four sub-stages. Putniņš & Henriksen (2017) point out that the channelized flow phase (phase III) and its sub-stages are closely associated with the deglaciation.

The study area (Fig. 1) is located directly to the southwest of the area covered by the work of Garnes & Bergersen (1980). There the deglaciation of the last inland ice sheet is described as being of a gradual down-wastage (Garnes & Bergersen 1980) where a stagnant and dead ice was existed at higher elevations while active ice was flowing in the valleys. Later, Sollid & Sørbel (1994) acknowledged the change from warm- to cold-based ice conditions at higher inland areas as streamlined landforms are found in these areas together with extensive supraglacial and lateral drainage systems. It is assumed that the vertical thinning of ice over the study area may have initiated simultaneously as at the Blåhø mountain (1617 m a.s.l.) situated roughly 70 km north (Putniņš & Henriksen 2017). Goehring *et al.* (2008) state that the thinning of ice at Blåhø began soon after 25.1 ± 1.0 ^{10}Be ka based on an exposure age from the summit, whereas lower-elevated samples yielded ages around 9.9 and 11.8 ^{10}Be ka.

In their work, Garnes & Bergersen (1980; also Bergersen & Garnes 1972) divides the deglaciation phase into the following substages (phases); the Nunatak phase (Da), the Krusgrav phase (Db), the Espedal phase (Dc), the Store Dølasjø phase (Dd) and the Gudbrandsdal phase (De). The pre-early and early substages of Phase III (Putniņš & Henriksen 2017) can be correlated to the Nunatak phase of Garnes & Bergersen (1980), while the middle and late substages of Phase III are correlated to the Krusgrav phase. Long-existing ice flow of Phase III is also connected with the Krusgrav phase. The whole deglaciation phase of Garnes & Bergersen (1980) corresponds to Vorren's (1977) Phase 4, assigned to represent the Preboreal age in the early Holocene.

Methods

Geomorphological mapping and the ground-truthing of landforms

The meltwater as well as other landforms investigated within this study were mapped manually using the same input data sources as in Putniņš & Henriksen (2017). The LiDAR data provided by the Norwegian Mapping Authority (Kartverket) was used as the primary source of terrain information. A Digital Elevation Model (DEM) of 3 m horizontal resolution was processed from the LiDAR and used to calculate a hillshade image. Additional sources of information (WMS servers) like the aerial imagery and topographic maps (Kartverket), maps of Quaternary deposits as well as the resource maps provided by the Geological Survey of Norway (NGU) were used to validate identified landforms and to exclude man-made objects (i.e. the road fragments, ditches, mounds or walls). The landform recognition and determination was carried out using ESRI software ArcGIS (version 10.3 and 10.5). In ArcGIS, a file geodatabase was established for the identified landforms (Putniņš & Henriksen 2017).

Subsequently to the geomorphological mapping of landforms, ground truthing was carried out. The aim was to clarify uncertainties of the genesis of various mapped landforms. Often the ground truthing constituted of identifying the sedimentary composition of landforms and, thus, to distinguish between glacigenic or glacifluvial genesis. After this step, the established database of identified landforms was updated in accordance to the fieldwork findings either adjusting the previously mapped landforms or including additional, previously unmapped landforms.

Implementation of the reference gradient surface and the correlations of meltwater landforms

Analysing the spatial and temporal distribution patterns of meltwater landforms over distances in areas where a distinct terrain slope exist can be a difficult task. Given the combination of such

topographic settings and the dome-shaped surface of the FIS ice sheet, correlating the marginal meltwater landforms simply along the same horizontal elevation (contour line) may introduce inaccurate results (Clark *et al*. 2012). For example, correlating two lateral meltwater features a few km apart along a valley side that are perched at the same absolute height above sea level, may wrongly suggest too thick ice in the down valley direction. Therefore the correlation of marginal meltwater landform should be carried out by following a gradient of the previous ice surface along the mountain and valley sides. Finding such gradient of a previous ice sheet at a certain stage (phase) in time is a complicated task, particularly for cases where lateral landforms cannot be traced along large distances on a regional scale. In a regional-scale studies from a nearby area, ca. 25 km to the northeast, Garnes & Bergersen (1980) states: 'observations of lateral marks, and the mapping of deposits assumed to correlate with them, indicate that the gradient of the ice surface in the area between eastern Jotunheimen and Mjøsa was approximately 1% during most of the deglaciation period'. Here we have chosen to use the same ice surface gradient of 1% with a dip towards southeast as the *Krusgrav phase* from Garnes & Bergersen (1980).

The reference gradient, i.e. the *ice surface of the Krusgrav phase*, was implemented in GIS as follow: First, the exact location of the profile line representing the Krusgrav phase was located on the topographic map (Fig. 1A) using figures from Garnes & Bergersen (1980). The start point was placed at the northern side of Heimdal and the endpoint placed at Lillehammer through the Flatstranda pass. The elevations of the ice surface (the Z values) were assigned in accordance to the profile graph (Fig. 5 in Garnes & Bergersen 1980) of the Krusgrav phase where Flatstranda is set to 1300 m a.s.l. Z values were calculated using simple mathematics of the distance from Flatstranda and 1% gradient. Then, the orientation of the profile line was compared to the direction of the regional ice flow (Phase II) pattern identified by Putniņš & Henriksen (2017) to validate suitability of the surface gradient for the study area. Since the ice flow pattern direction of Phase II (ibid.) corresponds fairly well to the orientation of the general slope of the terrain the profile line orientation was not adjusted. Further, the profile line with Z values were moved parallel roughly 25 km in southern direction for the surface gradient to cover the whole study area. The reference gradient surface was then generated using the 'Natural Neighbors' (ArcGIS System toolboxes, Spatial Analyst Tools, Interpolation) tool with the resolution of 5 m cell.

After the reference gradient surface was generated, the actual analyses of the spatial distribution and the temporal relations of meltwater landforms were performed. The analyses were carried out using both ArcGIS and ArcScene software from ESRI. In ArcScene, the possible ice surface of the Krusgrav phase was visualized over the DEM. To achieve this, the DEM, the gradient surface rasters and a polygon shapefile with the same extent as the gradient surface (to be used as the 'Virtual ice

surface') was added to the project. Then, under the 'Base heights' tab in the layer properties of the DEM layer, the elevation was set to be 'Floating on a custom surface' and the DEM raster itself was chosen as this surface. Similarly, the 'Virtual ice surface' layer was set to be 'Floating on a custom surface' with the selected reference gradient surface. These two simple operations allowed the ice surface of Krusgrav phase to be visualized and the spatial distribution of the meltwater landforms to be analysed in regards to their relations to the Krusgrav phase position. As a part of the analyses, the 'Virtual ice surface' was slid along the vertical (Z) axis visualizing different ice surface positions above and below the Krusgrav phase. This was achieved by modifying the layer offset of the 'Virtual ice surface' layer found under the same 'Base heights' tab in the layer properties. By doing this, several potentially interesting (regarding the locations of the meltwater landforms) possible ice marginal positions – levels (in m) above or below the Krusgrav phase surface – were noted for the further, detailed studies.

It should be pointed out that this simplistic method do not take into account that the profile of the previous ice surface was likely shaped more like a hyperbolic curve rather than a flat surface. Therefore, the approach implemented here do visualize the possible ice marginal positions including nunataks rather than visualizing the configuration of the actual ice surface.

After searching with a 'sliding' ice surface, a selection of illustrative maps showing possible ice marginal positions of the most informative levels were prepared in ArcGIS. To obtain these levels of ice surfaces, the height difference of DEM and the reference gradient (Krusgrav phase) surface was extracted using the raster calculator. These calculated surfaces were used in the 'Contour' tool (from the Spatial Analyst toolbox) to generate contour lines with 1 m intervals (the base contour set to 0 and the Z factor 1). Then the extracted contour lines representing the selected ice surfaces were filtered and the rest were neglected. Further, some smoothening and additional editing of the line features were carried out to improve the visual appearance of the outcome. In addition, ice thickness was calculated at four levels (+100 m, the Krusgrav phase, -100 m and -200m) using the raster calculator function described above. To ease the functionality of symbols, the calculated thickness maps were not converted to vector data but left as raster images.

Results

Meltwater landform examples

The analyses of meltwater landforms have been widely used for glacial reconstructions (Kleman *et al. 1997;* Greenwood *et al.* 2007; Greenwood & Clark 2009a, b; Margold *et al.* 2011, 2013a, b, 2015; Clark *et al.* 2012, 2017; Hughes *et al.* 2014) as this genetic group of landforms, in addition to glacigenic landforms, are well-known source of palaeoglaciological information on the thermal, dynamic conditions of ice and the deglaciation nature. Here we present a detailed study primarily focused on meltwater landforms and their characteristic in the study area, and discuss their implications in context to reconstruct the deglaciation.

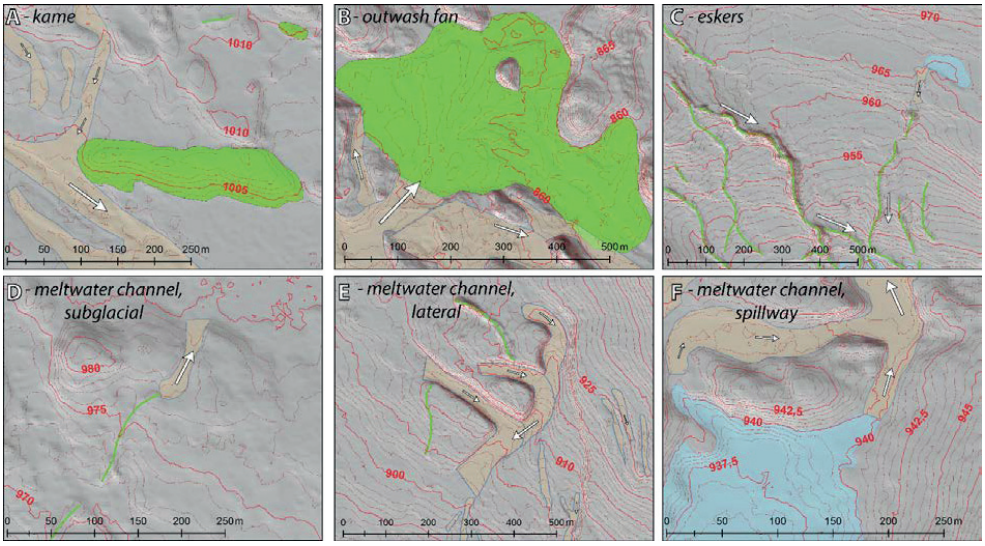

Figure 2. Examples of meltwater landforms used for glacial reconstructions. Red numbers indicate present day elevation (m a.s.l.). For legend, see Fig. 3. **A.** Kame terrace. **B.** Non-constrained outwash fan. **C.** Eskers. **D.** Subglacial meltwater channel. **E.** Lateral (marginal and submarginal) meltwater channels. **F.** Proglacial (spillway) meltwater channels.

Kames and kame terraces and constrained outwash fans. Depositional meltwater (glacifluvial) landforms as kame terraces (Fig. 2A) and constrained outwash fans are relatively abundant within the study area. They are predominantly located on the valley slopes and are used as indicators of lateral ice margins. Noticeably most of the mapped kame terraces are found at the northern side of Fjelldokka valley (Fig. 1A). As they are generally located at higher elevation, they indicate that this area was one of the first to become deglaciated by down-wastage of ice (c.f. Garnes & Bergersen 1980). I.e. the meltwater drainage and thus the deposition of glacifluvial material initiated earlier here and may have potentially happened for a longer time. At the northern side of Fjelldokka valley are also constrained outwash fans. Their morphology resembles the nearby ribbed moraine and were

likely accumulated in ice crevasses plausibly burying the underlying ribbed moraines (Putniņš & Henriksen 2017).

Commonly these landforms are found in close spatial associations with meltwater channels. The depositional landforms are either (a) located in distal (down-flow direction) ends of meltwater channels suggesting that they might have formed simultaneously, or (b) they are cut by meltwater channels, indicating that the channels are younger. Kames are also found on the valley sides, in some places together with kettle holes forming a so-called *kame and kettle topography* (Benn & Evans 2010).

Non-constrained outwash fans and deltas. Depositional glacifluvial landforms as non-constrained outwash fans and deltas have a district, typically conical shape (Fig. 2B). The non-constrained morphology indicates proglacial deposition away from the ice margin, either in a subaerial or glacilacustrine environment. The identified deltas must have been deposits in areas previously occupied by ice-dammed lakes, suggesting that these meltwater basins have existed for a sufficient time allowing formation of this landform. Both the deltas and non-constrained outwash fans are less common within the study area, and are usually found located at distal (down-flow direction) ends of meltwater channels.

Eskers. Eskers are one of the most abundant glacifluvial landforms (~965) found within the study area. Two groups of distributional pattern of eskers, parallel (Fig. 2C) and transverse to the general ice flow direction have been recognized by Putniņš & Henriksen (2017). The parallel eskers are usually morphologically more pronounced, i.e. wider, higher and longer, suggesting that they evolved over a longer period of time, whereas the transverse eskers form shorter, more fragmented systems. This indicates shorter time of development at a later stage of deglaciation. The esker systems parallel to ice flow are mainly found on the valley sides and have probably acted as conduits feeding the subglacial meltwater drainage system and thereby affected the ice flow dynamics further downstream. At the northern side of lake Fullsenn (Fig. 4) is one of the most prominent esker system (~6 km in total length), mainly consisting of parallel eskers but also some several cross-cutting eskers. This, combined with the overall location of the system, indicates that for a sufficient long period the subglacial meltwater drainage within this basin occurred predominantly through the pass in northeast towards the Fjelldokka valley.

Various patterns of spatial relationships between eskers and other meltwater landforms are observed. In some cases, eskers are accompanied by subglacial meltwater channels both upstream

and downstream, whereas lateral meltwater channels are often located higher above on the valley slope to the eskers. These spatial relationships indicate that these landforms may have been formed simultaneously or subsequently by the same meltwater drainage system. Eskers cut by meltwater channels, on the other hand, indicate a sequence of events as well as to a change of the mode in drainage pattern.

Meltwater basins / ice-dammed lakes. Meltwater basins, which for a relatively short time held ice-dammed lakes, are found in different topographical settings and at various elevations throughout the study area. Often these basins have formed within local depressions on valley slopes or cover relatively large areas of valley floors. Present day lakes are commonly found at the lowest parts of these basins. Such short-lived ice-dammed lakes are identified based on spillway channels, deltas and shore lines.

The levels of ice-dammed lakes have been mapped by identifying the lowest out-flowing spillways over pass-points. In some cases like Fullsenn, and possibly also Trollåsen, rudimentary remnants of older drainage pattern (Fig. 2F) are identified indicating that during earlier stages the water table was higher. This suggests another ice configuration. Basins with deltas point towards sufficient amount of time of existence of the ice-dammed lake allowing deltas to form. The relative age differences of the existence of ice-dammed lakes can be evaluated by following the concept of vertical down-wastage of ice (Garnes & Bergersen 1980) which implies that the meltwater basins located at higher elevations are older than their lower counterparts. Moreover, the geomorphological evidence suggest that the higher elevated meltwater basins have acted as a source for subglacial/englacial drainage as indicated by eskers lying lower in the terrain (Fig. 2C).

When mapping the meltwater basins (ice-dammed lakes), it is difficult to determine their maximum extent due to the unclear ice marginal positions at the time of basin existence. In some cases where a distinctive characteristic meltwater basin features (beach ridges, spillway channels, others) are lacking, it cannot be excluded that instead of meltwater the basins have been filled with remnant ice blocks. The boundaries of the meltwater basins adjoining the previous ice body are here delineated following the obstacles imposed by the underlying topography (i.e. the borders are drawn at the place where the underlying topography may have caused a separation of the ice mass). The observations (Supporting information Fig. S1) suggest that the most favourable conditions for formation of ice-dammed lakes are in front of the ice in areas where the slope of the underlying topography is dipping in the opposite direction of ice flow (Trollåsen, Fullsenn, valley north of Synnfjell). Such topographical setting gives favourable conditions for a longer existence of ice-

dammed lakes than a lateral setting in a valley where the meltwater basin is formed along the ice tongue. The potentially largest meltwater basin within the study area is located in the lake Fullsenn basin and could have covered up to 4-5 km^2, however, the ice-dammed lake area is uncertain as the exact ice position is hard to determine.

Meltwater channels. Meltwater channels are one the most distinctive erosional glacifluvial landforms found within the study area (Fig. 2). As pointed out by Greenwood *et al*. (2007), meltwater channels are a valuable source of information for deglacial reconstructions, however, it is important to distinguish the different channel types. Here, we have categorized meltwater channels into three groups following Greenwood *et al*. (2007); lateral, subglacial and proglacial meltwater channels (spillways) (Fig. 2D-F). Such categorizing is sometimes difficult due to the ambiguous nature of identified features. Observations suggest that in areas with certain topographic conditions, such as terrain slope oriented opposite the previous ice flow direction (Fig. 3), it is possible that the meltwater channels developed under lateral or subglacial conditions later operated as proglacial channels. Such reuse of exciting meltwater channels have also been acknowledged by similar studies elsewhere (e.g. Carrivick *et al.* 2017; Storrar & Livingstone 2017).

Subglacial meltwater channels. As pointed out above, it is in some cases hard to determine whether a meltwater channel is purely of a subglacial origin as that their functionality may have been changed over time. A few of meltwater channels within the study area are clearly identified as subglacial (Fig. 2D) based on the following diagnostic criteria summarized by Greenwood *et al*. (2007): (a) abrupt beginning and end (Sissons 1960, 1961; Glasser & Smith 1999); (b) close spatial relations with eskers (Kleman & Borgström 1996) and (c) lack of alluvial fans (Sissons 1961). Since the orientation of subglacial channels is governed by the disposition of the hydraulic head, which is approximately the direction of the steepest ice-surface slope (Sugden *et al.* 1991), these channels can therefore indicate ice flow direction close to the terminus and thus ice-front margins may be reconstructed orthogonal to the channel systems (Greenwood *et al.* 2007). Moreover, subglacial meltwater channels indicate a warm-based thermal regime (Greenwood *et al.* 2007).

Lateral meltwater channels. Lateral meltwater channels of both marginal and submarginal types are probably the most abundant type of meltwater channels in the study area. They are commonly found on valley slopes throughout the whole study area. The lateral meltwater channels are often found in sequential series at different elevation (Fig. 2E) indicating down-wasting of ice (Garnes & Bergersen

1980), considered as indicators of successive ice marginal positions drawn parallel to these channels (Greenwood *et al*. 2007). Such channels are interpreted as indicators of marginal cold-based ice where meltwater cannot drain through the englacial–subglacial conduits and therefore is deflected along the ice margins (Dyke 1993; Kleman *et al.* 1997; Hättestrand 1998; Greenwood *et al.* 2007; Evans *et al.* 2017). However, as proved by Syverson & Mickelson (2009), lateral meltwater channels may also form under temperate ice conditions.

Lateral meltwater channels are determined according to the following diagnostic criteria (summarized by Greenwood *et al*. 2007): (a) forms sequence of channels parallel to each other (Sissons 1961; Schytt 1956; Dyke 1993); (b) are perched on valley sides (Benn & Evans 2010); (c) may terminate in downslope chutes (Sissons 1961; Schytt 1956). The most prominent (the longest and widest) of the identified lateral meltwater channels (north of Trollåsen; Etne's tributary valley; south of lake Fullsenn) usually have gentle gradients pointing towards marginal origin whereas the shorter channels with steeper gradients and with a sudden change in direction may be of submarginal origin (Sissons 1961; Greenwod *et al.* 2007). Most prominent examples of sequential, sinuous lateral meltwater channels within the study area are found in Trollåsen (Figs 2E, 7, 8C) and on the northern side of Fjelldokka valley (Figs 7, 8A).

Occasionally the lateral meltwater channels are found in close spatial relations with depositional glacifluvial landforms such as kame terraces and constrained outwash fans (Fig. 8A) and rarer with meltwater basins (ice-dammed lakes) (Fig. 3), suggesting that these landforms may have formed contemporaneous or at least within a short time frame. When lateral meltwater channels are found in close spatial relations to eskers, it is important to distinguish between the type of distributional pattern of eskers (parallel or transverse to the general ice flow direction). Lateral channels in close spatial relations with parallel eskers (Fig. 3) are likely formed during different stages of deglaciation. Whereas, when lateral channels are found in proximity with transverse eskers (Fig. 8C) they may indicate a simultaneous processes of landform formation, as also presented in example by Syverson & Mickelson (2009).

Proglacial meltwater channels (spillways). A few of the meltwater channels within the study area are identified being of proglacial origin (Fig. 2F) based on the following criteria: (a) regular meander bends; (b) occasional bifurcation (Benn & Evans 2010); (c) direct downslope flow direction (Prince 1960). It is likely that proglacial meltwater channels may have originated as subglacial meltwater channels that have later undergone subaerial enlargement at the later stages of deglaciation (Benn & Evans 2010). The characteristic of these channels are that they have large (deep and wide)

dimensions that cannot be explained by the fluvial erosion processes in non-glacial conditions (Benn & Evans 2010). Often, spillways are accompanied by bare rock fields at their down-flow sides.

In areas where ice-dammed lakes (meltwater basins) have existed and spillways indicate water flow the opposite direction than present-day drainage (Figs 4, 7), water have occasionally drained the basins into adjacent valleys. Often the (non-constrained) depositional landforms like outwash fans and/or deltas are present at the downstream end of these channels (Fig. 8B).

Possible ice marginal positions

Valley north of Synnfjell

The valley north of Synnfjell was important for establishing the ice flow pattern evolution in Etne valley system as ice masses of considerable (~200m) thickness was flowing up-hill (eastwards) around the obstacle of the Synnfjell ridge until the latest stage of active ice flow (Putniņš & Henriksen, 2017). The development of this shift in ice flow pattern is further investigated here. All of the possible ice marginal positions within this area are located above the Krusgrav phase surface (0 m of reference surface).

Stages from +200 m to +100 m above the reference surface. A theoretical ice surface 200 m above the Krusgrav phase (+200 m) was delineated to illustrate the likely marginal position of the Nunatak phase (Garnes & Bergersen 1980) within this area. It revealed that the nearby peaks to the south (the Synnfjell ridge) and north were ice-free and that the ice flow was restricted within the valley (Fig. 3). The +100 m stage illustrates the disintegration of the ice masses where the several ice-free areas around topographic obstacles indicate partly deviated ice flow. Close to the water divide within the valley, the ice masses in the west and east became separated. With no further ice flowing from the west, the ice masses in east became stagnant. This separation is also indicated by the extensive development of eskers in the western area, whereas to the east abundance of meltwater channels are present (Fig. 3). In additional, surface run-off water (and meltwater) from the slopes to the north was draining towards the ice margin, joining to the meltwater system via lateral, subglacial or proglacial systems.

Stages from +82 m to +50 m above the reference surface. The possible ice marginal position at + 82 m illustrates a further retreat from the pass-point (Fig. 3). At this stage, the major esker system near the glacial front melted out from the ice whereas a distinct kame terrace formed laterally to the

north. To the northwest, a development of sequential proglacial meltwater basins can be seen. A noticeable proglacial drainage system (in central part) as well as a distinct fan-shaped esker system in the south started to evolve (Fig. 3). Further development of these systems are shown with the following marginal positions delineated. At the +67 m delineated stage a distinct kame terrace north of Lake Sæbu-Røssjøen started to emerge from the ice. Moreover, emerging eskers at the southern coast of the lake (Fig. 3) also indicate that at this point the ice body within Sæbu-Røssjøen became disintegrated from the rest of the ice. The +50 m stage, however, shows a possible ice marginal position when the dead ice block at Sæbu-Røssjøen had melted away and the distinct esker system in the south emerged from the ice (Fig. 3). At this point, the drainage direction of the proglacial water shifted from eastward to south- and westward flow towards the ice front where it joined the existing subglacial drainage system (Fig. 3). An ice-dammed lake evolved at the northern side of the ice tongue.

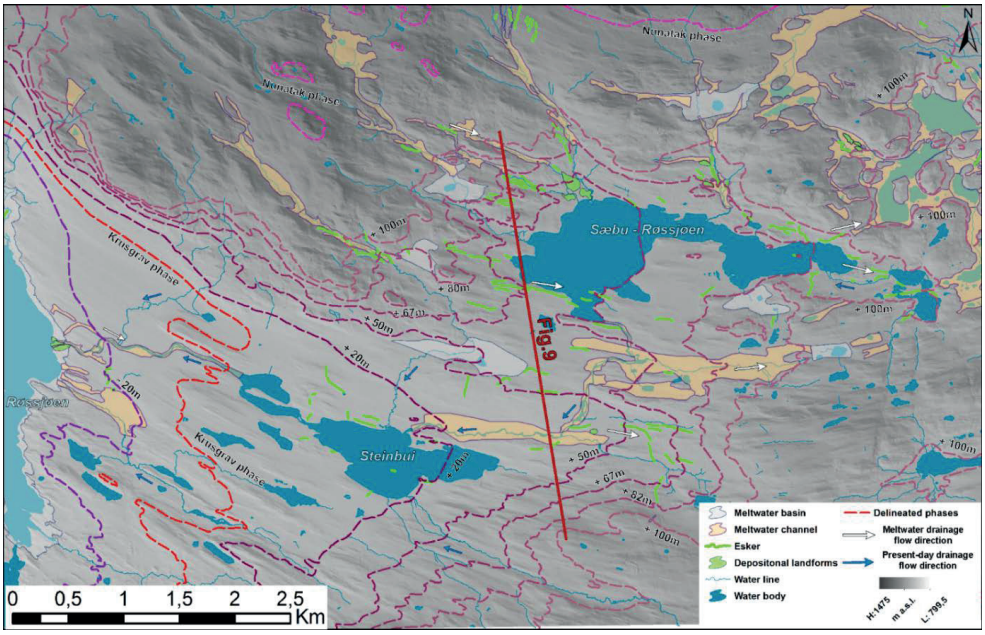

Figure 3. Possible ice marginal positions delineated at the valley north of Synnfjell.

Lower Etne valley and lake Fullsenn

Stages from +67 m to the Krusgrav phase. The first noteworthy of the delineated stages within this part of the study area is the +67 m stage. At this stage the ice-dammed lake (meltwater basin) within the lake Reinetjernet area, northeast of Svarthamar, started to evolve (Fig. 4). During this period, the meltwater basin was draining towards the northeast (out of the bounds from the study area) via a spillway. Later, the drainage occurred through two subsequent lateral meltwater channels that had developed at southern side of the basin due to the following glacial retreat. This meltwater basin

continued to evolve and roughly during the +50 m stage it was likely draining through an englacial-subglacial conduit system (as well as through the meltwater channel occupied by the present-day Reina river). As glacial retreat continued in the area between lake Reinetjernet and Svarthamar, several other local meltwater basins were formed and various meltwater channels evolved prior to the Krusgrav phase (Fig. 4).

Stages from the Krusgrav phase to -132 m. Area between Svarthamar and Røssjøen. Roughly around the Krusgrav phase (0 m) the valley between Svarthamar and lake Reinetjernet had become ice-free (Figs 4, 5A) and the present-day water catchment of lake Reinetjernet drained proglacially to the ice margin. The delineated possible ice marginal positions illustrate that the whole basin of lake Røssjøen was filled with ice during the Krusgrav phase. Only at the -55 m stage the ice had retreated from most of the lake and the lower part of Reina river allowing a local meltwater basin to drain into Røssjøen via a lateral channel (Figs 4, 5A). It is plausible that this ice-dammed lake had previously drained subglacially through a subglacial meltwater channel (present-day esker). As a consequence of continuous vertical down-wasting of ice, the ice tongue had further glacial retreated from the valley south of Svarthamar (Figs 4, 5A) until the ice completely left the area at the -100 m stage.

***Stages from the Krusgrav phase to -132 m. Lake Fullsenn*.** During the period from the Krusgrav phase to the -55 m stage a subglacial drainage pattern was dominant within the lake Fullsenn area. At this period the esker system at the northern side of the lake was likely active draining meltwater through the subglacial–englacial conduits to the pass-point to Fjelldokka valley (Fig. 4). At some point in this period, lateral drainage also occurred over this pass-point. Later, at the -63 m stage the ice masses over the passage had separated and the mode of meltwater drainage shifted to proglacial drainage allowing three sequential spillway outlets to develop (Figs 4, 5B). At around the same time, an ice-dammed lake started to form at the northeastern corner of the Fullsenn basin. Following the glacial retreat towards west, the ice-dammed lake continued to expand with drainage through the lowermost spillway in northeast. This basin system was stable until the ice surface lowered to the -75 m stage when ice retreated from an obstacle, allowing meltwater to drain southwards (Figs 4, 5C) and initiated a gradual change from proglacial to lateral drainage. It is plausible that a simultaneous drainage through the both ends of the basin may have existed for a while, however, from the -85m stage the lateral drainage southwards to the Etne valley became dominant (Figs 4, 5C) and the spillway in northeast was abandoned. A series of subsequent meltwater channels indicate a gradual

lowering of the lateral drainage system along the eastern side of valley between lake Fullsenn and Etne valley until the -100 m stage. At this stage a distinct lateral meltwater channel developed at the southern side of lake Fullsenn (Figs 4, 5C) and the ice masses in Fullsenn and Etne valley started to separate as topographic obstacles emerged from the ice. Although the exact sequential order of the channel development and the configuration of ice masses during the transition from -100 m to -107 m is uncertain, it is evident that the lowermost lateral channel in the valley between Fullsenn and Etne was formed while there still was some ice remains in this valley. In addition, the few eskers found here (Figs 4, 5C) suggest that earlier, when the ice was thicker, the drainage here may at least partly occurred through subglacial-englacial conduit system. The disintegration of ice masses between lake Fullsenn and Etne valley that initiated around -100 m to -107 m stages terminated at the -132 m stage when there were only few ice remnants left (Fig. 4).

Stages from -132 m to -197 m. ***Lower Etne valley (near Etnsenn).*** Between the -107 m to -150 m stages, including the -132 stage, lateral meltwater channels accompanied by a few kames indicate possible ice marginal positions in Etne valley (Fig. 4). The slightly higher elevated terrain along the north-eastern side of the valley suggests that the ice masses here were thinner than in the deeper southwestern part (Fig. 6), indicating that the ice at these stages was likely stagnant in the northeast while it could be active ice in the deepest part of valley. At the -150 m stage, the glacier was roughly covering the whole lake Etnsenn, while at the -180 m stage it had retreated to the northern shore of the lake (Figs 4, 6). The transition from the -150 m to -180 m stage is marked by a development of extensive lateral meltwater channel systems and kames on both sides of the valley (Fig. 4), of which the one located on the southern side is the most prominent. As down-wasting of ice progressed,

there were only small, thin and disintegrated remnants left within the deepest part of the valley at the -197m stage (Fig. 4), prior to the complete disappearance of ice.

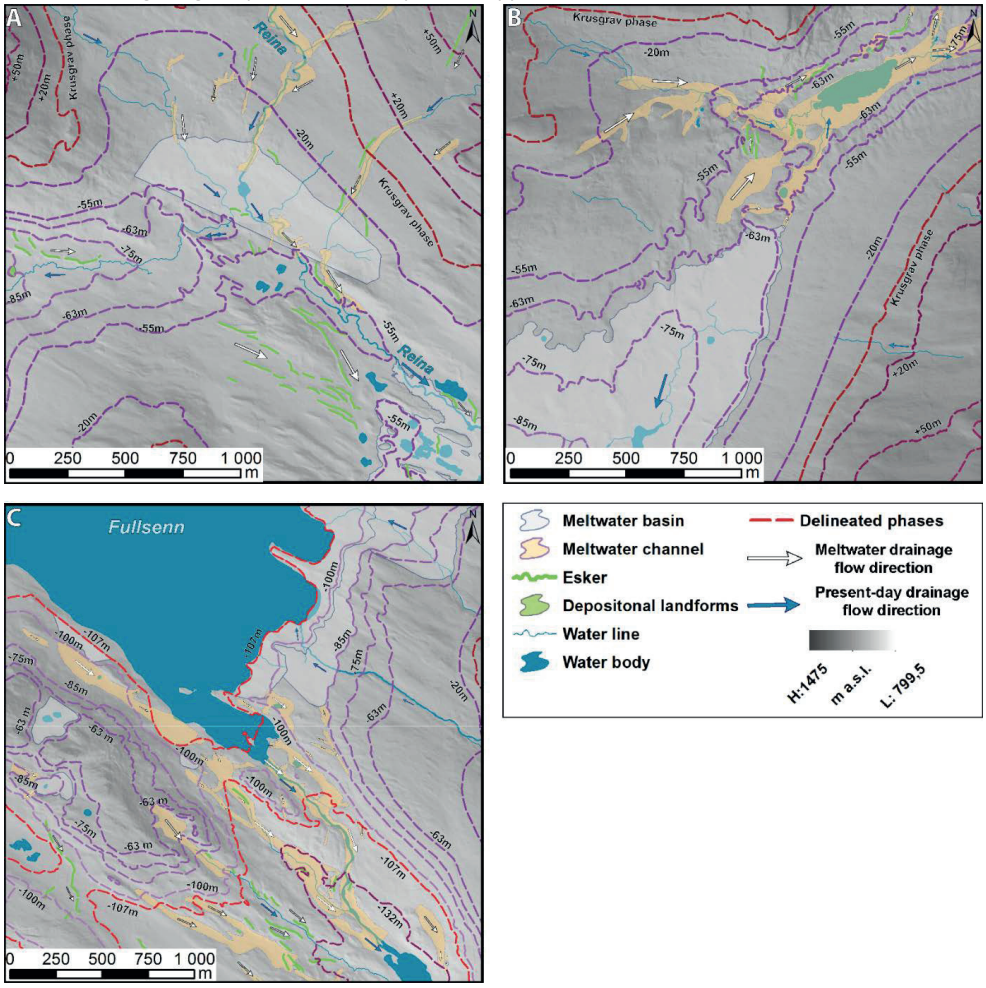

Figure 5. Close-up maps for areas selected in Lower Etne valley and lake Fullsenn. **A.** Area between Svarthamar and Røssjøen. **B.** Fullsenn–Fjelldokka pass (northeast of lake Fullsenn). **C.** Fullsenn–Lower Etne pass (southeast of lake Fullsenn).

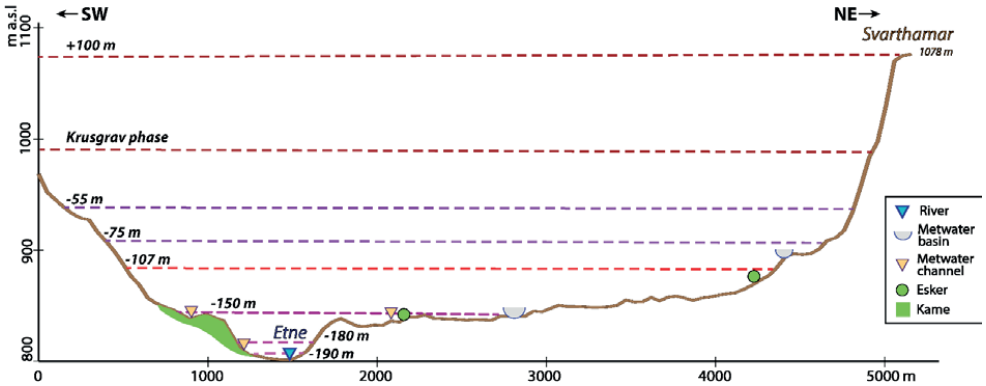

Figure 6. Cross-profile over the Lower Etne valley near Svarthamar (see Fig. 4 for profile location). Dashed lines indicate the ice surface gradients with possible ice marginal positions using the same colour-coding as used in map in Fig. 4.

Upper Etne, Fjelldokka and Trollåsen valleys

Stages from -75 m to -180 m. Fjelldokka and Upper Etne valley. As noted earlier, the northern side of Fjelldokka valley is located on a generally higher elevation than most of study area. Consequently, the deglaciation by down-wastage of ice initiated relatively early here and it is thought that drainage was especially heavy at the early stages (Garnes & Bergersen 1980). The deglaciation is marked by several lateral meltwater channels at different heights (Figs 7, 8A).

The most distinct channels are found between the marginal position of -75 m to the -85 m stage (Fig. 7). At the -85 m stage, the ice margin had retreated enough to allow a meandering lateral meltwater channel to form by cutting into the valley slope (Fig. 8A). At lower levels these meltwater channels developed further and are accompanied by depositional meltwater landforms, following the marginal positions delineated at -100 m and -107 m. The most prominent depositional meltwater landforms within this area could only have formed after further glacial retreat from the marginal positions of -107 m to -125 m stage, as seen by their spatial positions (Fig. 7).

The marginal position of -125 m stage indicates that the ice thickness had reduced to a level at which some of the ribbed moraine crests began to emerge above the ice surface, suggesting dead ice. This is in accordance with the observations that blocks of dead ice that might have existed nearby the depositional meltwater landforms described earlier (Figs 7, 8A). The ribbed moraine crests had emerged further from the ice surface when the marginal position reached -132 m stage. Following the further deglaciation (around -150 m stage), the ice had fully retreated from the Fjelldokka valley into the upper part of Etne valley. This retreat is illustrated by the sequence of various meltwater channels that had formed prior to the present day drainage of Etne river (Fig. 7). At the -180 m stage, as indicated by the delineated marginal positions (Fig. 7), the ice had retreated further to a lower

elevation level occupying only small area around Bjørnhaug, thus allowing the Etne river to evolve to what is its present day drainage. Further down the Etne valley, and roughly at the same time (from -150 m to -180m stage), lateral meltwater channels evolved on the side of the narrowest valley section between Etnehovda and Gråeberget (Fig. 7).

Stages from -75 m to - 180 m. ***Trollåsen–Etne passage.*** Although the Synhaugen ridge (Fig. 8B), between the southern Trollåsen and Upper Etne valleys, had been partly emerged from the ice at an earlier stage (-85 m) (Fig. 7), it was first around the -107 m stage Synberget peak started to appear indicating the two passages between these valleys. The northern of these two passages became ice-free at -180 m stage allowing meltwater to drain into Upper Etne valley. Correlating to the same stage are two distinct kame terraces located in close proximity to the southern passage, indicating that this passage was filled with ice. The drainage through these two passages may have occurred simultaneously but with different modes (Fig. 8B). The fact that the channel in northern passage is weakly developed (poorly eroded into the surrounding terrain) may indicate that the drainage through here, if compared to the southern passage, was a short-lived event.

Stages from -190m to –316 m. The delineated ice marginal positions illustrates that ice masses in the Trollåsen–Upper Etne passage separated completely between the -180 m to -190 m stage (Figs 7, 8B). Lateral and proglacial channels as well as ice-dammed lakes evolved at the ice margin in Trollåsen valley (Fig. 8B). At the same stage, the ice body in the narrow part of Upper Etne valley between Etnehovda and Gråeberget started to disintegrate (Fig. 7), leaving at least two separate ice bodies in the Upper Etne valley, where the one at the valley head still was fed by ice from NE. A possible third ice body existed in main part of Etne valley by a kame (Fig. 7).

As the ice retreated to the marginal position of -212 m stage, a distinct lateral meltwater channel (at least 1.5 km long) was formed along the northern side of the Trollåsen valley (Fig. 7). The ice-dammed lake in front of the ice margin reached its maximum extent, draining into Etne valley (Figs 7, 8B). At the same stage (-212 m), the active ice had retreated from catchment of present-day Etne river. Only a few thin ice remnants were left at the valley head southwest of Bjørnhaug (Fig. 7). Another ice remnant probably existed 3-5 km to the SE in the deepest part of Etne valley (Figs 7, 8B).

By the -228 m stage, the meltwater drainage along the northern side of the Trollåsen led to an intensive formation of various lateral meltwater channels (Figs 2E, 7, 8C). Further, a sequence of lateral meltwater channels (Figs 2E, 8C) was formed when the ice retreated from the -228 m to -245 m stage. During the ice surface lowering form -245 m to -263 m stage numerous other, less distinct

lateral meltwater channels, eskers and kames were formed. As the ice had retreated to the marginal position of -263 m stage, large kame terraces north of lake Yddin emerged from the ice.

The youngest meltwater landforms (lateral meltwater channels, eskers) in the study area were formed north of the present-day lake Yddin. Following the continuous glacial retreat, the ice marginal position was located there roughly at the -279 m stage. By the time the ice marginal position reached the -316 m stage, it had retreated to the western shore of lake Yddin and, thus, out of the bounds of the study area concluding the deglaciation here.

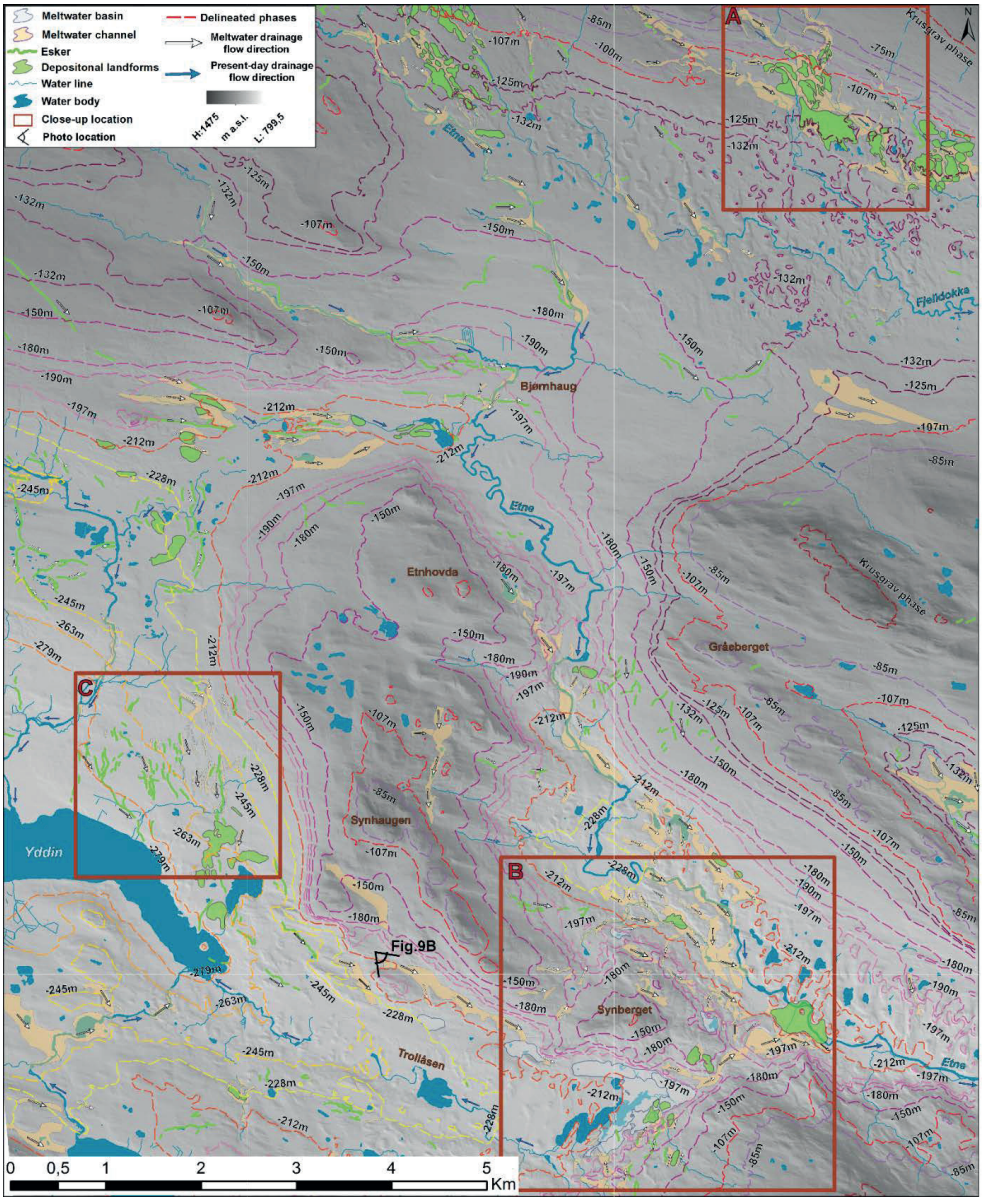

Figure 7. Possible ice marginal positions delineated in Upper Etne, Trollåsen and Fjelldokka valleys. Red boxes indicate locations of the close-up maps in Fig. 8.

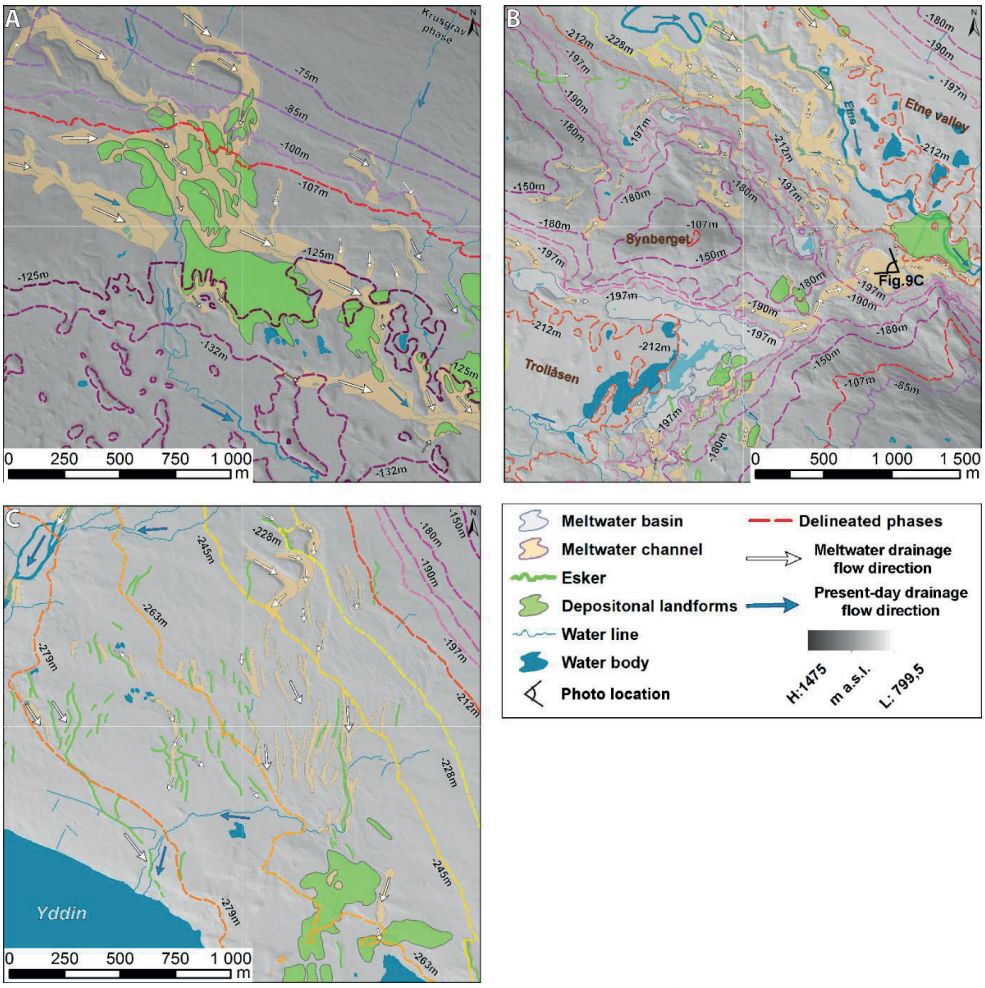

Figure 8. Close-up maps for areas selected in Upper Etne, Fjelldokka and Trollåsen valleys. **A.** Northern side of Fjelldokka valley. **B.** Trollåsen–Etne valley pass. **C.** Northeastern side of lake Yddin.

Figure 9. Panorama photos of various meltwater landforms within the study area. White arrows indicate the meltwater flow directions. For locations see Figs 4, 7, 8B. **A.** Meltwater basin west of lake Reinetjernet (dashed line indicate potential shore line). View towards east. **B.** Lateral meltwater channel north of Trollåsen. View towards southeast. **C.** Spillway between Trollåsen and Etne valley.

Discussion

The uncertainties of the delineated ice margin approach

Although the delineated ice marginal positions in combination with the identified meltwater landforms present a logical and plausible evolution of deglaciation, there are a few uncertainties with this conceptual approach. Here we have elaborated on them in attempt to rise readers' awareness on these issues.

Choice of the gradient steepness. The distributional patterns of meltwater landforms were analysed along an artificially generated reference surface sloping 1% towards the southeast, corresponds to the ice surface of the Krusgrav phase reported by Garnes & Bergersen (1980). Although the proposed deglaciation reconstructions and, thus, the ice surface gradients of the Nunatak, Krusgrav and Espedalen phases have been generally accepted (Sollid & Sørbel 1994; Mangerud 2004), Garnes & Bergersen (1980) point out that the gradient might have been less than the 1% prior the Nunatak phase and 2-4% at the distal parts of the ice sheet at the later stages. In order to check how the landforms aligned along different surface gradients, two other scenarios of 0.5% and 2% gradients were briefly tested. These tests indicate that the steepness gradient of 1% is the most reasonable for the large scale correlations. Also the identified lateral meltwater channels from the various localities within the study area (like north of Trollåsen, north of Fjelldokka and south of Fullsenn; Figs 4, 5B, 5C, 7 and 8) confirm the validity of the used reference surface gradient.

However, Garnes & Bergersen (1980) state that the ice surface gradient align more with the underlying valley terrain at the later stages of deglaciation, therefore the gradients could have to some extent varied throughout the valleys. This is also shown by the development of ice flow phases by Putniņš & Henriksen (2017). The exact timing and any change of the gradient is difficult to determine, it is, however, reasonable to assume that the ice surface had flattened out at the last stages of deglaciation. The implications is that the ice remnants could have stretched further down the valleys than what is reconstructed here.

Deviations of ice flow and surface gradient orientation. Another uncertainty is the local deviations between the ice flow direction and the surface gradient orientation, which may cause inaccuracies within the delineated ice marginal positions. Areas with a terrain slope oblique to the reference surface orientation are the valley north of Synnfjell, the area between Svarthamar and Røssjøen, the Fullsenn-Fjelldokka pass and the narrow valley near Etne's head (Fig. 7). The three latter areas are likely effected less due to their generally smaller topographical extent (~1 to 2 km wide).

The most noticeable example is the east-west trending valley north of Synnfjell (Fig. 3) where ice flow was oriented almost at right angle to the direction of the reference surface orientation. To evaluate the potential error caused by the oblique direction of this valley, a profile across the valley was constructed. As Fig. 10 illustrates, the surface gradient is roughly 15 m/km corresponding to a slightly higher elevated ice surface on the northern side of the valley. This reconstructed surface gradient is likely too steep, making correlations across the valley more uncertain. Some cross-valley features corresponding to two different delineation stages (up to 18 m difference) could instead

represent the same stage, and the actual ice marginal positions of various stages may have been located slightly further to the south than they are currently delineated. Therefore, when analysing the outcome, possible inaccuracies should be acknowledged in areas oriented obliquely to the slope gradient of the reference surface. Nevertheless, the mapped spillways and eskers corresponds well with the delineated possible ice marginal position (Fig. 3), indicating a reasonable reconstruction.

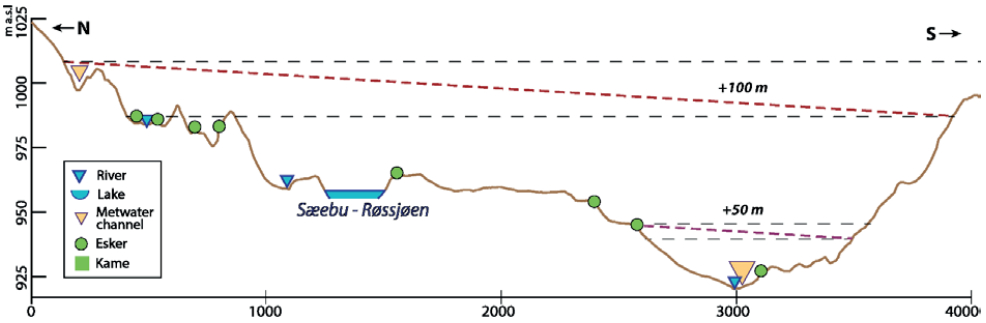

Figure 10. Cross-profile of the valley north of Synnfjell where the dashed red lines show the ice surface gradients of 100 and 50 m above the Krusgrav phase. Horizontal black dashed lines are marked where the ice surface gradients intersects with the topography.

***The 'static nature' of the reconstruction approach*.** The way the possible ice marginal positions have been delineated and presented here is static in regards to any change in the glacial dynamics that might have occurred throughout the deglaciation as it is relaying only on the reference surface with the Krusgrav phase as the reference point of time. Such approach, sliding an artificial ice surface up and down along the Z-axis of the reference surface, illustrates well the vertical down-wasting of ice (Garnes & Bergersen 1980). However, it neglect the possible influx of additional ice masses from the accumulation zone of the nearby ice dome that might have occurred after the Krusgrav phase, in particularly the western part of the study area may have received additional influx. Since the Skaget pass in the north of the study area became deglaciated shortly after the Krusgrav phase (similarly to the Krusgrav pass described in Garnes & Bergersen (1980)), any ice flow would had to move from the west around the mountains. This is indicated on the map reconstructing the ice thickness during the +100m stage (Fig. 11). Possibly, the diverging orientations of ribbed moraine crests within the Fjelldokka valley reported by Putniņš & Henriksen (2017), is the evidence for such influx of ice after the Krusgrav phase. Substantially influx of ice from the west may have caused the ice margins to advance or still stand even during continuous down wasting. Any indications of ice advance is not found within the study area.

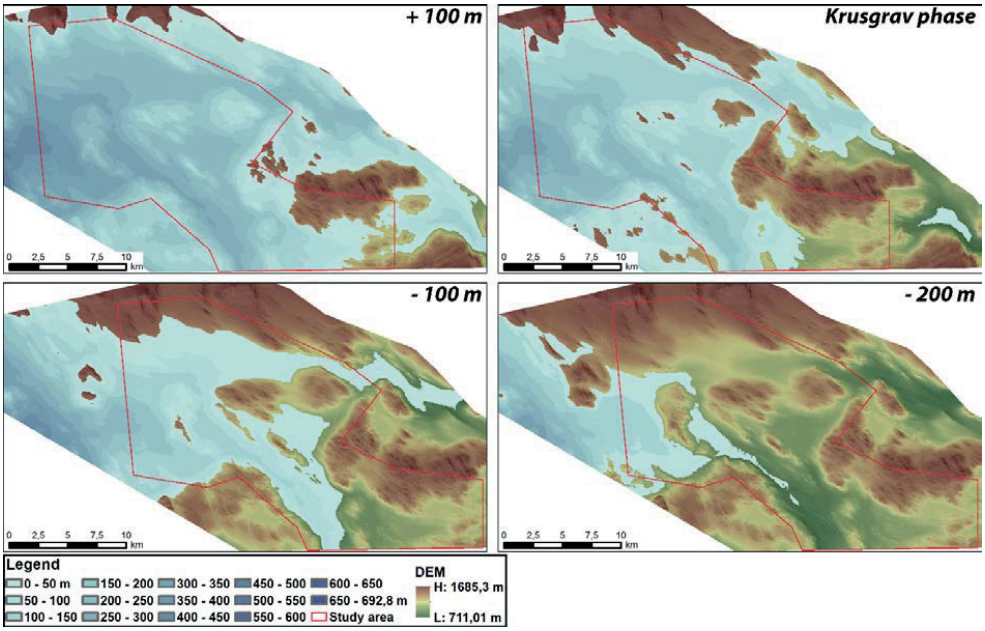

Figure 11. Estimated ice thickness within the study area at the 100 m above and during the Krusgrav phase, and 100 and 200 m below the Krusgrav phase**.**

Although the change from warm- to cold-based ice conditions at later stages of deglaciation has been acknowledged (Sollid & Sørbel 1994; Kleman *et al.* 1997), Garnes & Bergersen (1980) stated that stagnant, dead ice was located at higher elevations while active ice was flowing in the valleys as the inland ice sheet gradually down-wasted. Reconstruction of the ice thickness during the +100m stage (Fig. 11) indicates that the ice was substantially thick to maintain sliding conditions at the ice-bed interface.

Summarizing the above, the complete pattern of deglaciation is near-to-impossible to determine due to the static nature of the reconstruction approach and other uncertainties. The possible influxes of additional ice masses after the Krusgrav phase imply that the evolution of deglaciation occurred in an asynchronous manner. Although the presented reconstructions show a generally reasonable pattern of deglacial in a regional scale, it should be considered more as the local reconstructions of the given areas and straight-forward correlations of delineated stages over long distances should be avoided.

The delineated ice marginal positions

The presented findings show that the implementation and use of the reference gradient for delineating the possible ice marginal positions has allowed to illustrate the vertical down-wasting of

ice in a more detailed way than what Garnes & Bergersen (1980) did for the neighbouring area to the north. The combination of mapped meltwater landforms and the delineated ice marginal positions give a reasonable sequence of deglaciation stages.

The vertical melting of ice is best illustrated by the formation and development of the meltwater drainage system consisting of ice-dammed lakes, meltwater channels, eskers and kames in valley north of Synnfjell (Fig. 3) between the Nunaktak phase and the +50 m stage as well as in the area northeast of Svarthammar (Fig. 4) between the +67 m and -55 m stage. Similarly, the sequential lateral channels from the northern side of Fjelldokka valley (Figs 7, 8A) between the -75 m to -125 m stages and from the northern side of Trollåsen valley between the -212 m to -245 m stages (Figs 7, 8C) illustrates the same pattern of down-wasting.

In some areas where the general slope of terrain is oriented in the opposite direction of the previous ice flow (like in valley north of Synnfjell, Trollåsen valley and the head of Etne valley), the reconstructed deglaciation pattern of down-wasting partly coincides with ice front retreat. In the lowest parts of the terrain, ice remnants belonging to various delineated stages were blocking the (present-day) drainage routes (like upper part of Fjelldokka, upper part of the main Etne valley and the Fullsenn–Etne valley connection) (Figs 4, 7). Often these blockages resulted in forming frontal ice-dammed lakes in basins with drainage through spillways into adjacent valleys flowing in the opposite direction than present as it is shown by spillways northeast of lake Fullsenn and the Trollåsen–Etne passage. Elsewhere, smaller, presumably short-lasting lateral ice-dammed lakes were formed in basins at the sides of the outlet glaciers (e.g. Fig. 9A). The given above examples illustrate the influence of the general (underlying) landscape on the landform distribution patterns.

The delineated ice marginal positions illustrate that at some deglacial stages thin, dead-ice conditions existed at some parts of the study area (mainly in Etne valley). Often these areas do not resemble the typical dead-ice field with hummocky moraine (Eyles *et al.* 1999) but there are a few smaller kettles found within kames – indicating the presence of buried ice during the sediment deposition (southern side of Etne valley). At the northern side of Etne valley, the lack of distinct kame and kettle morphology can be explained by the strong influence of underlying terrain (streamlined landforms and ribbed moraine) and/or later erosional meltwater action. Whereas additional meltwater sedimentation may have buried any features in the northern side of Fjelldokka valley.

The established ice thickness estimations (Fig. 11) in combination with the findings of various meltwater landforms improves the understanding of the thermal conditions of the ice sheet during its deglaciation. The reconstructed ice retreat pattern suggests that ice flow was active for longer time within the deepest parts of the terrain (Figs 4, 6**,** 7, 11) confirming earlier findings (e.g. Soliid &

Sørbel 1994; Kleman et. al. 1997). As illustrated by Fig. 11, several stages when blocks of ice of considerable sizes became disintegrated from the main ice are delineated. Such disintegration seems to have occurred where there are bedrock thresholds or saddles along the valley longitudinal profile, thus, even further illustrating the influence of the general underlying terrain on the deglaciation.

The reconstructed down-wasting pattern indicates a gradual retreat of the ice margin from east to west (Fig. 11), confirming the reconstructions flow pattern proposed by Putniņš & Henriksen (2017). Furthermore, such westward retreat of ice (Fig. 11) align with the general reconstructions of the last stages of the Fennoscandian Ice Sheet that the last remaining glaciers were probably located on the floors of deep valleys near the former ice divide (Hughes et al. 2016).

Conclusions

- The use of the 'virtual ice surface' originating from the implemented reference gradient surface has enabled to improve the meltwater landform correlations and to delineate possible ice marginal positions in greater detail. It has further increased the general understanding of the final stages of deglaciation with its many stages in the Upper Etne valley.
- During the final stages of deglaciation the inflow shifted from coming from north and northwest to being more from the west. The overall deglaciation pattern confirms the vertical down-wasting of ice.
- The existence and evolution of several small-scale and short-lived ice-dammed lakes and rerouting of meltwater are documented in detail, including the most prominent ice-dammed lakes within the Fullsenn basin and Trollåsen valley.
- Dead ice existed in the deeper valleys as ice bodies became separated from the main glacier, recognised by numerous transverse eskers and constrained outwash fans. Existence of several other dead-ice fields are indicated by the use of the 'virtual ice surface', although they are lacking typical landform features.
- Due to the vertical down-wasting ice and a gentle-sloping terrain oriented in the same direction as the main ice flow, the Upper Etne valley area is well-suited for the proposed delineation-surface approach. Factors increasing the unreliability of the 'virtual ice surface' are: (i) incorrect choice of surface gradient, (ii) deviating orientation of surface gradient with the ice flow and/or terrain, and (iii) any changes of the glacier's gradient and orientation over time. The static nature of the delineation of ice marginal positions should preferably be coupled with a more dynamic reference surface(s).

Acknowledgements. – The authors acknowledge Cecilie Rolstad Denby for the valuable input and discussion at an early stage of the manuscript. We gratefully acknowledge Renata Lapinska-Viola (NGU) for the help on acquiring additional geological data sets as well as Norwegian Mapping Authority (Kartverket) for providing the access to LiDAR data 'the old fashioned way' before the introduction of their web-service (www.hoydedata.no).

References

Benn, D. & Evans, A.J. 2010: *Glaciers and Glaciation.* 2nd edition. 802 pp. Hodder Education, London.

Bergersen, O. F. & Garnes, K. 1972: Ice movements and till stratigraphy in the Gudbrandsdal area. Preliminary results. *Norsk Geografisk Tidsskrift 26*, 1-16.

Bergersen, O. F. & Garnes, K. 1983: Glacial deposits in the culmination zone of the Scandinavian ice sheet. *In* Ehlers, J. (ed.): *Glacial deposits in north-west Europe*, 29-40, A. A. Balkema, Rotterdam.

Briner, J. P., Miller, G. H., Davis, P. T. & Finkel, R. C. 2006: Cosmogenic radionuclides from fiord landscapes support differential erosion by overriding ice sheets. *Bulletin of the Geological Society of America 118*, 406-420.

Carlson, A. B. & Sollid, J. L. 1979: *Fullsenn, kvartærgeologisk kart 1717 III - 1:50 000*. Norges geologiske undersøkelse, Trondheim.

Carlson, A. B. & Sollid, J. L. 1983: Fullsenn. Beskrivelse til kvartærgeologisk kart 1717 III – M 1:50 000. *Norges geologiske undersøkelse* 390, 35 pp. NGU, Trondheim.

Carrivick, J. L., Yde, J., Russell, A. J., Quincey, D. J., Ingeman-Nielsen, T. & Mallalieu, J. 2017: Ice-margin and meltwater dynamics during the mid-Holocene in the Kangerlussuaq area of west Greenland. *Boreas 46*, 369-387.

Clark, C. D., Hughes, A. L. C., Greenwood, S. L., Jordan, C. & Sejrup, H. P. 2012: Pattern and timing of retreat of the last British-Irish Ice Sheet. *Quaternary Science Reviews 44*, 112-146.

Clark C. D., Ely J. C., Greenwood S. L., Hughes A. L. C., Meehan, R., Barr I. D., Bateman M. D., Bradwell, T., Doole, J., Evans D. J. A., Jordan C. J., Monteys, X., Pellicer X. M. & Sheehy, M. 2017: BRITICE Glacial Map, version 2: a map and GIS database of glacial landforms of the last British–Irish Ice Sheet. *Boreas 47*, 11-18.

Dyke, A. S. 1993: Landscapes of cold-centred Late Wisconsinan ice caps, Arctic Canada. *Progress in Physical Geography: Earth and Environment 17*, 223-247.

Eyles, N., Boyce, J. I. & Barendregt, R. W. 1999: Hummocky moraine: sedimentary record of stagnant Laurentide Ice Sheet lobes resting on soft beds. *Sedimentary Geology 123*, 163-174.

Evans, D. J. A., Hughes, A. L. C., Hansom, J. D. & Roberts, D. H. 2017: Scottish Landform Examples 43: glacifluvial landforms of Strathallan, Perthshire. *Scottish Geographical Journal 133*, 42-53.

Fabel, D., Ballantyne, C. K. & Xu, S. 2012: Trimlines, blockfields, mountain-top erratics and the vertical dimensions of the last British–Irish Ice Sheet in NW Scotland. *Quaternary Science Reviews 55*, 91-102.

Finlayson, A., Fabel, D., Bradwell, T. & Sugden, D. 2014: Growth and decay of a marine terminating sector of the last British–Irish Ice Sheet: a geomorphological reconstruction. *Quaternary Science Reviews 83*, 28-45.

Garnes, K. & Bergersen, O. F. 1980: Wastage features of the inland ice sheet in central South Norway. *Boreas 9*, 251-269.

Glasser, N. F. & Smith, G. H. S. 1999: Glacial meltwater erosion of the Mid-Cheshire Ridge: implications for ice dynamics during the Late Devensian glaciation of northwest England. *Journal of Quaternary Science 14*, 703-710.

Goehring, B. M., Brook, E. J., Linge, H., Ralsbeck, G. M. & Yiou, F. 2008: Beryllium-10 exposure ages of erratic boulders in southern Norway and implications for the history of the Fennoscandian Ice Sheet. *Quaternary Science Reviews 27*, 320-336.

Greenwood S. L., Clark C. D. & Hughes A. L. C. 2007: Formalising an inversion methodology for reconstructing ice-sheet retreat patterns from meltwater channels: application to the British Ice Sheet. *Journal of Quaternary Science 22*, 637-645.

Greenwood, S. L. & Clark, C. D. 2009a: Reconstructing the last Irish Ice Sheet 1: changing flow geometries and ice flow dynamics deciphered from the glacial landform record. *Quaternary Science Reviews 28*, 3085-3100.

Greenwood, S. L. & Clark, C. D. 2009b: Reconstructing the last Irish Ice Sheet 2: a geomorphologically-driven model of ice sheet growth, retreat and dynamics. *Quaternary Science Reviews 28*, 3101-3123.

Greenwood, S. L., Clason, C. C., Helanow, C. & Margold, M. 2016: Theoretical, contemporary observational and palaeo-perspectives on ice sheet hydrology: Processes and products. *Earth-Science Reviews 155*, 1-27.

Heim, M., Schärer, U. & Milnes, A. G. 1977: The nappe complex in the Tyin-Bygdin-vang region, central southern Norway. *Norsk Geologisk Tidsskrift 57*, 171-181.

Hättestrand, C., 1998. The glacial geomorphology of central and northern Sweden. Sveriges Geologiska Undersökning, Serie Ca 85, 1-47.

Hughes, A. L. C., Clark, C. D. & Jordan, C. J. 2014: Flow-pattern evolution of the last British Ice Sheet. *Quaternary Science Reviews 89*, 148-168.

Hughes, A. L. C., Gyllencreutz, R., Lohne, Ø. S., Mangerud, J. & Svendsen, J. I. 2016: The last Eurasian ice sheets – a chronological database and time-slice reconstruction, DATED-1. *Boreas 45*, 1-45.

Kleman, J. & Borgström, I. 1996: Reconstruction of palaeo-ice sheets: the use of geomorphological data. *Earth Surface Processes and Landforms 21*, 893-909.

Kleman, J., Hattestrand, C., Borgstrom, I. & Stroeven, A. 1997: Fennoscandian palaeoglaciology reconstructed using a glacial geological inversion model. *Journal of Glaciology 43*, 283-299.

Kleman, J., Hättestrand, C., Stroeven, A. P., Jansson, K. N., De Angelis, H. & Borgström, I. 2006: Reconstruction of palaeo-ice sheets - inversion of their glacial geomorphological record. *Glacier Science and Environmental Change*, 192-198.

Livingstone, S. J., Evans, D. J. A., Ó Cofaigh, C., Davies, B. J., Merritt, J. W., Huddart, D., Mitchell, W. A., Roberts, D. H. & Yorke, L. 2012: Glaciodynamics of the central sector of the last British–Irish Ice Sheet in Northern England. *Earth-Science Reviews 111*, 25-55.

Mangerud, J. 2004: Ice sheet limits in Norway and on the Norwegian continental shelf. *In* Ehlers, J. & Gibbard, P. L. (eds.): *Developments in Quaternary Sciences*, 271-294 pp. Elsevier. Amsterdam.

Mangerud, J., Gyllencreutz, R., Lohne, Ø. & Svendsen, J. I. 2011: Glacial History of Norway. *In* Ehlers, J., Gibbard, P. L. & Hughes, P. D. (eds.): *Developments in Quaternary Sciences*, 279-298 pp. Elsevier.

Margold, M., Jansson, K. N., Kleman, J. & Stroeven, A. P. 2011: Glacial meltwater landforms of central British Columbia. *Journal of Maps 7*, 486-506.

Margold, M., Jansson, K. N., Kleman, J. & Stroeven, A. P. 2013a: Lateglacial ice dynamics of the Cordilleran Ice Sheet in northern British Columbia and southern Yukon Territory: retreat pattern of the Liard Lobe reconstructed from the glacial landform record. *Journal of Quaternary Science 28*, 180-188.

Margold, M., Jansson, K. N., Kleman, J., Stroeven, A. P. & Clague, J. J. 2013b: Retreat pattern of the Cordilleran Ice Sheet in central British Columbia at the end of the last glaciation reconstructed from glacial meltwater landforms. *Boreas 42*, 830-847.

Margold, M., Stokes, C. R. & Clark, C. D. 2015: Ice streams in the Laurentide Ice Sheet: Identification, characteristics and comparison to modern ice sheets. *Earth-Science Reviews 143*, 117-146.

Ng, F. S. L., Barr, I. D. & Clark, C. D. 2010: Using the surface profiles of modern ice masses to inform palaeo-glacier reconstructions. *Quaternary Science Reviews 29*, 3240-3255.

Olsen, L. 1985: Weichselian till stratigraphy in the Lillehammer area, southeast Norway. *Norges geolologiske undersøkelse 401*, 59-81.

Price, R. J. 1960: Glacial meltwater channels in the Upper Tweed drainage basin. *The Geographical Journal 126*, 483-489.

Putniņš, A. & Henriksen, M. 2017: Reconstructing the flow pattern evolution in inner region of the Fennoscandian Ice Sheet by glacial landforms from Gausdal Vestfjell area, south-central Norway. *Quaternary Science Reviews 163*, 56-71.

Schytt, V. 1956: Lateral drainage channels along the northern side of the Moltke Glacier, Northwest Greenland. *Geografiska Annaler 38*, 64-77.

Sissons, J. B. 1960: Some aspects of glacial drainage channels in Britain: Part I. *Scottish Geographical Magazine 76*, 131-146.

Sissons, J. B. 1961: Some aspects of glacial drainage channels in Britain. Part II. *Scottish Geographical Magazine 77*, 15-36.

Sollid, J. L. & Sørbel, L. 1994: Distribution of glacial landforms in southern Norway in relation to the thermal regime of the last continental ice sheet. *Geografiska Annaler. Series A, Physical Geography 76*, 25-35.

Storrar, R. D. & Livingstone, S. J. 2017: Glacial geomorphology of the northern Kivalliq region, Nunavut, Canada, with an emphasis on meltwater drainage systems. *Journal of Maps 13*, 153-164.

Stroeven, A. P., Hättestrand, C., Kleman, J., Heyman, J., Fabel, D., Fredin, O., Goodfellow, B. W., Harbor, J. M., Jansen, J. D., Olsen, L., Caffee, M. W., Fink, D., Lundqvist, J., Rosqvist, G. C., Strömberg, B. & Jansson, K. N. 2016: Deglaciation of Fennoscandia. *Quaternary Science Reviews 147*, 91-121.

Sugden, D. E., Denton, G. H. & Marchant, D. R. 1991: Subglacial meltwater channel systems and ice sheet overriding, Asgard Range, Antarctica. *Geografiska Annaler, Series A 73 A*, 109-121.

Syverson, K. M. & Mickelson, D. M. 2009: Origin and significance of lateral meltwater channels formed along a temperate glacier margin, Glacier Bay, Alaska. *Boreas 38*, 132-145.

Vorren T. O. 1977: Weichselian ice movement in South Norway and adjacent areas. *Boreas 6*, 247-257.

Supporting Information

Fig. S1. An overview map of the study area with findings – mapped glacifluvial landforms and several delineated deglacial stages.

Final stages of deglaciation reconstructed from meltwater landforms in the Upper Etne valley, south-central Norway

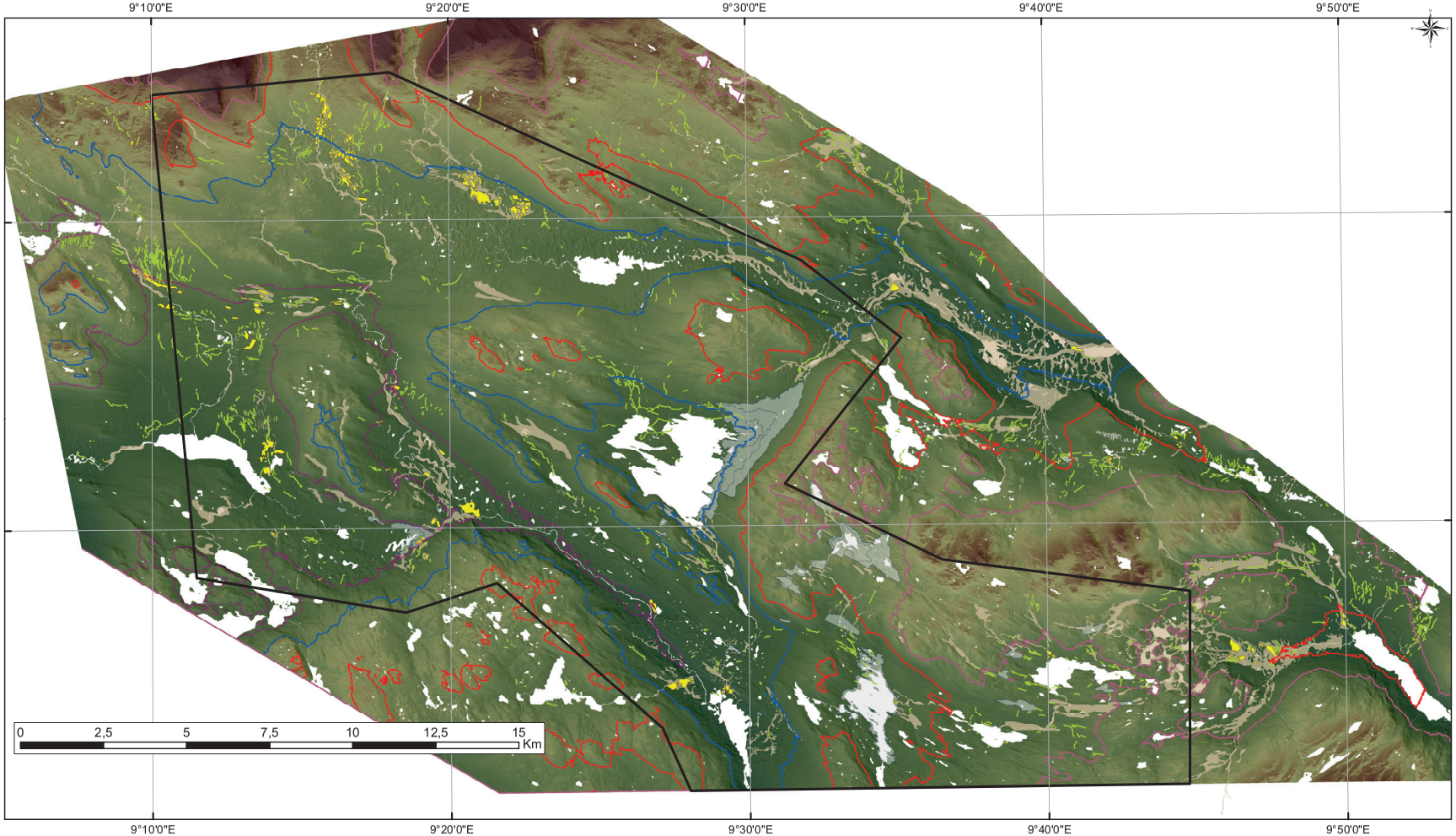

Legend

- Study area
- Water body
- +100m
- Krusgrav phase
- -100m
- -200m
- Eskers
- Depositonal landforms
- Meltwater channels
- Meltwater basins

© Artūrs Putniņš [a],*, Mona Henriksen [a]
[a] Faculty of Environmental Sciences and Natural Resource Management,
Norwegian University of Life Sciences,
P.O. Box 5003, 1432 Ås, Norway
* Corresponding author. Tel. +47 67231815. E-mail address: arturs.putnins@nmbu.no

ISBN: 978-82-575-1536-2
ISSN: 1894-6402

Norwegian University
of Life Sciences

Postboks 5003
NO-1432 Ås, Norway
+47 67 23 00 00
www.nmbu.no

100037 / ANDVORDGRAFISK.NO